Aus der Chirurgischen Klinik,
der Medizinischen Fakultät Charité – Universitätsmedizin Berlin

DISSERTATION

Rebesiedlung von xenogenen Gefäßmatrizen als Modell-System für eine optimierte Reendothelialisierung von parenchymatösen Gewebekonstrukten

zur Erlangung des akademischen Grades
Doctor medicinae (Dr. med.)

vorgelegt der Medizinischen Fakultät
Charité – Universitätsmedizin Berlin

von

Nicolai Seiffert

aus Berlin

Datum der Promotion: 25. November 2022

Inhaltsverzeichnis

1. Abstrakt

Hintergrund: Mit Hilfe des *tissue engineering* (TE) und dem Verfahren der De- und Rezellularisierung wird versucht, Ersatz für geschädigte, funktionseingeschränkte Organe zu schaffen. Grundvoraussetzung für die Implantation solcher Konstrukte – und somit der Vollblutperfusion *in vivo* – ist eine erfolgreiche Reendothelialisierung des Gefäßsystems. Bislang wurden für die Zellbesiedlung weitestgehend Zellen von gesunden Probanden oder Labortieren verwendet. Ungeklärt ist, ob auch Endothelzellen aus vorgeschädigten Gefäßen – isoliert von Patienten mit hohem kardiovaskulärem Risikoprofil – für solche Zwecke geeignet sind. Die Reendothelialisierung dezellularisierter boviner Karotiden (BCA) mit von Patienten gewonnenen Zellen kann dabei als Modellsystem für die Entwicklung eines *tissue engineerten* Gefäßersatzes (TEVG) dienen. Resultierende Erkenntnisse könnten in komplexen vaskulären Systemen getestet werden.

Methodik: BCA wurden ohne Zusatz von Natriumlaurylsulfat (*sodium dodecyl sulfate,* SDS) dezellularisiert, charakterisiert und mit endothelialen Vorläuferzellen (*endothelial colony forming cells*, ECFC), isoliert von Patienten mit kardiovaskulärem Risikoprofil, in Monokultur bzw. mit MSC in Kokultur reendothelialisiert. Des Weiteren wurden Rattenpankreata und -lebern dezellularisiert und mittels allogenen Langerhans Inseln rebesiedelt sowie Rattenlebern zusätzlich mit Endothelzellen (RAEC) und mesenchymalen Stromazellen (MSC) reendothelialisiert.

Ergebnisse: Alle Matrices zeigten eine erfolgreiche Dezellularisierung bei erhaltener Komposition der extrazellulären Matrix. Die biomechanischen Eigenschaften der BCA waren nach Dezellularisierung weitestgehend erhalten. Trotz erfolgreicher Isolierung von ECFC von kardiovaskulär-vorerkrankten Patienten mit typischem Phänotyp war die Reendothelialiserung von BCA-Chips ausschließlich in Kokultur mit MSC erfolgreich. Die Kokultur zeigte ein konfluentes Zellwachstum, welches bei Verwendung von Ratten-MSC im Vergleich zu humanen MSC ausgeprägter war. Humane Zellen konnten bis zu 14 Tage in xenogener Zellkultur nachgewiesen werden. Parenchymatöse Organe konnten durch allogene Zellen rebesiedelt werden.

Fazit: Bei Verwendung von aus Patientenblut-isolierten ECFC und Kultivierung unter statischen Bedingungen konnte nur in Kokultur mit MSC eine konfluente Endothelzellschicht ausgebildet werden. Die Rebesiedlung parenchymatöser Organe mit organtypischen sowie organfremden Zellen, die von Labortieren isoliert wurden, war erfolgreich.

2. Abstract

Background: Tissue engineering (TE) and the sub-area of decellularization and recellularization attempts to create replacements for damaged, dysfunctional organs. For implantation of such constructs - and thus whole blood perfusion *in vivo* - a successful reendothelialization of the vascular system is inevitable. So far, cells from healthy volunteers or laboratory animals have largely been used for recellularization. It is unclear whether endothelial cells from previously damaged vessels - isolated from patients with a high cardiovascular risk profile - can also be used for such purposes. The reendothelialization of decellularized bovine carotid arteries (BCA) with patient-derived cells can serve as a model system for the development of a tissue-engineered vascular graft (TEVG). Resulting findings could then be tested in complex vascular systems.

Methods: Bovine carotid arteries (BCA) were decellularized through a novel protocol without usage of sodium dodecyl sulfate (SDS), characterized and reendothelialized using endothelial progenitor cells (ECFC), isolated from patients with cardiovascular risk factors, in monoculture or coculture with MSC. Rat pancreata and livers were de- and recellularized using allogenic islets of Langerhans while rat livers were also reendothelialized using allogenic endothelial (RAEC) and mesenchymal stromal cells (MSC).

Results: All matrices showed successful decellularization while composition of extracellular matrix was retained. Biomechanical properties of decellularized BCA remained largely intact. While ECFC isolation form cardiovascular risk patients was successful and showed a typical ECFC-phenotype, recellularization of BCA-chips could only be achieved in coculture with MSC with a tendency for more confluent results using rat MSC compared to human MSC. Human cells were detectable for up to 14 days in xenogeneic cell culture. Recellularization of decellularized parenchymal organs with allogenic cells was successful.

Conclusion: Upon usage of ECFC isolated from hospitalized patients under static conditions, no confluent endothelial layer was detected. A tendency for better reendothelialization in coculture with rat MSC or human MSC could be observed. Recellularization of decellularized parenchymal organs using cells from young and healthy laboratory animals could be achieved even in matrices from different organs.

3. Einleitung

Das *Tissue Engineering* (TE), also die Gewebezüchtung, dient perspektivisch u.a. auch dazu, transplantierbares Gewebe und Organe zu generieren, um so dem Mangel an geeigneten Spenderorganen entgegenzuwirken. Hierbei ist die Methodik der De- und Rezellularisierung ein vielversprechender Teilbereich, bei welchem aus Geweben oder Organen alle zellulären Bestandteile entfernt werden, jedoch die extrazelluläre Matrix (EZM) mit spezifischen Eigenschaften für die zelluläre Repopulation erhalten bleibt [1]. Auf diese Weise könnten aus tierischen Geweben oder auf zellulärer Ebene vorgeschädigten Organen ggf. funktionstüchtige humane Organe geschaffen werden. Ein – konzeptionell vergleichsweise einfaches – Beispiel stellt ein mit Methoden des TE erzeugter Gefäßersatz (*tissue-engineered vascular graft,* TEVG) zur Anwendung bei peripherer arterieller Verschlusskrankheit (pAVK) dar, da insbesondere in fortgeschrittenen Krankheitsstadien patienteneigene Gefäße nicht mehr verfügbar und künstliche Ersatzmaterialien zum Teil nicht geeignet sind [2]. Die Generierung dieser TEVG würde ein erstes Modellsystem darstellen, um die Bedingungen der Reendothelialisierung untersuchen zu können und diese im Weiteren auf komplexere vaskuläre Systeme zu übertragen. Die Anwendung im Kontext einer Rebesiedlung entsprechender dezellularisierter Gefäße von implantierbaren Organen mit Empfänger-eigenen Zellen könnte die notwendige Immunsuppression reduzieren oder sogar obsolet machen [3].

Aufgrund der Thrombogenität der Extrazellulärmatrix ist eine erfolgreiche, möglichst vollständige Reendothelialisierung des Gefäßsystems Grundvoraussetzung für die Implantation solcher Konstrukte und somit der Vollblutperfusion *in vivo* [2]. Das Erreichen einer konfluenten Endothelschicht ist insbesondere bei soliden Organen durch die komplexe Mikroarchitektur und schlechtere Erreichbarkeit der oberflächenfernen Areale erschwert. Weiterhin scheint die Güte der Dezellularisation auch durch die genutzten Detergenzien beeinflusst zu werden. Hierbei wird häufig Natriumlaurylsulfat (*sodium dodecyl sulfate*, SDS) genutzt, welches eine Schädigung der Basalmembran bedingt und somit eine schlechtere Ausgangssituation für die Rebesiedelung schafft [4]. Insofern ist die Heranziehung eines Modell-Systems zur Evaluierung von Optimierungsmöglichkeiten hilfreich.

Bisher publizierte Studien beschränken sich auf die Verwendung gesunder Zellen für die Rebesiedlung. Es stellt sich die Frage, ob auch Endothelzellen von kardiovaskulär vorerkrankten Patienten in gleichem Maße verwendet werden können. Kürzlich zeigten

Stroncek et al. beispielsweise, dass von Adipozyten gewonnene mesenchymale Stromazellen (MSC) ein abweichendes Zellverhalten zeigen [5].

Zielsetzung der vorliegenden Arbeit ist die Optimierung der Methoden der Reendothelialisierung von zuvor dezellularisierten Konstrukten unter Verwendung isolierter Zellen von Patienten mit hohem kardiovaskulärem Risiko zur Generierung eines humanisierten Gefäßes als Modell-System für die Verbesserung der Rezellularisierung von parenchymatösen Organen.

4. Methodik

Materialien	Bezugsquelle
Antigen Retrieval Solution	Agilent Technologies, Santa Clara, CA, USA
Aquatex	Merck KGaA, Darmstadt, Deutschland
Chondroitin-4-Sulfat	Carl Roth GmbH, Karslruhe, Deutschland
DiI-Ac-LDL	Merck KGaA, Darmstadt, Deutschland
Dithizone	Merck KGaA, Darmstadt, Deutschland
DNA Blood and Tissue Kit	Qiagen, Venlo, Niederlande
DNase	F. Hoffmann-La Roche AG, Basel, Schweiz
EBM-2 Medium	Lonza Group AG, Basel, Schweiz
EGM-2 SingleQuots Supplements	Lonza Group AG, Basel, Schweiz
EGM-2 Medium	PromoCell GmbH, Heidelberg, Deutschland
EGTA	Merck KGaA, Darmstadt, Deutschland
Ethanol	Carl Roth GmbH, Karslruhe, Deutschland
Fetal Bovine Serum	Merck KGaA, Darmstadt, Deutschland
Fibronektin	Merck KGaA, Darmstadt, Deutschland
Ficoll	Merck KGaA, Darmstadt, Deutschland
Fluorescein Diacetate	Thermo-Fisher Scientific, Waltham, MA, USA
Gelatine	Merck KGaA, Darmstadt, Deutschland
Heparin	Rotexmedia, Trittau, Deutschland
Histoacryl	B. Braun, Melsungen, Deutschland
Isofluran-Gas	abbvie, North Chicago, IL, USA
Ketamin	Pfizer, New York City, NY, USA
Kollagenase	Merck KGaA, Darmstadt, Deutschland
Lipidol	Guerbet, Villepinte, Frankreich
LSAB2 Kit	Agilent Technologies, Santa Clara, CA, USA
M-199	Thermo-Fisher Scientific, Waltham, MA, USA
Medetomidin	CP Pharma, Burgdorf, Deutschland
Metamizol	Ratiopharm, Burgdorf, Deutschland
1,9-Dimethylmethylene blau (DMMB)	Merck KGaA, Darmstadt, Deutschland
MSC Basal Medium	ATCC, Manassas, VA, USA
MSC Growth Kit	ATCC, Manassas, VA, USA
Natriumlaurylsulfat	Carl Roth GmbH, Karslruhe, Deutschland

Paraformaldehyd	Carl Roth GmbH, Karslruhe, Deutschland
Penicillin/Streptomycin	Merck KGaA, Darmstadt, Deutschland
Peressigsäure	Merck KGaA, Darmstadt, Deutschland
Phosphat-gepufferte Salzlösung	Merck KGaA, Darmstadt, Deutschland
Propidiumiodid	Merck KGaA, Darmstadt, Deutschland
RPMI-1640	Thermo-Fisher Scientific, Waltham, MA, USA
Tissue Freezing Medium	Leica Biosystems, Wetzlar, Deutschland
Triton X-100	Carl Roth GmbH, Karslruhe, Deutschland
Trypsin	Merck KGaA, Darmstadt, Deutschland
Venenverweilkanüle 16G, 20G, 22G	B. Braun, Melsungen, Deutschland
Venenverweilkanüle 17G, 24G	Becton Dickinson Corporation, Franklin Lakes, NJ, USA

Tabelle 1: Auflistung der im Rahmen der Projekte verwendeten Materialien (Eigene Darstellung, basierend auf den Veröffentlichungen von *Seiffert et al.*, *Napierala et al.* und *Everwien et al.* [6–8]).

Geräte	Bezugsquelle
Allura Xper FD20/20 Angiographieeinheit	Philips Medical Systems, Hamburg, Germany
Zeiss Axiovert 40 CFL Mikroskop	Carl Zeiss AG, Oberkochen, Deutschland
Cytospin 4	Thermo-Fisher Scientific, Waltham, MA, USA
EVOS FL Auto Mikroskop	Thermo-Fisher Scientific, Waltham, MA, USA
GraphPad Prism	GraphPad Software Inc., La Jolla, CA, USA
MATLAB	The MathWorks, Natick, MA, USA
NanoDrop 2000c	Thermo-Fisher Scientific, Waltham, MA, USA
Zeiss Axio Observer Z1 Mikroskop	Carl Zeiss AG, Oberkochen, Deutschland
Rollschüttler RM 5	Glaswarenfabrik Karl Hecht, Sondheim, Deutschland
Spritzenpumpe	B. Braun, Melsungen, Deutschland
Zugtestmaschine	ElectroForce LM1, BOSE, Eden Prairie, MN, USA

Tabelle 2: Auflistung der im Rahmen der Projekte verwendeten Geräte (Eigene Darstellung, basierend auf den Veröffentlichungen von *Seiffert et al.*, *Napierala et al.* und *Everwien et al.* [6–8]).

4.1. Versuchstiere

Alle Tierexperimente erfolgten unter Einhaltung lokaler gesetzlicher Vorgaben und nach Genehmigung durch das Landesamt für Gesundheit und Soziales (T0139/13, T0301/17, O0365/11, O0262/13, O264/13, L0013/18). Detaillierte Angaben sind in den Veröffentlichungen von *Napierala et al.* und *Everwien et al.* aufgeführt [7,8].

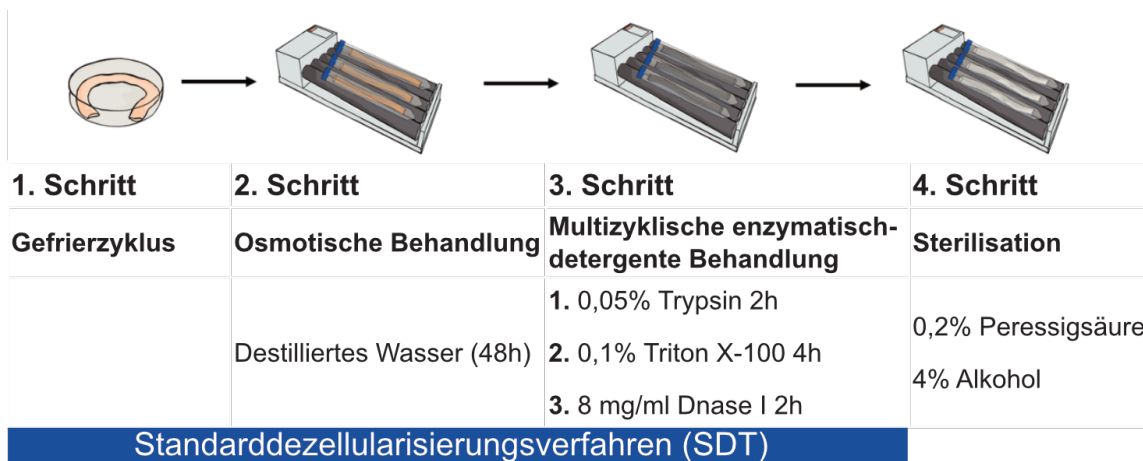## 4.2. Entnahme von Rinderkarotiden

Bovine Karotiden wurden in einem lokalen Schlachthof entnommen, in steriler gekühlter phosphat-gepufferter Salzlösung (PBS) ins Labor überführt, von überschüssigem Gewebe befreit und bei -80°C gefroren bis zur weiteren Verwendung gelagert [6].

4.3. Dezellularisierung von bovinen Karotiden

Die Dezellularisierung von bovinen Karotiden (BCA) erfolgte durch einen mehrschrittigen Prozess [6]:

1. Schritt (Gefrierzyklus): Bei -80°C für 24h gefrorene BCA wurden bei 5°C aufgetaut.
2. Schritt (osmotische Behandlung): Inkubation der BCA für 48h in destilliertem Wasser auf eliptischem Rollschüttler.
3. Schritt (multizyklische enzymatisch-detergente Behandlung): Über drei Tage wurden die BCA auf einem Rollschüttler bei 37°C inkubiert. Die tägliche Inkubation erfolgte in 0,05% Trypsin (2 Stunden) und 0,1% Triton X-100 (4 Stunden), jeweils gelöst in 0,05% EGTA. Anschließend wurden die BCA in 8mg/ml DNase-I inkubiert. Zwischen den Versuchsschritten und über Nacht wurde mit PBS gespült. Zur Identifikation der optimalen Exposition erfolgten fünf Zyklen (=5 Tage).

1. Schritt	2. Schritt	3. Schritt	4. Schritt
Gefrierzyklus	Osmotische Behandlung	Multizyklische enzymatisch-detergente Behandlung	Sterilisation
	Destilliertes Wasser (48h)	1. 0,05% Trypsin 2h 2. 0,1% Triton X-100 4h 3. 8 mg/ml Dnase I 2h	0,2% Peressigsäure 4% Alkohol
Standarddezellularisierungsverfahren (SDT)			

Abbildung 1 Dezellularisierungsprozess von bovinen Karotiden
(modifiziert nach *Seiffert et al.* [6] CC BY 4.0 http://creativecommons.org/licenses/by/4.0)

4.4. Isolierung von humanen endothelialen Vorläuferzellen

Die Isolierung humaner endothelialer Vorläuferzellen (*endothelial colony forming cells – ECFC*) wurde unter Modifikation publizierter Protokolle [9,10] nach Genehmigung durch die Ethikkommission der Charité – Universitätsmedizin Berlin (EA1/256/14) und unter Einhaltung der Deklaration von Helsinki durchgeführt. Nach schriftlichem Einverständnis hospitalisierter Probanden erfolgte die Isolierung mononukleärer Zellen mittels Biocoll-Dichtegradient aus einer peripheren Blutprobe mit anschließender Aussaat auf einer Gelatine-Fibronektin-Beschichtung für 4 Tage bei 37°C und 5% CO_2 in EBM-2 Zellkulturmedium, welches durch EGM2-SingleQuots, 18% FBS und 1% P/S (EGM-2) angereichert wurde. Nach Entfernung nicht-adhärenter Zellen wurde die Inkubation in frischem EGM-2 fortgesetzt [6].

4.5. Isolierung und Kultur von mesenchymalen Stromazellen

Die Isolierung von MSC erfolgte aus dem Knochenmark des Rattenfemurs nach einem adaptiertem Protokoll von *Soleimani und Nadri* [11] für die Versuche der Publikation von *Seiffert et al.* [6]. Der intramedulläre Kanal wurde mit RPMI 1640 Medium, angereichert mit 10% fetalem bovinen Serum (FBS) und 1% Penicillin/Streptomycin (P/S), gespült, die Zellsuspension in eine Zellkulturflasche überführt, bei 37°C 5% CO_2 für 4 Tage inkubiert, von nicht-adhärenten Zellen befreit und mit frischem Medium inkubiert. Ab einer Konfluenz von >70% erfolgte die Aufteilung auf neue Zellkulturflaschen [6]. Die in der Publikation von Everwien et al. verwendeten MSC wurden nach einem adaptierten Protokoll von *Nayernia et al.* [12] isoliert. Hier wurde der intramedulläre Kanal mit RPMI 1640 Medium, angereichert mit 20% FBS und 1% P/S, gespült, die Zellsuspension in eine Zellkulturflasche überführt, bei 37°C 5% CO_2 für 3 Tage inkubiert, von nicht-adhärenten Zellen befreit und mit frischem Medium inkubiert. Bei einer Konfluenz von 100% wurden die Zellen eingefroren und bei -150°C auf flüssigem Stickstoff gelagert [8]. Kommerziell erworbene humane mesenchymale Stromazellen (hMSC, PCS-500-010, ATCC, Manassas, VA, USA) wurden nach Herstellerangaben in MSC Basal Medium, angereichert mit 10% FBS, 1% P/S und MSC Growth Kit (hMSC-Medium), kultiviert [6].

4.6. Rezellularisierung von bovinen Karotiden

Nach Sterilisation der dezellularisierten BCA durch Inkubation in 0,2% Peressigsäure (PAA) und 4% Ethanol für 6 Stunden folgten PBS-Waschschritte, der Zuschnitt der dezellularisierten BCA in 0,5 cm^2 Stücke (BCA-Chips) und die Inkubation in EGM-2 über Nacht. 80µl Zellsuspension aus EGM-2 mit ca. $3,6x10^5$ humanen ECFC (hECFC) wurde auf die luminale Seite der BCA-Chips gegeben. Für Kokultur-Versuche mit Ratten-MSC (rMSC) wurde EGM-2 im Verhältnis 1:1 mit M-199 Zellkulturmedium sowie für Versuche mit humanen MSC EGM-2 im Verhältnis 1:1 mit hMSC-Medium gemischt. Expandierte hECFC, rMSC oder hMSC wurden trypsiniert, gewaschen und im jeweiligen Rebesiedlungsmedium resuspendiert. 80µl Zellsuspension mit $5,5x10^5$ ECFC und $4,2x10^4$ rMSC oder hMSC wurden auf die luminale ECM-Chipseite gegeben. Nach einstündiger Inkubation bei 37°C und 5% CO_2 wurden 4ml des jeweiligen Rebesiedlungsmediums ergänzt, die Inkubation für 72 Stunden fortgeführt und nach Überführen der Matrizen in neue 12-Well-Platten für weitere 12 Tage bei

Monokulturversuchen (n=8) bzw. 14 Tage (n=6) oder 23 Tage (Ratten-MSC: n=5 oder humane MSC: n=6) bei Kokulturversuchen inkubiert [6].

4.7. Entnahme von Rattenpankreas und Rattenleber

Zur Entnahme der Rattenpankreata wurde eine modifizierte Spenderpankreatektomie nach *Klempnauer und Settje* [13] durchgeführt [7]. Es erfolgte die Kanülierung der V. cava inferior (IVC), V. portae (PV) und Aorta jeweils mit Venenverweilkanüle retrograd sowie des Pankreasgangs (PG) anterograd. Rattenlebern wurden entsprechend eines modifizierten Entnahmeprotokolls von *Hillebrandt et al.* [14] entnommen. Es erfolgte die Kanülierung des Gallenganges (GG), der IVC sowie der PV mittels Venenverweilkanüle. Entnommene Rattenlebern wurden in Ringer-Laktat-Puffer überführt und sofort verwendet oder bei -80°C gelagert [7,8].

4.8. Isolierung von Langerhans Inseln der Ratte

Die Isolierung von Langerhans Inseln erfolgte analog zu *Schubert et al*. [15] mittels Entnahme des Pankreas nach Finalisierung und anterograder Gabe einer Digestionslösung aus Kollagenase und DNase über den gemeinsamen GG. Nach Inkubation für 13-15 Minuten in einem Wasserbad bei 37°C erfolgte ein diskontinuierlicher Ficoll-Gradient, die Kultivierung in RPMI 1640 Medium über Nacht und Evaluation der Zellreinheit und Anzahl mittels Dithizon-Färbung [7,8].

4.9. Dezellularisierung von Rattenpankreata

Die Pankreata wurden über die PV mit 1% Triton X-100 (Flussrate: 10ml/min; Dauer: 60 Minuten), 0,5% SDS (Flussrate: 10 ml/min; Dauer: 120 Minuten) und erneut Triton X-100 (Flussrate: 10 ml/min; Dauer: 15 Minuten) perfundiert sowie anschließend mit PBS (Flussrate: 2 ml/min; Dauer: 4 Stunden) gespült [7].

4.10. Dezellularisierung von Rattenlebern

Rattenlebern wurden nach einem modifizierten Protokoll von *Butter et al.* [16] dezellularisiert. Nach Auftauen der Leber bei 4°C über Nacht folgte die Perfusion mit PBS (Flussrate: 5 ml/min; Dauer: 15 Minuten), 1% Triton X-100 SDS (Flussrate: 5 ml/min; Dauer: 90 Minuten), 1% SDS (Flussrate: 5ml/min; Dauer: 90 Minuten) und 50 U/ml DNase (Flussrate: 5 ml/min, Dauer: 15 Minuten). Über Nacht folgte eine Perfusion mit PBS [8].

4.11. Rezellularisierung des Rattenpankreas

Zur Evaluierung der besten Applikationsroute wurden ca. 2000 Langerhans Inseln in 3 ml RPMI 1640 supplementiert mit 10% FBS (inselmedium P) manuell über die Aorta, V. portae oder den Pankreasgang gegeben. Dann wurde nach Inkubation in Inselmedium P bei 37°C und 5% CO_2 5 ml Inselmedium P über den Pankreasgang gegeben. Langerhans Inseln wurden in 3 Schritten à je 2 ml (insg. 6 ml mit ca. 17.500 Langerhans Inseln), unterbrochen von Zelladhäsionspausen, gegeben. Vor Beginn der Perfusion mit Inselmedium P mit verschiedenen Glukosekonzentrationen wurde die Perfusion für eine Stunde pausiert und das Organ in einen Bioreaktor überführt [7].

4.12. Rezellularisierung der Rattenleber

Die Reendothelialisierung erfolgte durch aortale Rattenendothelzellen (RAEC), welche freundlicherweise durch Prof. Dr. rer. nat. Martina Seifert (Medizinische Immunologie, Charité – Universitätsmedizin Berlin) zur Verfügung gestellt wurden. Zur Reendothelialisierung (*n* = 16) erfolgte die Gabe einer Zellsuspension, bestehend aus RAEC und MSC in 5ml Medium-Mix (1:1 Mischung aus EGM-2 und RPMI 1640), jeweils über die PV und IVC schrittweise mit anschließender zweistündiger Inkubation in Medium-Mix. Das Organ wurde dann in einer abgewandelten Version des von *Gassner et al.* [17] gezeigten Bioreaktors zur Perfusion (PV, IVC) und Gabe von Langerhans Inseln (GG) platziert. Nach Perfusion mit oxygeniertem Medium-Mix bei 37°C und 5% CO_2 über Nacht erfolgte am 2. Tag mittels Spritzenpumpe die Gabe von RAEC in 10 ml EGM-2 über die IVC und PV. Es folgte eine vierstündige Adhäsionspause, bevor die Perfusion durch Medium-Mix aufgenommen wurde. Die Kultivierung wurde im Bioreaktor für 9 Tage mit täglichem Wechsel des Perfusionsweges (PV oder IVC), Spülen des GG sowie kontinuierlicher Erhöhung der Perfusionsrate bis zur maximalen Geschwindigkeit von 3 ml/min fortgesetzt. An Tag 9 erfolgte die Rebesiedlung mit Langerhans Inseln (*n* = 10) nach Resuspension in 10ml RPMI 1640 und Aufblähen der Matrix mit 2,5 ml RPMI 1640 manuell über den GG, bevor die Perfusion mit Inselmedium L wieder aufgenommen wurde [8].

4.13. Histologische Analyse von bovinen Karotiden sowie Rattenpankreas und -leber

De- und rezellularisierte Gewebe wurden durch Paraformaldehyd (PFA) fixiert, dehydriert, paraffiniert und 7µm (BCA) bzw. 5 µm (sonstige Gewebe) Gewebeschnitte

angefertigt. Für rezellularisierte BCA wurden 7 µm-Kryoschnitte nach Einbettung in Tissue Freezing Medium hergestellt. Es erfolgten Hämatoxylin und Eosin (HE)- sowie 4',6-Diamidin-2-phenylindol (DAPI)-Übersichtsfärbungen. Immunhistologische und Immunfluoreszenzfärbungen mittels der in Tabelle 3 genannten Antikörper erhielten vor Einbettung in Aquatex eine entsprechende Gegenfärbung. Die Auswertung erfolgte unter Verwendung eines Zeiss Axio Observer Z1 oder EVOS FL Auto Mikroskops.

Alle dezellularisierten Gewebe wurden durch Kollagen-I und Kollagen-IV-Färbungen charakterisiert. Weitere Analysen wurden für dezellularisierte Pankreata und BCA mittels Sirius Red sowie Laminin und Fibronektin durchgeführt. Nach Deparaffinierung und Rehydrierung wurde ein 3% Peroxidase Block und die Antigen-Demaskierung mittels Citratpuffer durchgeführt. Die Primärantikörper für Kollagen-I und Fibronektin wurden bei 37°C für 2h inkubiert. Für Laminin und Kollagen-IV wurde ein Schritt zur Blockierung unspezifischer Bindungen durch Zugabe von 3% Ziegenserum ergänzt und anschließend die Proben mit dem Primärantikörper für eine Stunde sowie mit dem Sekundärantikörper für 30 Minuten bei 37°C inkubiert. Alle weiteren Schritte erfolgten unter Verwendung des LSAB2 Kits nach Herstellerangaben. Reendothelialisierte Konstrukte wurden mit monoklonalen Antikörpern gegen CD31, CD90 (Pankreas, BCA), von Willebrand Faktor (vWF, BCA), *human nuclear antigen* (HNA, BCA) und Ki-67 (Leber) angefärbt. Für CD31 und Ki-67 erfolgte die Verarbeitung der Proben wie bei o.g. Charakterisierung dezellularisierter Gewebe durch Peroxidaseblock und Citratpuffer-Demaskierung, Inkubation mit Primärantikörper über Nacht (CD31) bzw. 2 Stunden (Ki-67-Antikörper) und Verwendung des LSAB2-Kits. Für die CD90 und HNA-Färbung wurde nach Behandlung mit der Dampfkochermethode für 5 Minuten in kochendem TRIS/EDTA-Puffer zur Epitop-Freilegung anschließend ein Peroxidaseblock (CD90) bzw. Proteinblock (HNA) durchgeführt. Der jeweilige Primärantikörper wurde bei Raumtemperatur über Nacht sowie der jeweilige Sekundärantikörper für 45 Minuten bei 37°C oder 30 Minuten bei Raumtemperatur inkubiert. Weitere Schritte erfolgten nach Herstellerangaben unter Verwendung des LSAB2-Kits. Für die Immunfluoreszenzfärbungen (CD31, vWF) wurden die Proben für 20 Minuten in kochender Antigen-Retrieval-Solution inkubiert. Danach erfolgte ein Blocking-Schritt mit 1% BSA, 1% Ziegenserum und 0,3% Triton X-100 bevor die Primärantikörper bei 4°C über Nacht aufgetragen wurden. Der Sekundärantikörper wurde anschließend für 45 Minuten bei 37°C inkubiert. Isolierte ECFC wurden mittels Cytospin-Verfahren fixiert. Nach Proteinblock (CD31, 45 Minuten) oder Inkubation mit

bovinem Serumalbumin (BSA, vWF, 10 Minuten) bei Raumtemperatur erfolgte das Aufbringen der jeweiligen Primärantikörper für CD31 (1h, 37°C) und vWF (über Nacht, 4°C) und die Inkubation mit dem Sekundärantikörper für 45 Minuten bei 37°C. Isolierte ECFC wurden mit EGM-2 Medium, versetzt mit 10μg DiI-ac-LDL, für 4h bei 37°C und 5% CO_2 inkubiert, mit DAPI gegengefärbt und in PFA fixiert [6–8].

Primärantikörper

Ziel	Wirt	Verdünnung	Kat.-Nr.	Hersteller
Collagen-I	Mouse	1:400	H00001278-M03	Abnova, Taipei, Taiwan
Collagen-IV	Rabbit	1:400	Ab6586	abcam, Cambridge, UK
Fibronectin	Rabbit	1:400	Ab23751	abcam, Cambridge, UK
Laminin	Rabbit	1:50	Ab11575	abcam, Cambridge, UK
vWF	Rabbit	1:400	Ab6994	abcam, Cambridge, UK
CD31	Rabbit	1:100	Bs-0195R	Bioss Antibodies, Woburn, USA
CD90	Rabbit	1:10	Ab92574	abcam, Cambridge, UK
Ki-67	Rabbit	1:1000	PA5-19462	Thermo-Fisher Sci., Waltham, USA
HNA	Mouse	1:200	Ab191181	abcam, Cambridge, UK

Sekundärantikörper

Ziel	Wirt	Verdünnung	Kat.-Nr.	Hersteller
Rabbit	Goat	1:400	Ab6721	abcam, Cambridge, UK
Mouse	Donkey	1:400	715-035-150	Dianova, Hamburg, Deutschland
Rabbit	Goat	1:400	Ab150080	abcam, Cambridge, UK

Tabelle 3: Verwendete Antikörper (modifiziert nach *Seiffert et al.* [6])

4.14. Biochemische Analyse von bovinen Karotiden

Alle biochemischen Analysen erfolgten aus jeweils 10mg homogenisierten, gefriergetrockneten Proben. Der DNA-Gehalt wurde mit *DNA Blood and Tissue Kit* bei nativen und dezellularisierten Pankreata und BCA ermittelt und im *NanoDrop 2000C* gemessen. Der Gehalt von sulfatierten Glykosaminoglykanen (sGAG) wurde zwischen nativem und dezellularisiertem Gewebe sowie täglich nach dem Dezellularisierungszyklus an 5 Tagen verglichen. Es wurde ein publiziertes Verfahren nach *Farndale et al.* [18] verwendet. Native und verarbeitete Proben wurden mit Chondroitin-4-Sulfat (0-200μg/ml) zur Generierung einer Standardkurve in Papain-Puffer inkubiert. Danach wurden die Proben zu gleichen Teilen mit 1,9-

Dimethylmethylene blau (DMMB) vermischt und bei einer Wellenlänge von 525nm photometrisch mittels NanoDrop 2000c gemessen [6].

4.15. Mechanische Analyse von bovinen Karotiden

Dezellularisierte BCA wurden in 5mm dicke Ringe mit 5 mm Durchmesser zugeschnitten und in einer Zugtestmaschine nach Vorspannung bei 1N mit einer Rate von 0,166 mm/s bis zum Versagen gedehnt. Kraft und Verschiebung wurden durch 100Hz-Abtastrate ermittelt. Ein in MATLAB (The MathWorks, Natick, MA, USA) selbsterstelltes Programm wurde zur Berechnung von Zug und Dehnung aus Kraft und Verschiebung verwendet. Die Zug-Dehnungs-Kurven wurden erstellt und hieraus die Parameter Elastizitätsmodul (E coll und E ela), Zug- und Bruchfestigkeit, Fließspannung sowie Gleichmaß-, Fließ- und Bruchdehnung berechnet (Tabelle 4). Native Kontrollen (n = 12) wurden mit Proben nach Gefrierzyklus, Standarddezellularisierungsverfahren (SDT) und Sterilisation (jeweils n = 8) sowie SDT ohne Gefrierzyklus (n = 9) verglichen [6].

4.16. Angiographie von dezellularisierten Rattenpankreata und -lebern

Zur Visualisierung der duktalen und vaskulären Anatomie der Pankreata und Lebern wurde eine digitale Subtraktionsangiographie in Kooperation mit der radiologischen Abteilung (Institut für Radiologie, Charité – Universitätsmedizin Berlin) durchgeführt. Lipidol und Histoacryl wurden zu gleichen Teilen vermischt als Kontrastmittel verwendet. Unter fluoroskopischer Kontrolle wurde nach Spülung mit 10%iger Glukoselösung das Kontrastmittel manuell über die kanülierten Zugangswege gegeben und die Bilder mittels Angiographieeinheit aufgenommen [7,8].

4.17. Statistik

Für die statistische Analyse und graphische Darstellung wurde GraphPad Prism in den Versionen 6.0 und 7.0 verwendet. Kontinuierliche Variablen wurden mit dem *Shapiro-Wilk-Test* auf Normalverteilung geprüft, sofern die Stichprobengröße die Annahme einer Normalverteilung zuließ. Parametrische kontinuierliche Variablen wurden als Mittelwert mit Standardfehler angegeben, während nicht-parametrische Variablen als Median mit Interquartilsabstand (IQR) dargestellt wurden. Parametrische kontinuierliche Variablen wurden bei Nachweis einer Normalverteilung mittels *Mann-Whitney-U Test* untersucht, andernfalls fand ein Vergleich mittels *t-Test für*

unabhängige Stichproben oder des *One-Way ANOVA* bei Gruppenvariablen Anwendung. Bei nichtparametrischen Variablen erfolgte die Testung mittels *Friedman-Test*, *Wilcoxon-Rangsummentest* oder *Kruskal-Wallis-Test* gefolgt von *Dunn's multiplem Vergleichstest* bei Gruppenvariablen. Als signifikant wurden *p*-Werte < 0,05 erachtet [6–8].

5. Ergebnisse

5.1. Dezellularisierung von bovinen Karotiden, Rattenpankreas und -leber

Die histologische Analyse zeigte eine vollständige Entfernung aller zellulärer Bestandteile in den jeweiligen HE- und DAPI-Färbungen bei weiterhin typischer Gewebearchitektur der BCA, Rattenlebern und Pankreata. Zusätzliche immunhistochemische Analysen für Kollagen-I und -IV in allen dezellularisierten Geweben konnten einen Erhalt der EZM-Proteine zeigen. Sirius-Red und histochemische Laminin- und Fibronektinfärbungen konnten im Vergleich mit nativen Kontrollen ein vergleichbares Vorkommen der Matrixproteine in typischer EZM-Lokalisation bei dezellularisiertem Pankreas und BCA nachweisen [6–8].

5.2. Biochemische Analyse von bovinen Karotiden

Es erfolgte die Messung von sGAG in nativen und dezellularisierten BCA-Proben, nach osmotischer Behandlung und jeweils nach erfolgtem enzymatisch-detergentem Behandlungszyklus für bis zu fünf Zyklen. Initial zeigte sich ein Anstieg des sGAG-Gehaltes nach Dezellularisierung, welcher gegenüber nativen Proben (4,93 μg/mg [IQR 1,61 μg/mg] Trockengewicht) ein statistisch-signifikantes (*p* = 0,007) Maximum nach 3 Behandlungszyklen bei 7,87 μg/mg (IQR 0,43 μg/mg) Trockengewicht erreichte. Durch weitere Behandlungszyklen folgte im Anschluss ein Abfall des sGAG-Gehaltes, welcher sich nach fünf Zyklen im Vergleich zum Maximum nach drei Zyklen erneut signifikant zeigte (4,15 μg/mg [IQR 0,90 μg/mg] Trockengewicht, *p* = 0,0013). Zum biochemischen Nachweis einer erfolgreichen Dezellularisierung wurde nach abgeschlossenem Dezellularisierungsprotokoll (SDT) der DNS-Gehalt gemessen und mit nativen Kontrollen verglichen. Es konnte eine signifikante Reduktion von 2157,00 ng/mg (IQR 709,00 ng/mg) Trockengewicht bei nativen BCA auf 30,00 ng/mg (IQR 51,83 ng/mg; *p* = 0,031) Trockengewicht nach SDT nachgewiesen werden [6].

5.3. Mechanische Analyse von bovinen Karotiden

Um die Veränderung mechanischer Eigenschaften der BCA im Verlauf des Dezellularisierungsverfahrens untersuchen zu können, wurden native Kontrollen (n = 12) mit Proben nach Gefrierzyklus (n = 8), SDT (n = 8) und Sterilisation (n = 8), den zu rebesiedelnden Konstrukten, verglichen. Gleichmaß- (p = 0,01, Abb. 2 h), Fließ- (p = 0,03; Abb. 2 d) und Bruchdehnung (p < 0,01; Abb. 2 f) wiesen statistisch signifikant reduzierte Messwerte gegenüber nativen Kontrollen auf, während das Elastizitätsmodul E ela (p = 0,008; Abb. 2 a) einen statistisch signifikanten Anstieg zeigte. Alle weiteren Messpunkte zeigten keinen signifikanten Unterschied zu nativen Proben nach vollständiger Dezellularisierung und Sterilisation. Vollständig dezellularisierte und sterilisierte Proben behielten 91% Zugwiderstand im Vergleich zu nativen Kontrollen im Hinblick auf die Bruchfestigkeit. Weitere Messpunkte im Verlauf des Dezellularisierungsverfahrens zeigten unterschiedliche mechanische Eigenschaften (Tabelle 4, Abbildung 2) [6].

| Probe	E ela [MPa]	E coll [MPa]	Zugfestigkeit [MPa]	Gleichmaßdehnung []	Fließspannung [MPa]	Fließdehnung []	Bruchfestigkeit [MPa]	Bruchdehnung []
Nativ								
25% Perzentile	0,23	2,37	0,89	0,89	0,25	0,37	1,02	0,71
Median	**0,31**	**2,77**	**1,06**	**1,00**	**0,37**	**0,52**	**1,23**	**0,85**
75% Perzentile	0,61	3,14	1,23	1,16	0,41	0,62	1,46	1,08
IQR	**0,38**	**0,76**	**0,34**	**0,27**	**0,16**	**0,25**	**0,44**	**0,37**
Gefrierzyklus								
25% Perzentile	0,33	1,68	0,73	0,66	0,25	0,38	0,97	0,74
Median	**0,48**	**2,14**	**0,96**	**0,71**	**0,41**	**0,43**	**1,09**	**0,89**
75% Perzentile	0,82	2,40	1,02	0,86	0,42	0,52	1,11	1,05
IQR	**0,49**	**0,73**	**0,29**	**0,20**	**0,18**	**0,14**	**0,13**	**0,31**
SDT								
25% Perzentile	0,33	1,39	0,69	0,54	0,25	0,24	0,73	0,58
Median	**0,54**	**1,45**	**0,73**	**0,69**	**0,30**	**0,37**	**0,80**	**0,74**
75% Perzentile	0,86	2,34	0,96	0,74	0,44	0,42	1,05	0,80
IQR	**0,52**	**0,94**	**0,28**	**0,21**	**0,19**	**0,18**	**0,32**	**0,22**
SDT + Sterilization								
25% Perzentile	0,77	1,85	0,81	0,40	0,32	0,17	0,90	0,48
Median	**1,28**	**3,05**	**0,96**	**0,42**	**0,40**	**0,22**	**1,11**	**0,53**
75% Perzentile	1,52	3,46	1,05	0,67	0,45	0,40	1,28	0,73
IQR	**0,75**	**1,61**	**0,24**	**0,27**	**0,13**	**0,23**	**0,37**	**0,24**
SDT ohne Gefrierzyklus								
25% Perzentile	0,18	2,86	0,89	0,53	0,21	0,24	0,96	0,60
Median	**0,21**	**3,12**	**1,00**	**0,67**	**0,23**	**0,35**	**1,09**	**0,68**
75% Perzentile	0,34	3,26	1,16	0,68	0,23	0,37	1,22	0,72
IQR	**0,17**	**0,41**	**0,27**	**0,15**	**0,02**	**0,13**	**0,26**	**0,12**

Tabelle 4: Ergebnisse der mechanischen Untersuchung von dezellularisierten bovinen Karotiden (modifiziert aus *Seiffert et al.*[6])
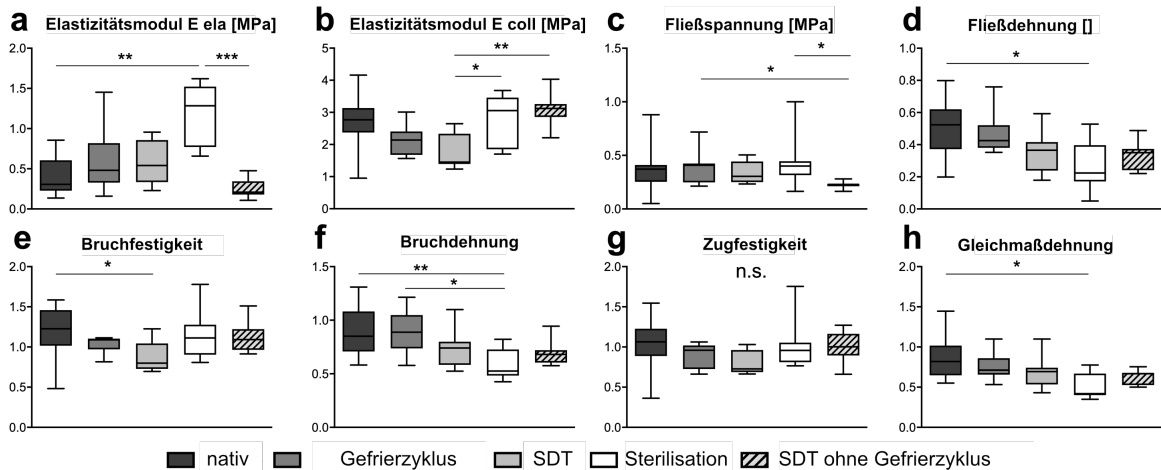
Abbildung 2: Mechanische Eigenschaften von BCA während des Dezellularisierungs- und Sterilisierungsprozesses
(modifiziert aus *Seiffert et al.* [6] CC BY 4.0 http://creativecommons.org/licenses/by/4.0/).
Es zeigte sich eine moderate Reduktion von Elastizitätsmodul E col (b), Bruchfestigkeit (e) und Zugfestigkeit (g) nach dem Gefrierzyklus (*n* = 8) und dem Standarddezellularisierungsverfahren (SDT, *n* = 8) beim Vergleich mit nativen Kontrollen (*n* = 12). Statistisch signifikante Unterschiede wurden in der Sterilisierungsgruppe bezüglich Elastizitätsmodul E ela (a), Gleichmaß- (h), Fließ- (d) und Bruchdehnung (f) im Vergleich zu nativen Kontrollen beobachtet. Final dezellularisierte und sterilisierte BCA (Sterilisation, *n* = 8) zeigten vergleichbare Ergebnisse zu nativen Kontrollen bezüglich Elastizitätsmodul E col (b), Bruchfestigkeit (e), Zugfestigkeit (g) und Fließspannung (c). SDT ohne Gefrierzyklus wurden nicht zur Rebesiedlung verwendet.
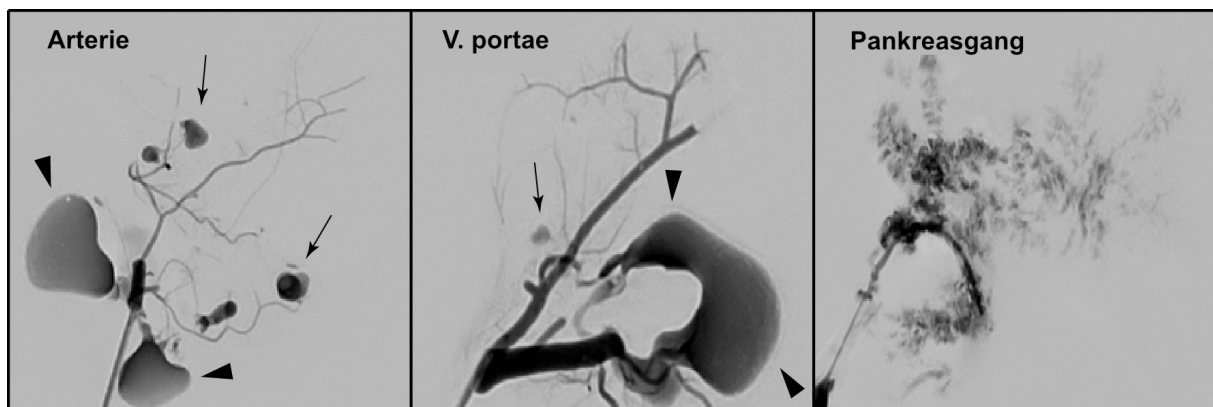
Abbildung 3: Angiographie von dezellularisierten Rattenpankreata
(aus *Napierala et al.* [7] *CC BY 4.0 http://creativecommons.org/licenses/by/4.0*)
Ein Austritt von Kontrastmittel (KM) bei Gabe über das vaskuläre System wurde erst distal im Parenchymbereich (schwarze Pfeile) beobachtet. Abweichend trat das KM bei Gabe über den Pankreasgang im Verlauf in den dezellularisierten Parenchymbereich aus. KM trat auch durch extra-pankreatische Gefäße außerhalb des Organs aus (schwarze Pfeilköpfe).

5.4. Angiographie von dezellularisierten parenchymatösen Organen

Mittels Gabe von Kontrastmittel (KM) über das arterielle und portalvenöse System des dezellularisierten Pankreas konnte die Integrität des vaskulären Netzwerkes nachgewiesen werden. Ein geringer Austritt von KM wurde an den parenchymatösen Kapillaren beobachtet, wohingegen ein diffuser Austritt von KM über den Verlauf des Pankreasganges gezeigt wurde (Abbildung 3). Bei dezellularisierten Rattenlebern

waren die Ergebnisse vergleichbar, während hier jedoch kein KM-Austritt aus dem portalvenösen System beobachtet wurde und der Gallengang einen unmittelbaren Austritt von Kontrastmittel in den parenchymatösen Bereich aufwies [7,8].

5.5. Patientencharakteristika

Insgesamt wurden ECFC von 10 Probanden isoliert, welche gleichermaßen aus Männern (50%) und Frauen (50%) mit einem Durchschnittsalter von 62 Jahren (±21 Jahre) bestand. Alle Probanden durchliefen einen onkologischen (40%), endokrinologischen (20%) oder allgemeinchirurgischen (20%) Eingriff vor der Isolierung. Bluthochdruck (80%), chronisches Nierenversagen (40%) und Diabetes mellitus (30%) waren die häufigsten Nebenerkrankungen. Alle Probanden waren Nichtraucher [6].

5.6. Isolierung von *endothelial colony forming cells*

Es zeigte sich eine Zellisolierungs-Effizienz von 80%, definiert als erfolgreiche Zellisolation bei 8 von 10 Patienten. Typische kopfsteinpflasterartige Kolonien traten durchschnittlich nach 10-12 Tagen Zellkultur in EGM-2 im Inkubator auf. Isolierte Zellen inkorporierten acLDL. CytoSpin-Proben konnten CD31- und vWF-positive Signale an typischer Lokalisation wie Zelloberfläche (CD31) oder innerhalb von Vesikeln, vereinbar mit Weibel-Palade-Körperchen (vWF), nachweisen [6].

### 5.7. Besiedlung von EZM-Chips mit humanen *endothelial colony forming cells*

Mittels ECFC rebesiedelte EZM-Chips zeigten nach 12 Tagen Monokultur nur in einem Versuch (n = 9) vereinzelte Zellen in der HE-Färbung (Abb. 4a) ohne Nachweis von Zellkernen in der DAPI-Färbung (Abb. 4b). Bei ECFC in Kokultur mit rMSC konnte ein konfluentes Zellwachstum auf der luminalen EZM-Chipseite bei allen für 14 (n = 8) und 23 Tage (n = 5) kultivierten Proben in den HE- und DAPI-Färbungen mit einem typischen Auftreten CD31- und vWF-positiver Zellen nachgewiesen werden (Abb. 4e-j). CD90-positive Areale wurden bei Versuchen mit rMSC und hMSC nach 23 Tagen Kultivierung identifiziert (Abb. 4k,l). In wenigen Zellen konnte ein HNA-positives Signal nach 14 aber kein Signal nach 23 Tagen Zellkultur beobachtet werden (Abb. 4m,n). Ähnliche Ergebnisse zeigten Kokulturversuche von ECFC mit hMSC mit teilweise konfluentem Zellwachstum nach 23 Tagen. CD31- (Abb. 4o) und CD90- positive Areale (Abb. 4l) konnten nach 23 Tagen nachgewiesen werden [6].

5.8. Besiedlung von dezellularisiertem Rattenpankreas mit Langerhans Inseln

Bei der Rebesiedlung zeigten sich deutliche Unterschiede in Abhängigkeit von der Applikationsroute: Zellen wurden hauptsächlich im dezellularisierten vaskulären oder duktalen System nachgewiesen. Bei Zellgabe über den Pankreasgang traten die Langerhans Inseln schneller und häufiger ins parenchymatöse Kompartment über als bei Gabe über das Gefäßsystem [7].

5.9. Besiedlung von dezellularisierter Rattenleber

Durch HE-Färbung konnten hauptsächlich Zellen im Bereich der Gefäße nachgewiesen werden, die durch positive CD31-Färbung als Endothelzellen identifiziert werden konnten. Für einige Zellen konnte durch Ki-67-positive Areale eine Proliferation nachgewiesen werden. CD90-Färbungen wiesen MSC innerhalb des Gefäßnetzwerkes nach. Langerhans Inseln wurden im Parenchym nachgewiesen [8].
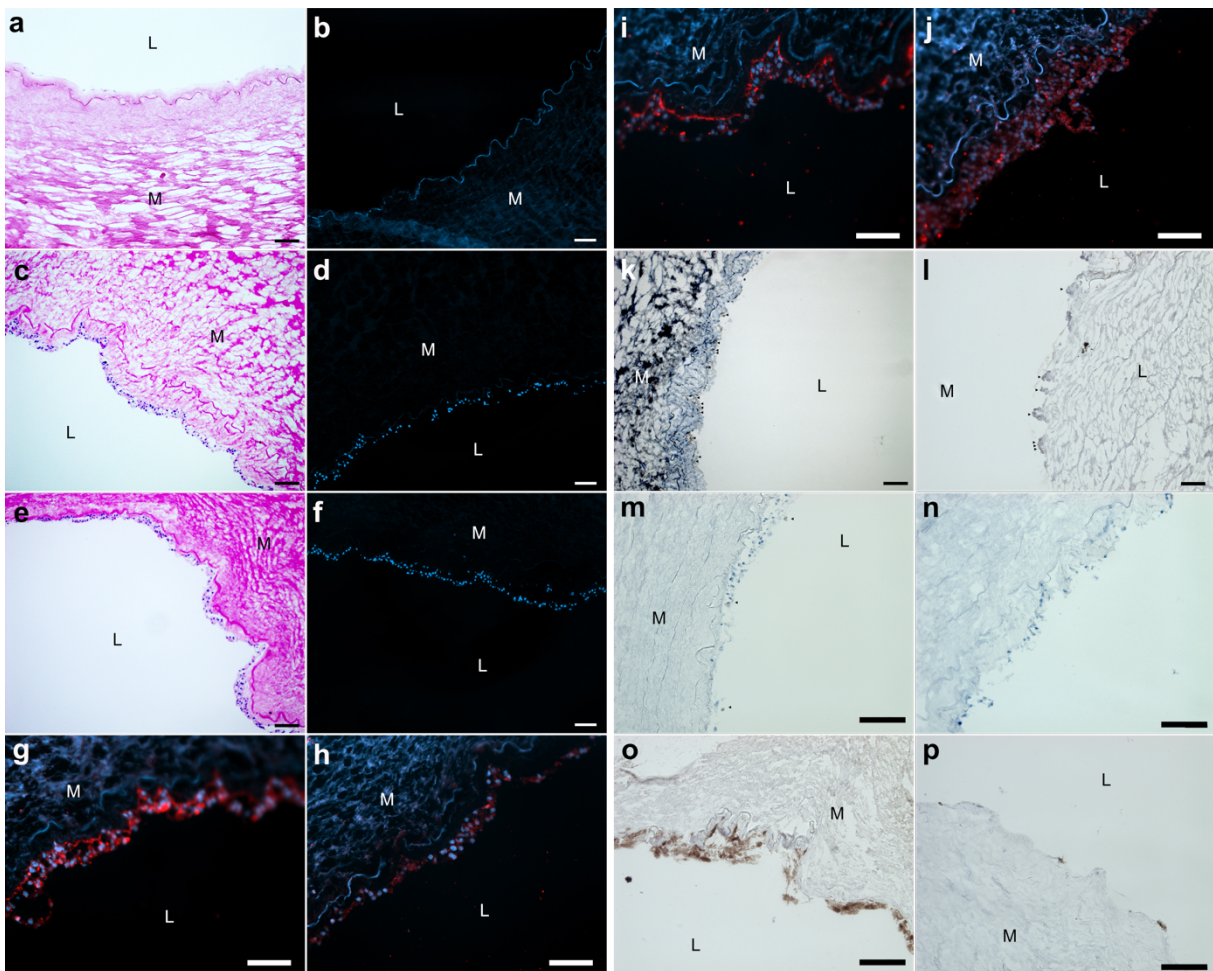
Abbildung 4: Histologische Untersuchung rezellularisierter boviner Karotiden mit Durchlicht- und Immunfloreszenzmikroskopie
(modifiziert aus *Seiffert et al.* [6] CC BY 4.0 http://creativecommons.org/licenses/by/4.0/*)*

EZM-Chips wurden mit endothelial colony forming cells (ECFC) in Mono- (a, b) oder in Kokultur mit Ratten- (rMSC, c-k, m, n) oder humanen mesenchymalen Stromazellen (hMSC, l, o, p) rebesiedelt und für 14 (a-d, g, h, m) oder 23 Tage (e, f, i, j, k, l, n-p) inkubiert. HE- (a, c, e), DAPI- (b, d, f), vWF- (g, i) und CD31-Färbungen (h, j, o) zeigten konfluentes Zellwachstum auf luminaler EZM-Chip-Seite. Ein Trend zu mehrschichtigem Zellwachstum konnte in Proben mit einer Inkubation für 23 Tage (e, f, i, j) beobachtet werden. CD90- (k, l, Pfeile) und HNA-positive Zellen (m, n, p) konnten nachgewiesen werden. Der Maßstabsbalken entspricht 100μm.

6. Diskussion

Die Dezellularisierung und Rezellularisierung ist eine Methode des *Tissue Engineering* mit dem Ziel, implantierbare Gewebe und Organe zu generieren und so den Mangel an geeigneten Organen und Geweben zu begegnen. Hierfür können allogene oder xenogene Gewebe herangezogen werden, die nach erfolgreicher Dezellularisierung und Erhalt ihres dreidimensionalen Gerüsts der Extrazellulärmatrix zur Rebesiedlung mit autologen Zellen dienen können. Grundvoraussetzung für eine anschließende Implantation solcher neu-geschaffener Gewebsstrukturen ist eine vollständige Reendothelialisierung mit funktionsfähigen Endothelzellen, um ein direktes, durch die Thrombogenität der freien Extrazellulärmatrix vermitteltes ischämisches Transplantatversagen zu verhindern [1].

Zur Vermeidung eingeschränkter mechanischer [19] und verminderter Rezellularisierungseigenschaften durch SDS-vermittelte [4] drastische EZM-Modifikationen, modifizierten wir ein klinisch-angewandtes SDS-freies Verfahren von *Olausson et al.* [20] zur Dezellularisierung von BCA-Chips als Modellsystem für die De- und Rezellularisierung parenchymatöser Organe. Obwohl nur ein milder Effekt von Triton X-100 auf sGAG bekannt ist [21], wurde eine signifikante sGAG-Reduktion nach fünf Dezellularisierungszyklen beobachtet und entsprechend auf drei Zyklen verkürzt. Während der unterschiedlichen Phasen der Dezellularisierung und Sterilisierung zeigten sich die mechanischen Eigenschaften unterschiedlich. Nach abgeschlossenem Herstellungsverfahren zeigte sich ein steiferes Konstrukt ohne statistisch signifikanten Verlust der Widerstandskraft. Im Prozessverlauf abweichende Ergebnisse könnten durch beeinträchtigte Kollagenfasern [22] und den Einfluss von PAA [23] bei erhaltenen Rebesiedlungseigenschaften erklärt werden [24]. Zusammengefasst erfüllt das gezeigte Dezellularisierungs- und Sterilisierungsverfahren wichtige Voraussetzungen für eine Anwendung aufgrund einer weitgehenden Konservierung mechanischer Eigenschaften, einer höchstwahrscheinlich konservierten EZM mit fortbestehendem sGAG-Gehalt und, im Vergleich zu nativen Gefäßen und dezellularisierten Pankreata, vergleichbaren Nachweis von EZM-Proteinen [6,7].

In Vorbereitung einer möglicherweisen zukünftigen klinischen Anwendung wurde die Verwendung von humanen ECFC – isoliert aus peripherem Blut von kardiovaskulär-vorerkrankten Patienten – zur Rebesiedlung dezellularisierter BCA-Chips als Modell-System für die Reendothelialiserung von xenogenen parenchymatösen Gewebekonstrukten evaluiert [6].

Krawiec et al. [5] isolierten MSC aus Adipozyten von Patienten mit kardiovaskulären Risikofaktoren und formulierten die Forderung nach weiteren Untersuchungen der Eignung von Zellen aus ähnlichen Patientenkohorten zur Rebesiedlung dezellularisierter ECM. Für ECFC konnte eine veränderte Funktion und reduzierte Anzahl bei älteren Patienten sowie bei Patienten mit Diabetes mellitus, Bluthochdruck und chronischer Niereninsuffizienz als Vorerkrankungen, bekannten Risikofaktoren für pAVK, gesehen werden [25]. Es zeigte sich, dass in diesem Patientenkollektiv mittels peripherer Blutentnahme ECFC erfolgreich isoliert und expandiert werden konnten [6]. Im Gegensatz zur gegenwärtigen Literatur, die gesunden ECFC eine gute Rebesiedlungsfähigkeit zuspricht [26], konnten dezellularisierte BCA-Chips mit patienten-isolierten ECFC im eigenen Versuchsansatz nur unzureichend rebesiedelt werden. Da von verbesserten Proliferationseigenschaften bei gemeinsamer Besiedelung mit MSC berichtet wurde [27], ist es denkbar, dass insbesondere aus kardiovaskulär-vorerkrankten Patienten isolierte ECFC auf diese Unterstützung angewiesen sind. Es wurden daher leicht zugängliche rMSC oder kommerziell erworbene hMSC in Kokultur verwendet. Interessanterweise zeigte sich, dass durch den xenogenen Kobesiedlungsansatz eine konfluente Endothelschicht mit CD31- und vWF- Expression in typischer Lokalisation erreicht werden konnte, jedoch bei längerer Kultivierung kein positives HNA-Signal detektierbar war. Es muss insofern angenommen werden, dass rMSC im Verlauf der Kultivierung begonnen haben, CD31- und vWF-Antigen zu exprimieren sowie ECFC nach Kulturdauern von 14 und 23 Tagen zu verdrängen [6]. *Joddar et al.* [28] konnten ebenfalls eine CD31 Exprimierung von MSC in Kokultur mit Endothelzellen beobachten. Kokultivierung von hMSC und ECFC unter ähnlichen Zellkulturbedingungen zeigten im direkten Vergleich mit rMSC eine schlechtere Reendothelialisierungrate [6]. Auch bereits publizierte Ergebnisse zeigten einen positiven und limitierenden Effekt auf Zellproliferation und Zellüberleben beim Vergleich von allogenen und xenogenen Kokulturen von ECFC und MSC [29].

Für die Anwendung der Erkenntnisse aus dem Modellsystem wurde die Rezellularisierung des Pankreas als parenchymatöses Organ mit komplexer

Gefäßarchitektur ausgewählt [7]. Nach erfolgter Dezellularisierung konnte mittels Angiographie bei Rattenpankreata ein weitestgehend intaktes arterielles und portalvenöses Gefäßsystem dargestellt werden. Erst im Kapillarbereich wurde ein Austritt von Kontrastmittel beobachtet. Im Gegensatz hierzu zeigte sich der Pankreasgang im gesamten Verlauf durchlässig für Kontrastmittel. Es wurde daher postuliert, dass durch die durchlässige Pankreasgangwand auch größeren Langerhans Inseln einen Zugang in das Pankreasparenchym ermöglicht wird. Durch Repopulationsversuche mit Langerhans Inseln wurde bei Zellgaben über den Pankreasgang ein vermehrter und schnellerer Übertritt in das periduktale Parenchym gesehen [7]. Unklar blieb, ob der beobachtete Kontrastmittel-Austritt im kapillaren Gefäßsystem symptomatisch für eine Schädigung der Basalmembran sein könnte.

Da sich das dezellularisierte Pankreasgewebe in der Handhabung als sehr fragil erwies, wurde die Möglichkeit evaluiert, dezellularisierte Rattenlebern über eine Rebesiedlung mit Langerhans Inseln, MSC und Endothelzellen zu einem endokrinen Neo-Pankreas zu maturieren [8]. Da bereits gezeigt werden konnte, dass nicht-organspezifische EZM-Strukturen zur Rebesiedlung verwendet werden können und es bei der Leber ebenso über Arterie, PV und GG drei mögliche Besiedlungs- bzw. Perfusionswege gibt, die sich in der angiographischen Untersuchung vergleichbar mit dem Pankreas zeigen, scheint es möglich, dass auch organfremde Zellen eine Rebesiedlung erreichen können [30]. Bemerkenswert ist zudem, dass das Volumen der Rattenleber theoretisch ausreicht, um sämtliche Langerhans Inseln des humanen Pankreas zu beherbergen [8]. Für die notwendige Reendothelialisierung zur zukünftigen Implantation fanden die Erkenntnisse aus dem BCA-Chip-Modell Anwendung, die eine verbesserte Konfluenz durch Kokultur endothelialer Zellen mit MSC zeigen konnten [6]. Nach erfolgreicher Dezellularisierung wurde die Reendothelialisierung der dezellularisierten Leber über zwei Tage mit RAEC und allogenen MSC mit anschließender Perfusion im Bioreaktor durchgeführt. Nach erfolgter Reendothelialisierung wurden Langerhans Inseln über den Pankreasgang appliziert. In der histologischen Untersuchung zeigte sich ein konfluentes Endothel mit Langerhans Inseln in der EZM eines zellfremden Organs [8].

Insgesamt zeigte sich im Vergleich zu der aktuell publizierten Datenlage eine gleichwertige bis unzureichende Rebesiedlungsfähigkeit von ECFC, welche aus Patientenblut mit kardiovaskulärem Risikoprofil isoliert wurden [31]. Die dargestellten Ergebnisse machen deutlich, dass vorgeschädigte, aus Patienten der möglichen

Zielgruppe isolierte Zellen möglicherweise andere Charakteristika aufweisen als bislang verwendete Zellen. Da EZM-Chips unter statischen Bedingungen rebesiedelt wurden, bleibt es denkbar, dass konfluentes Wachstum und eine physiologische ECFC- und MSC-Zellfunktion unter *in vivo* Bedingungen möglich sein könnte. Um einen humanisierten TEVG aus BCA zu generieren, wären die Entwicklung einer, vorzugsweise Gefäßen entsprechenden, zylindrischen Form, deren Maturierung und schließlich die experimentelle Implantation *in vivo* im Tiermodell die nächsten Schritte [6].

7. Fazit

Erstmalig konnte in dieser Arbeit gezeigt werden, dass aus peripherem Patientenblut isolierte ECFC nicht in der Lage waren eine konfluente Endothelzellschicht auf SDS-frei dezellularisierten BCAs auszubilden. Eine erfolgreiche Reendothelialiserung wurde unter Verwendung von ECFC in Kokultur mit MSC beobachtet. Unter statischen Bedingungen formten rMSC eine konfluente Zellschicht und exprimierten typische Endothelzellmarker. Weiterhin konnte eine SDS-freie Dezellularisierungsstrategie zur Generierung verfügbarer BCAs unter Erhaltung wichtiger mechanischer und EZM-Charakteristika für eine perspektivische Anwendung als peripherer Gefäßersatz von kleinem Durchmesser bei pAVK-Patienten etabliert werden. Es konnte gezeigt werden, dass durch die Verwendung von allogenen Zellen, isoliert von Labortieren, die Rezellularisierung von dezellularisierten Rattenpankreata und Rattenlebern, auch bei zellfremder Umgebung, gelingt.

8. Literaturverzeichnis

[1] K.H. Hillebrandt, H. Everwien, N. Haep, E. Keshi, J. Pratschke, I.M. Sauer, Strategies based on organ decellularization and recellularization, Transpl. Int. 32 (2019) 571–585.
[2] S. Pashneh-Tala, S. MacNeil, F. Claeyssens, The Tissue-Engineered Vascular Graft-Past, Present, and Future, Tissue Eng. Part B Rev. 22 (2016) 68–100.
[3] D. Rana, H. Zreiqat, N. Benkirane-Jessel, S. Ramakrishna, M. Ramalingam, Development of decellularized scaffolds for stem cell-driven tissue engineering: Decellularized scaffolds for tissue engineering, J. Tissue Eng. Regen. Med. 11 (2017) 942–965.
[4] P.F. Gratzer, R.D. Harrison, T. Woods, Matrix alteration and not residual sodium dodecyl sulfate cytotoxicity affects the cellular repopulation of a decellularized matrix, Tissue Eng. 12 (2006) 2975–2983.
[5] J.T. Krawiec, J.S. Weinbaum, H.-T. Liao, A.K. Ramaswamy, D.J. Pezzone, A.D. Josowitz, A. D'Amore, J.P. Rubin, W.R. Wagner, D.A. Vorp, In vivo functional

evaluation of tissue-engineered vascular grafts fabricated using human adipose-derived stem cells from high cardiovascular risk populations, Tissue Eng. Part A. 22 (2016) 765–775.

[6] N. Seiffert, P. Tang, E. Keshi, A. Reutzel-Selke, S. Moosburner, H. Everwien, D. Wulsten, H. Napierala, J. Pratschke, I.M. Sauer, K.H. Hillebrandt, B. Struecker, In vitro recellularization of decellularized bovine carotid arteries using human endothelial colony forming cells, J. Biol. Eng. 15 (2021) 15.

[7] H. Napierala, K.-H. Hillebrandt, N. Haep, P. Tang, M. Tintemann, J. Gassner, M. Noesser, H. Everwien, N. Seiffert, M. Kluge, E. Teegen, D. Polenz, S. Lippert, D. Geisel, A. Reutzel Selke, N. Raschzok, A. Andreou, J. Pratschke, I.M. Sauer, B. Struecker, Engineering an endocrine Neo-Pancreas by repopulation of a decellularized rat pancreas with islets of Langerhans, Sci. Rep. 7 (2017) 41777.

[8] H. Everwien, E. Keshi, K.H. Hillebrandt, B. Ludwig, M. Weinhart, P. Tang, A.S. Beierle, H. Napierala, J.M. Gassner, N. Seiffert, S. Moosburner, D. Geisel, A. Reutzel-Selke, B. Strücker, J. Pratschke, N. Haep, I.M. Sauer, Engineering an endothelialized, endocrine Neo-Pancreas: Evaluation of islet functionality in an ex vivo model, Acta Biomater. 117 (2020) 213–225.

[9] M. Vasa, S. Fichtlscherer, K. Adler, A. Aicher, H. Martin, A.M. Zeiher, S. Dimmeler, Increase in circulating endothelial progenitor cells by statin therapy in patients with stable coronary artery disease, Circulation. 103 (2001) 2885–2890.

[10] J.M. Melero-Martin, Z.A. Khan, A. Picard, X. Wu, S. Paruchuri, J. Bischoff, In vivo vasculogenic potential of human blood-derived endothelial progenitor cells, Blood. 109 (2007) 4761–4768.

[11] M. Soleimani, S. Nadri, A protocol for isolation and culture of mesenchymal stem cells from mouse bone marrow, Nat. Protoc. 4 (2009) 102–106.

[12] K. Nayernia, J.H. Lee, N. Drusenheimer, J. Nolte, G. Wulf, R. Dressel, J. Gromoll, W. Engel, Derivation of male germ cells from bone marrow stem cells, Laboratory Investigation. 86 (2006) 654–663.

[13] J. Klempnauer, A. Settje, Vascularized pancreas transplantation in the rat - details of the microsurgical techniques, results, and complications, Transpl. Int. 2 (1989) 84–91.

[14] K. Hillebrandt, D. Polenz, A. Butter, P. Tang, A. Reutzel-Selke, A. Andreou, H. Napierala, N. Raschzok, J. Pratschke, I.M. Sauer, B. Struecker, Procedure for Decellularization of Rat Livers in an Oscillating-pressure Perfusion Device, J. Vis. Exp. (2015) e53029.

[15] U. Schubert, J. Schmid, S. Lehmann, X.Y. Zhang, H. Morawietz, N.L. Block, W. Kanczkowski, A.V. Schally, S.R. Bornstein, B. Ludwig, Transplantation of pancreatic islets to adrenal gland is promoted by agonists of growth-hormone-releasing hormone, Proc. Natl. Acad. Sci. U. S. A. 110 (2013) 2288–2293.

[16] A. Butter, K. Aliyev, K.-H. Hillebrandt, N. Raschzok, M. Kluge, N. Seiffert, P. Tang, H. Napierala, A.I. Muhamma, A. Reutzel-Selke, A. Andreou, J. Pratschke, I.M. Sauer, B. Struecker, Evolution of graft morphology and function after recellularization of decellularized rat livers, J. Tissue Eng. Regen. Med. 12 (2018) e807–e816.

[17] J.M.G.V. Gassner, M. Nösser, S. Moosburner, R. Horner, P. Tang, L. Wegener, D. Wyrwal, F. Claussen, R. Arsenic, J. Pratschke, I.M. Sauer, N. Raschzok, Improvement of Normothermic Ex Vivo Machine Perfusion of Rat Liver Grafts by Dialysis and Kupffer Cell Inhibition With Glycine, Liver Transpl. 25 (2019) 275–287.

[18] R.W. Farndale, D.J. Buttle, A.J. Barrett, Improved quantitation and discrimination of sulphated glycosaminoglycans by use of dimethylmethylene blue, Biochim. Biophys. Acta. 883 (1986) 173–177.

[19] L. Mancuso, A. Gualerzi, F. Boschetti, F. Loy, G. Cao, Decellularized ovine arteries as small-diameter vascular grafts, Biomed. Mater. 9 (2014) 045011.

[20] M. Olausson, P.B. Patil, V.K. Kuna, P. Chougule, N. Hernandez, K. Methe, C. Kullberg-Lindh, H. Borg, H. Ejnell, S. Sumitran-Holgersson, Transplantation of an allogeneic vein bioengineered with autologous stem cells: a proof-of-concept study, Lancet. 380 (2012) 230–237.

[21] D.M. Faulk, C.A. Carruthers, H.J. Warner, C.R. Kramer, J.E. Reing, L. Zhang, A. D'Amore, S.F. Badylak, The effect of detergents on the basement membrane complex of a biologic scaffold material, Acta Biomater. 10 (2014) 183–193.

[22] P.M. Crapo, T.W. Gilbert, S.F. Badylak, An overview of tissue and whole organ decellularization processes, Biomaterials. 32 (2011) 3233–3243.

[23] D.O. Freytes, S.F. Badylak, T.J. Webster, L.A. Geddes, A.E. Rundell, Biaxial strength of multilaminated extracellular matrix scaffolds, Biomaterials. 25 (2004) 2353–2361.

[24] A.M. Matuska, P.S. McFetridge, The effect of terminal sterilization on structural and biophysical properties of a decellularized collagen-based scaffold; implications for stem cell adhesion, J. Biomed. Mater. Res. B Appl. Biomater. 103 (2015) 397–406.

[25] G.P. Fadini, D. Losordo, S. Dimmeler, Critical reevaluation of endothelial progenitor cell phenotypes for therapeutic and diagnostic use, Circ. Res. 110 (2012) 624–637.

[26] B. Denecke, L.D. Horsch, S. Radtke, J.C. Fischer, P.A. Horn, B. Giebel, Human endothelial colony-forming cells expanded with an improved protocol are a useful endothelial cell source for scaffold-based tissue engineering, J. Tissue Eng. Regen. Med. 9 (2015) E84-97.

[27] J.M. Melero-Martin, M.E. De Obaldia, S.-Y. Kang, Z.A. Khan, L. Yuan, P. Oettgen, J. Bischoff, Engineering robust and functional vascular networks in vivo with human adult and cord blood-derived progenitor cells, Circ. Res. 103 (2008) 194–202.

[28] B. Joddar, S.A. Kumar, A. Kumar, A Contact-Based Method for Differentiation of Human Mesenchymal Stem Cells into an Endothelial Cell-Phenotype, Cell Biochem. Biophys. 76 (2018) 187–195.

[29] D. Reichert, J. Friedrichs, S. Ritter, T. Käubler, C. Werner, M. Bornhäuser, D. Corbeil, Phenotypic, Morphological and Adhesive Differences of Human Hematopoietic Progenitor Cells Cultured on Murine versus Human Mesenchymal Stromal Cells, Sci. Rep. 5 (2015) 15680.

[30] P. Zhou, Y. Guo, Y. Huang, M. Zhu, X. Fan, L. Wang, Y. Wang, S. Zhu, T. Xu, D. Wu, Y. Lu, Z. Wang, The dynamic three-dimensional culture of islet-like clusters in decellularized liver scaffolds, Cell Tissue Res. 365 (2016) 157–171.

[31] J.D. Stroncek, B.S. Grant, M.A. Brown, T.J. Povsic, G.A. Truskey, W.M. Reichert, Comparison of endothelial cell phenotypic markers of late-outgrowth endothelial progenitor cells isolated from patients with coronary artery disease and healthy volunteers, Tissue Eng. Part A. 15 (2009) 3473–3486.

9. Eidesstattliche Versicherung

„Ich, Nicolai Seiffert, versichere an Eides statt durch meine eigenhändige Unterschrift, dass ich die vorgelegte Dissertation mit dem Thema: ***Rebesiedlung von xenogenen Gefäßmatrizen als Modell-System für eine optimierte Reendothelialisierung von parenchymatösen Gewebekonstrukten*** selbstständig und ohne nicht offengelegte Hilfe Dritter verfasst und keine anderen als die angegebenen Quellen und Hilfsmittel genutzt habe.

Alle Stellen, die wörtlich oder dem Sinne nach auf Publikationen oder Vorträgen anderer Autoren/innen beruhen, sind als solche in korrekter Zitierung kenntlich gemacht. Die Abschnitte zu Methodik (insbesondere praktische Arbeiten, Laborbestimmungen, statistische Aufarbeitung) und Resultaten (insbesondere Abbildungen, Graphiken und Tabellen) werden von mir verantwortet.

Ich versichere ferner, dass ich die in Zusammenarbeit mit anderen Personen generierten Daten, Datenauswertungen und Schlussfolgerungen korrekt gekennzeichnet und meinen eigenen Beitrag sowie die Beiträge anderer Personen korrekt kenntlich gemacht habe (siehe Anteilserklärung). Texte oder Textteile, die gemeinsam mit anderen erstellt oder verwendet wurden, habe ich korrekt kenntlich gemacht.

Meine Anteile an etwaigen Publikationen zu dieser Dissertation entsprechen denen, die in der untenstehenden gemeinsamen Erklärung mit dem/der Erstbetreuer/in, angegeben sind. Für sämtliche im Rahmen der Dissertation entstandenen Publikationen wurden die Richtlinien des ICMJE (International Committee of Medical Journal Editors; www.icmje.og) zur Autorenschaft eingehalten. Ich erkläre ferner, dass ich mich zur Einhaltung der Satzung der Charité – Universitätsmedizin Berlin zur Sicherung Guter Wissenschaftlicher Praxis verpflichte.

Weiterhin versichere ich, dass ich diese Dissertation weder in gleicher noch in ähnlicher Form bereits an einer anderen Fakultät eingereicht habe.

Die Bedeutung dieser eidesstattlichen Versicherung und die strafrechtlichen Folgen einer unwahren eidesstattlichen Versicherung (§§156, 161 des Strafgesetzbuches) sind mir bekannt und bewusst."

_____

Datum   Unterschrift

10. Anteilserklärung an den erfolgten Publikationen

Nicolai Seiffert hatte folgenden Anteil an den folgenden Publikationen:

Publikation 1: Seiffert N, Tang P, Keshi E, Reutzel-Selke A, Moosburner S, Everwien H, Wulsten D, Napierala H, Pratschke J, Sauer IM, Hillebrandt KH, Struecker B**. [In vitro recellularization of decellularized bovine carotid arteries using human endothelial colony forming cells]**, Journal of Biological Engineering, 2021.

Beitrag im Einzelnen:
Ich half bei der Planung der Studie und beschaffte alle notwendigen Ausgangsmaterialien inklusive boviner Karotiden und Patientenblutproben. Ich führte die beschriebenen Versuche, zum Teil mit Hilfe der Ko-Autoren, durch, analysierte die Ergebnisse der Versuche und erstellte die hierauf-basierenden Abbildungen 2-6 und Tabellen 1-2. Ich schrieb das Manuskript der Veröffentlichung, antwortete auf die Fragen der Reviewer, erarbeitete die Revisionen und reichte die notwendigen Folgeunterlagen ein. Bis zur Veröffentlichung führte ich die Korrespondenz mit den Editoren.

Publikation 2: Napierala H, Hillebrandt KH, Haep N, Tang P, Tintemann M, Gassner JMGV, Noesser M, Everwien H, **Seiffert N**, Kluge M, Teegen E, Polenz D, Lippert S, Geisel D, Reutzel-Selke A, Raschzok N, Andreou A, Pratschke J, Sauer IM, Struecker B. **Engineering an endocrine Neo-Pancreas by repopulation of a decellularized rat pancreas with islets of Langerhans**, Scientific Reports, 2017.

Beitrag im Einzelnen:
Ich half bei der Analyse der Experimente inklusiver histologischer Untersuchungen, die zur Erstellung der Abbildung 3 geführt haben. Ich diskutierte die Ergebnisse kritisch mit den weiteren Autoren und las das Manuskript der Veröffentlichung Korrektur.

Publikation 3: Everwien H, Keshi E, Hillebrandt KH, Ludwig B, Weinhart M, Tang P, Beierle AS, Napierala H, Gassner JMGV, **Seiffert N,** Moosburner S, Geisel D, Reutzel-Selke A, Struecker B, Pratschke J, Haep N, Sauer IM. **[Engineering an endothelialized, endocrine Neo-Pancreas: Evaluation of islet functionality in an ex vivo model],** Acta Biomaterialia, 2020.

Beitrag im Einzelnen:
Ich etablierte die Zellkultur von Endothel- und endothelialen Vorläuferzellen sowie spezifische Anfärbemethoden in der Arbeitsgruppe, die zur Erstellung von Abbildung 6 beigetragen haben. Weiterhin half ich bei der Isolierung und Kultivierung von MSC sowie der Etablierung des Ko-Seedings von Endothelzellen mit MSC mit spezifischem Medium-Mix, die als Grundlag der Abbildungen 7 und 8 dienten. Ich half bei der Durchführung der Perfusionsversuche, diskutierte die Ergebnisse kritisch mit den weiteren Autoren und las das Manuskript der Veröffentlichung Korrektur.

_____
Unterschrift, Datum und Stempel des erstbetreuenden Hochschullehrers

_____
Unterschrift des Doktoranden

11. Ausgewählte Publikationen

N. Seiffert, P. Tang, E. Keshi, A. Reutzel-Selke, S. Moosburner, H. Everwien, D. Wulsten, H. Napierala, J. Pratschke, I.M. Sauer, K.H. Hillebrandt, B. Struecker, **In vitro recellularization of decellularized bovine carotid arteries using human endothelial colony forming cells**, J. Biol. Eng. 15 (2021) 15.
DOI: http://dx.doi.org/10.1186/s13036-021-00266-5
PubMed PMID: 33882982
Impact Factor: 4,355 im Jahr 2020

H. Napierala, K.-H. Hillebrandt, N. Haep, P. Tang, M. Tintemann, J. Gassner, M. Noesser, H. Everwien, N. Seiffert, M. Kluge, E. Teegen, D. Polenz, S. Lippert, D. Geisel, A. Reutzel Selke, N. Raschzok, A. Andreou, J. Pratschke, I.M. Sauer, B. Struecker, **Engineering an endocrine Neo-Pancreas by repopulation of a decellularized rat pancreas with islets of Langerhans**, Sci. Rep. 7 (2017) 41777
DOI: http://dx.doi.org/10.1038/srep41777
PubMed PMID: 28150744
Impact Factor: 4,379 im Jahr 2020

H. Everwien, E. Keshi, K.H. Hillebrandt, B. Ludwig, M. Weinhart, P. Tang, A.S. Beierle, H. Napierala, J.M. Gassner, N. Seiffert, S. Moosburner, D. Geisel, A. Reutzel-Selke, B. Strücker, J. Pratschke, N. Haep, I.M. Sauer, **Engineering an endothelialized, endocrine Neo-Pancreas: Evaluation of islet functionality in an ex vivo model**, Acta Biomater. 117 (2020) 213–225.
DOI: http://dx.doi.org/10.1016/j.actbio.2020.09.022
PubMed PMID: 32949822
Impact Factor: 8,947 im Jahr 2020

N. Seiffert, P. Tang, E. Keshi, A. Reutzel-Selke, S. Moosburner, H. Everwien, D. Wulsten, H. Napierala, J. Pratschke, I.M. Sauer, K.H. Hillebrandt, B. Struecker, **In vitro recellularization of decellularized bovine carotid arteries using human endothelial colony forming cells**, J. Biol. Eng. 15 (2021) 15.
DOI: http://dx.doi.org/10.1186/s13036-021-00266-5
PubMed PMID: 33882982
Impact Factor: 4,355 im Jahr 2020

ibe
Advancing Biology-Inspired Engineering
Official publication of the Institute of Biological Engineering

RESEARCH   **Open Access**

In vitro recellularization of decellularized bovine carotid arteries using human endothelial colony forming cells

Nicolai Seiffert[1,2], Peter Tang[1], Eriselda Keshi[1], Anja Reutzel-Selke[1], Simon Moosburner[1], Hannah Everwien[1,3], Dag Wulsten[3,4], Hendrik Napierala[1], Johann Pratschke[1], Igor M. Sauer[1*] , Karl H. Hillebrandt[1,5†] and Benjamin Struecker[5,6†]

Abstract

Background: Many patients suffering from peripheral arterial disease (PAD) are dependent on bypass surgery. However, in some patients no suitable replacements (i.e. autologous or prosthetic bypass grafts) are available. Advances have been made to develop autologous tissue engineered vascular grafts (TEVG) using endothelial colony forming cells (ECFC) obtained by peripheral blood draw in large animal trials. Clinical translation of this technique, however, still requires additional data for usability of isolated ECFC from high cardiovascular risk patients. Bovine carotid arteries (BCA) were decellularized using a combined SDS (sodium dodecyl sulfate) -free mechanical-osmotic-enzymatic-detergent approach to show the feasibility of xenogenous vessel decellularization. Decellularized BCA chips were seeded with human ECFC, isolated from a high cardiovascular risk patient group, suffering from diabetes, hypertension and/or chronic renal failure. ECFC were cultured alone or in coculture with rat or human mesenchymal stromal cells (rMSC/hMSC). Decellularized BCA chips were evaluated for biochemical, histological and mechanical properties. Successful isolation of ECFC and recellularization capabilities were analyzed by histology.

Results: Decellularized BCA showed retained extracellular matrix (ECM) composition and mechanical properties upon cell removal. Isolation of ECFC from the intended target group was successfully performed (80% isolation efficiency). Isolated cells showed a typical ECFC-phenotype. Upon recellularization, co-seeding of patient-isolated ECFC with rMSC/hMSC and further incubation was successful for 14 ($n = 9$) and 23 ($n = 5$) days. Reendothelialization (rMSC) and partial reendothelialization (hMSC) was achieved. Seeded cells were CD31 and vWF positive, however, human cells were detectable for up to 14 days in xenogenic cell-culture only. Seeding of ECFC without rMSC was not successful.

(Continued on next page)

* Correspondence: igor.sauer@charite.de
†Karl H. Hillebrandt and Benjamin Struecker contributed equally to this work.
[1]Charité – Universitätsmedizin Berlin, corporate member of Freie Universität Berlin and Humboldt- Universität zu Berlin, Department of Surgery, Campus Charité Mitte | Campus Virchow-Klinikum, Augustenburger Platz 1, 13353 Berlin, Germany
Full list of author information is available at the end of the article

BMC

(Continued from previous page)

Conclusion: Using our refined decellularization process we generated easily obtainable TEVG with retained ECM- and mechanical quality, serving as a platform to develop small-diameter (< 6 mm) TEVG. ECFC isolation from the cardiovascular risk target group is possible and sufficient. Survival of diabetic ECFC appears to be highly dependent on perivascular support by rMSC/hMSC under static conditions. ECFC survival was limited to 14 days post seeding.

Keywords: Endothelial Colony forming cells (ECFC), Mesenchymal stromal cells (MSC), Tissue engineering, Bovine carotid artery, Decellularization, Recellularization, Target group specific cells / sick cells, Impaired cell function

Background

Cardiovascular diseases continue to be the leading cause of death in the United States [1]. Peripheral artery disease (PAD), especially in its advanced form critical limb ischemia (CLI), remains a major cause of vascular-related morbidity and mortality [2] while being a burden clinically and economically to western world healthcare systems [3, 4]. Bypass surgery is one of the most commonly applied surgical treatment of PAD today [5, 6], with patient-derived grafts remaining the gold standard to bypass constricted areas. Unfortunately, up to 30% of patients suffering from PAD are unable to provide suitable autologous vessel grafts [7, 8]. Synthetic prosthetic grafts may be used as an alternative for large diameter arteries (> 6 mm), however, mechanical mismatch, adverse host response, reduced patency rates and increased susceptibility to infections have impeded clinical applicability, especially for medium or small diameter arteries (inner diameter $\leq$ 6 mm) [8–12]. To address these problems and create viable alternatives, tissue engineered vascular grafts (TEVG) have been developed using self-assembly and biodegradable scaffold techniques of both synthetic and natural origin [13]. While the results seem promising and are pursued up to clinical trials, no widespread clinical application has been established so far [13, 14].

Promising, in this context, is the technique of decellularization, whereby all cellular material is removed and the extracellular matrix (ECM) is preserved with favorable mechanical and biochemical properties [13–18]. Decellularized constructs are seen as interesting platforms [19] for cellular repopulation and have been tolerated in xenogeneic applications [20]. Resulting acellular vascular scaffolds from bovine origin have been commercialized and are available for off-the-shelf purchase as alternatives to expanded polytetrafluoroethylene (ePTFE) prostheses for both hemodialysis access and treatment of CLI in cases of infected implantation sites [21, 22]. After cell removal, however, functional endothelium is absent and the underlying vascular ECM is exposed to blood which may cause both early and late graft failure by thrombosis and intimal hyperplasia [23]. As a prevention, reendothelialization should be pursued to mask thrombocyte-activating ECM and to control smooth muscle cell (SMC) proliferation and contractility [24].

Although recellularized grafts using endothelial cells (EC) have shown improved patency (89% seeded vs. 29% acellular) [25] and remodeling capacity [20, 26], the isolation of EC is associated with invasive procedures causing donor site complications, providing a low cell yield and may not be feasible for cell isolation due to vessel quality or availability [27, 28]. Endothelial colony forming cells (ECFC) may be isolated by peripheral blood draw and have successfully been expanded to large-scale in vitro experiments [29–31]. Additionally, ECFC seem not only to be able to cover exposed subendothelial ECM but may actually be of a superior thrombo-protective and intimal hyperplasia limiting phenotype when exposed to shear stress [32, 33]. Moreover, to support and stabilize ECFC the importance of co-culture with mesenchymal stromal cells (MSC) has been emphasized [29, 34]. Also, MSC have shown to be of immuno-modulatory characteristic and used successfully in xenogenic application [35–37].

ECFC have been in the focus of research for years [38]. In most cases umbilical cord blood-derived ECFC and ECFC isolated from young and healthy donors have been used, although an altered function of adult peripheral ECFC has been reported [39]. Additionally, mounting evidence suggests altered function and proliferation rate of ECFC from aging patients with high cardiovascular risk, including diabetes, hypertension and chronic renal disease [40–42]. Scaffold-reendothelialization using patient-derived ECFC has only been researched to cover synthetic vascular scaffolds so far [43–45]. To our knowledge, the suitability of endothelial colony forming cells sourced by peripheral blood draw from cardiovascular risk patients, the intended clinical target group, for reendothelialization of decellularized vascular scaffolds, has not yet been explored. Therefore, this study focused on isolation, expansion and usage of patient-derived ECFC for recellularization purposes while comparing seeding efficiency of ECFC-mono- with ECFC-rMSC and ECFC-hMSC-coculture approaches on decellularized BCA-chips. Healthy rMSC were used due to easy availability and reported low immunogenicity [37]. Furthermore, a refined decellularization strategy was explored.
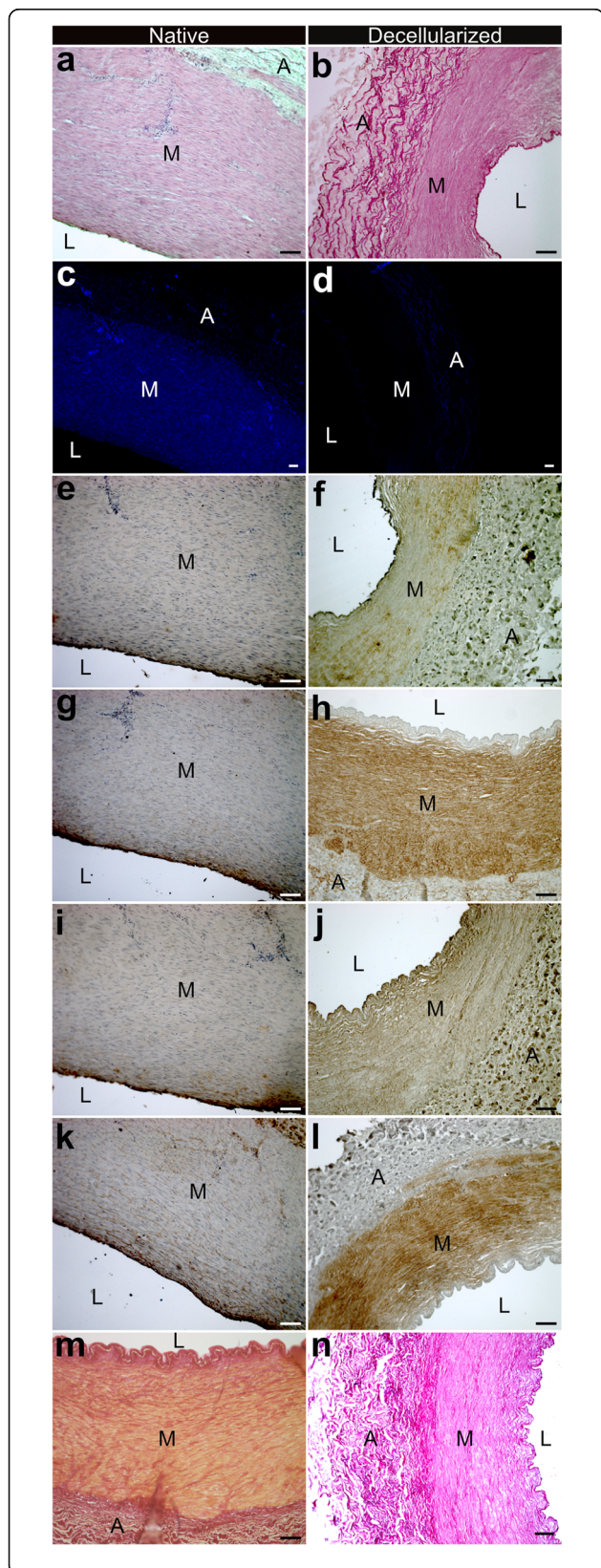
Fig. 1 Native bovine carotid arteries (BCA, **a, c, e, g, i, k, m**) were compared to decellularized BCA (**b, d, f, h, j, l, n**). Following decellularization, complete removal of nuclei (**b, d**) was observed in H/E- (**a, b**) and DAPI (**c**, d) staining. Further histochemical characterization of ECM for collagen I (**e, f**), collagen IV (**g, h**), fibronectin (**i, j**), laminin (**k, l**) and Picrosirius red (**m, n**) showed successful retention of abundant ECM components. L, M and A indicate lumen, media and adventitia, respectively. Scale bar represents 100 μm

Results

Successful decellularization of bovine carotid arterial grafts

Histological evaluation of decellularized matrices showed complete removal of cellular material throughout the entire vessel wall in H&E- and DAPI-Staining. While typical arterial wall architecture remained intact, a thinner *tunica media* and *tunica adventitia* configuration was observed in decellularized samples (Fig. 1a-d). Immunohistochemical stainings for laminin, fibronectin, collagen-I and collagen-IV in addition to conventional picrosirius red staining were performed to characterize decellularized extracellular matrix and compared to native controls. Microscopic evaluation of ECM showed no loss of abundant ECM components in respective areas of typical appearance, however, the compressed configuration following cell removal resulted in an intensified appearance of ECM-elements, especially in the area of the *tunica media* (Fig. 1e-l). Picrosirius red staining showed collagen retention after decellularization with removal of cytoplasm (yellow, Fig. 1m, n).

Biochemical analysis of decellularized matrices

To evaluate content of sulfated glycosaminoglycans (sGAG) during decellularization process, sGAG content was measured in native tissue, after osmotic treatment and after multi-cyclic detergent-enzymatic treatment for up to five cycles (Fig. 2a). An increase of sGAG content was observed during decellularization, reaching a peak after three cycles of detergent-enzymatic treatment at 7.87 median (IQR 0.43) μg/mg dry weight. This was statistically significant ($p = 0.007$) when compared to native specimens (4.93 IQR 1.61 μg/mg dry weight, Fig. 2a). Further incubation with detergent-enzymatic treatment resulted in reduced sGAG content that reached significance after five consecutive cycles (4.15 IQR 0.90 μg/mg dry weight) when compared to maximum sGAG content after three detergent-enzymatic cycles ($p = 0.0013$, Fig. 2a). Therefore, standard decellularization treatment (SDT) was limited to detergent-enzymatic exposure for three consecutive cycles to prevent sGAG loss. To show effective decellularization, DNA content was measured after SDT and compared to native specimens. DNA content declined significantly during decellularization from 2157.00 (IQR 709.00) ng/mg
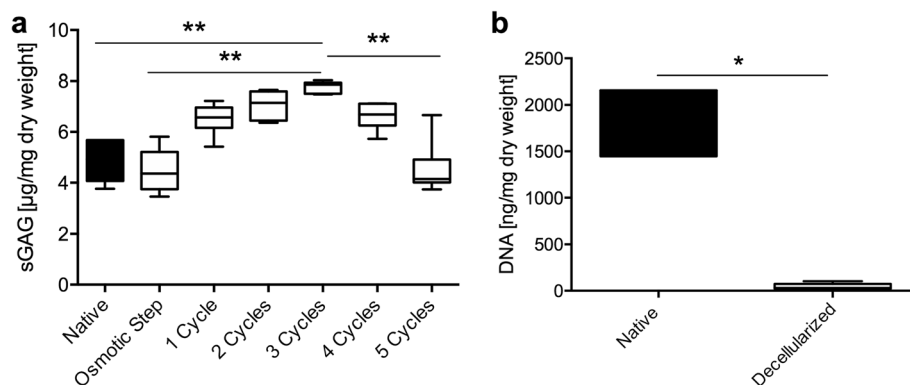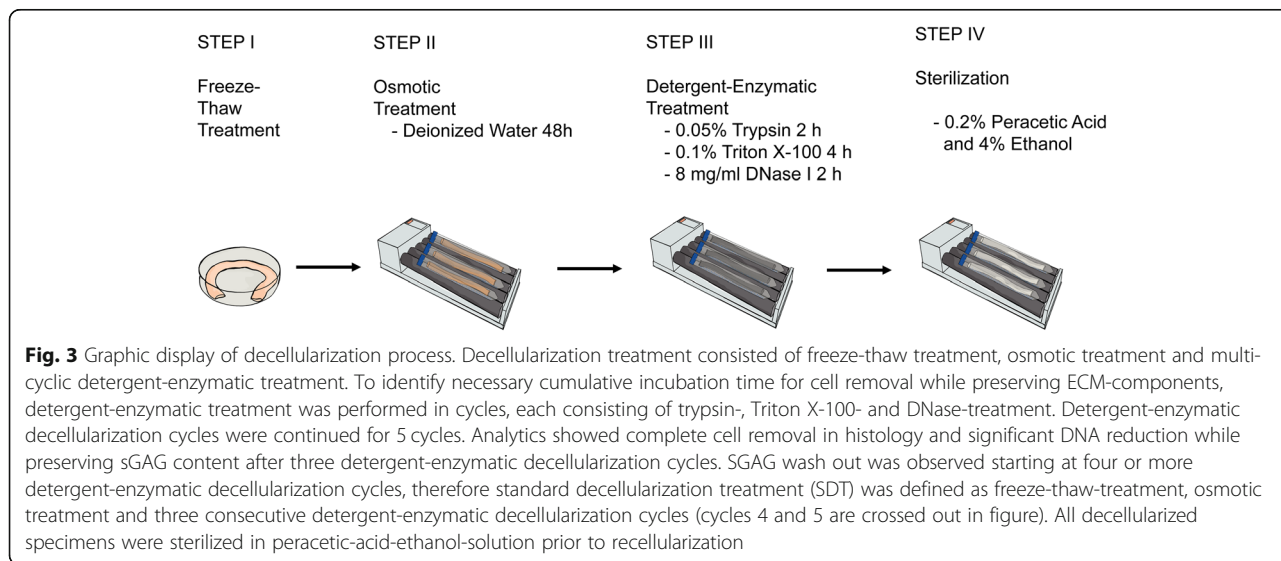
Fig. 2 a The content of sulfated glycosaminoglycans (sGAG) per dry weight increased statistically significant following decellularization treatment after three consecutive detergent-enzymatic treatment cycles. Further incubation for four or five treatment cycles resulted in reduced sGAG content, which reached significance after five cycles. **b** DNA amount was reduced significantly after complete standard decellularization treatment (SDT) compared to native controls. * $p < 0.05$, ** $p < 0.01$

dry weight in native BCAs to 30.00 (IQR 51.83) ng/mg dry weight after SDT (Fig. 2b).

Mechanical properties of decellularized matrices

To assess mechanical properties altered through the process of decellularization, native specimens ($n = 12$) were compared to samples acquired after freeze-thaw treatment ($n = 8$), SDT ($n = 8$), sterilization ($n = 8$) and SDT without Freeze-Thaw-Treatment ($n = 9$). The time point 'sterilization' represents the final vascular graft to be used for recellularization. SDT without Freeze-Thaw-Treatment is shown only for informatory purposes but was neither sterilized nor used for graft generation. Figure 3 better illustrates the decellularization and sterilization process. All samples were analyzed with regard to Young's Modulus E during low (E ela, Fig. 4a) and high strain (E col., Fig. 4b), point of transition from E ela to E col. in regard to stress (Trans stress, Fig. 4c) and strain (Trans strain, Fig. 4d), maximum tolerated stress (Max stress, Fig. 4e) and strain (Max strain, Fig. 4f) and stress (UTC, Fig. 4g) and strain tolerated before rupture (Failure strain, Fig. 4h). Completely decellularized and sterilized samples showed comparable results to native controls by maintaining roughly 91% of initial stress resilience with regards to Max stress (native 1.23 IQR 0.44 MPa, sterilization 1.11 IQR 0.37 MPa, $p > 1$). Similar results were also observed for E col. (native 2.77 IQR 0.76 MPa, sterilization 3.05 IQR 1.61 MPa, p > 1), UTS (native 1.06 IQR 0.34 MPa, sterilization 0.96 IQR 0.24 N, $p > 1$) and Trans stress (native 0.37 IQR 0.16 MPa, sterilization 0.40 IQR 0.13 MPa, $p > 1$). Further characterization of mechanical behavior of samples acquired throughout the decellularization process revealed differing results. A limited decline of Max stress resilience was recorded after freeze-thaw treatment (1.09 IQR 0.13 MPa, 89% initial stress resilience) which reached statistical

significance ($p = 0.04$) after SDT (Max stress 0.80 IQR 0.32 MPa, 65% initial stress resilience). Likewise, a decline of E col. could be seen in samples after freeze-thaw treatment and SDT (Freeze-Thaw-Cycle 2.14 IQR 0.73 MPa, SDT 1.43 IQR 0.94 MPa) which was followed by a statistically significant increase ($p = 0.04$) after sterilization (3.05 IQR 1.61 MPa) compared to SDT but comparable to native specimens. Max strain (native 0.85 IQR 0.37, sterilization 0.53 IQR 0.24 $p < 0.01$), Failure strain (native 1.00 IQR 0.27, sterilization 0.42 IQR 0.27 $p = 0.01$) and Trans strain (native 0.52 IQR 0.25, sterilization 0.22 IQR 0.23 $p = 0.03$) was reduced up to statistical significance after sterilization but showed no statistically relevant abbreviation to native controls for all other timepoints during graft generation for Max strain (Freeze-Thaw-Cycle 0.89 IQR 0.31, SDT 0.74 IQR 0.22), Failure strain (Freeze-Thaw-Cycle 0.71 IQR 0.20, SDT 0.70 IQR 0.21) and Trans strain (Freeze-Thaw-Cycle 0.43 IQR 0.14, SDT 0.37 IQR 0.18). While a reduction of UTS was observed for all groups (Freeze-Thaw-Cycle 0.96 IQR 0.29, SDT 0.73 IQR 0.28), it did not reach statistical significance. Trans stress did not show any statistically significant changes throughout graft generation process (Trans stress 0.30 IQR 0.19 MPa). E ela, however, showed an increase during graft generation that reached statistical significance after sterilization (native 0.31 IQR 0.34 MPa, Freeze-Thaw-Cycle 0.48 IQR 0.49 MPa, SDT 0.54 IQR 0.52 MPa, sterilization 1.28 IQR 0.75 MPa $p = 0.008$). SDT without Freeze-Thaw-Cycle showed significantly altered mechanical test results compared to sterilization (E ela 0.21 IQR 0.17 MPa, $p < 0.001$, Trans stress 0.23 IQR 0.02 MPa, $p = 0.016$), SDT (E col. 3.12 IQR 0.40 MPa, $p = 0.004$) and Freeze-Thaw-Cycle (Trans stress 0.41 IQR 0.18 MPa, $p = 0.049$) while alle other measurements remained comparable (UTS 1.00 IQR 0.27 MPa, Failure strain 0.67 IQR 0.15, Trans strain 0.35 IQR 0.13, Max stress 1.09 IQR

Fig. 3 Graphic display of decellularization process. Decellularization treatment consisted of freeze-thaw treatment, osmotic treatment and multi-cyclic detergent-enzymatic treatment. To identify necessary cumulative incubation time for cell removal while preserving ECM-components, detergent-enzymatic treatment was performed in cycles, each consisting of trypsin-, Triton X-100- and DNase-treatment. Detergent-enzymatic decellularization cycles were continued for 5 cycles. Analytics showed complete cell removal in histology and significant DNA reduction while preserving sGAG content after three detergent-enzymatic decellularization cycles. SGAG wash out was observed starting at four or more detergent-enzymatic decellularization cycles, therefore standard decellularization treatment (SDT) was defined as freeze-thaw-treatment, osmotic treatment and three consecutive detergent-enzymatic decellularization cycles (cycles 4 and 5 are crossed out in figure). All decellularized specimens were sterilized in peracetic-acid-ethanol-solution prior to recellularization

0.26 MPa, Max strain 0.68 IQR 0.12). Complete data is available as a supplemental file.

Patient characteristics
In total, ECFC were isolated from 10 patients in this study (Table 1). The patients were equally male (50%) and female (50%), and the median age of patients at the time of ECFC-isolation was 62 years. All patients underwent surgery prior to ECFC-isolation. Oncological, general and endocrinological surgery was performed in 40, 40 and 20% of the patients, respectively. Most common

comorbidities were arterial hypertension (80%), renal failure (40%) and diabetes (30%). None of the patients were active smokers.

Isolation of endothelial colony forming cells
Cell-Isolation via peripheral blood draw from hospitalized patients was successful in 8 of 10 patients. Cell culture contamination led to the exclusion of two cell-isolations, leaving a total of 8 cell-isolations used for further experiments. All included patients were suffering from either diabetes, hypertension, chronic renal failure

Fig. 4 Mechanical properties of specimens during decellularization and sterilization process were determined and a moderate reduction of Young's Modulus E col. (**b**), Max Stress (**e**) and UTS (**g**) was observed following freeze-thaw-cycle (*n* = 8) and standard decellularization treatment (SDT, *n* = 8) when compared to native controls (*n* = 12). Statistical significance was reached in the sterilization group with regards to Young's Modulus E ela (**a**), Max Strain (**f**), Failure Strain (**h**) and Trans Strain (**d**). Final decellularized and sterilized BCAs (sterilization, *n* = 8) showed comparable results to native controls in regard to Youngs-Modulus E col. (**b**), Max Stress (**e**), UTS (**g**) and Trans Stress (**c**). SDT without freeze-thaw treatment (SDT w/o Freeze-Thaw-Cycle, *n* = 8) is shown for informatory purposes only but was not used to generate specimens intended for recellularization

Table 1 Characteristics of donors of endothelial colony forming cells

Characteristics	N = 10
Male sex, %	50
Median age at isolation (range), years	62 (41–83)
Non-Smoking, %	100
Post-surgical, %	100
Co-morbidities, %	
Arterial hypertonia	80
Diabetes	30
Renal failure	40
Coronary heart disease	10
Admission by surgical departments, %	
Oncological surgery	40
General surgery	40
Endocrinological surgery	20

or a combination thereof (Table 1). Cell cultures were screened daily until cobblestone-like colonies emerged at a mean of 10-12d (Fig. 5). Rapid doubling times followed colony appearance. Acetylated low-density lipoprotein (acLDL) uptake was observed in ECFC cultures incubated with DiI-acLDL by means of colocalization of DAPI- and surrounding DiI-signal (Fig. 5b). Immunofluorescence staining for CD31 (Fig. 5c) and vWF (Fig. 5d) was performed on CytoSpin specimens. Due to the manner of CytoSpin-preparation, no results in regard to cell-cell interaction or cell-colony formation could be obtained. Cells generally appeared dense and layered and stained positive on cell surface area for CD31 or within vesicle-like structures consistent with Weibel-Palade-Bodies for vWF.

Seeding of hECFC on ECM-chips

Decellularized ECM-chips were seeded with human endothelial colony forming cells (hECFC). Recellularized ECM-chips were examined for cell growth using brightfield and fluorescence microscopy. DAPI- and H/E-staining of ECM-chips recellularized with hECFC in monoculture for 12 days showed limited to no seeding efficiency. Solitary cells or cell residue on luminal ECM-chip-side could be found in only one of nine recellularized samples (*n* = 9) in H&E staining (Fig. 6a). We were unable to confirm any cell nuclei in DAPI-staining (Fig. 6b).
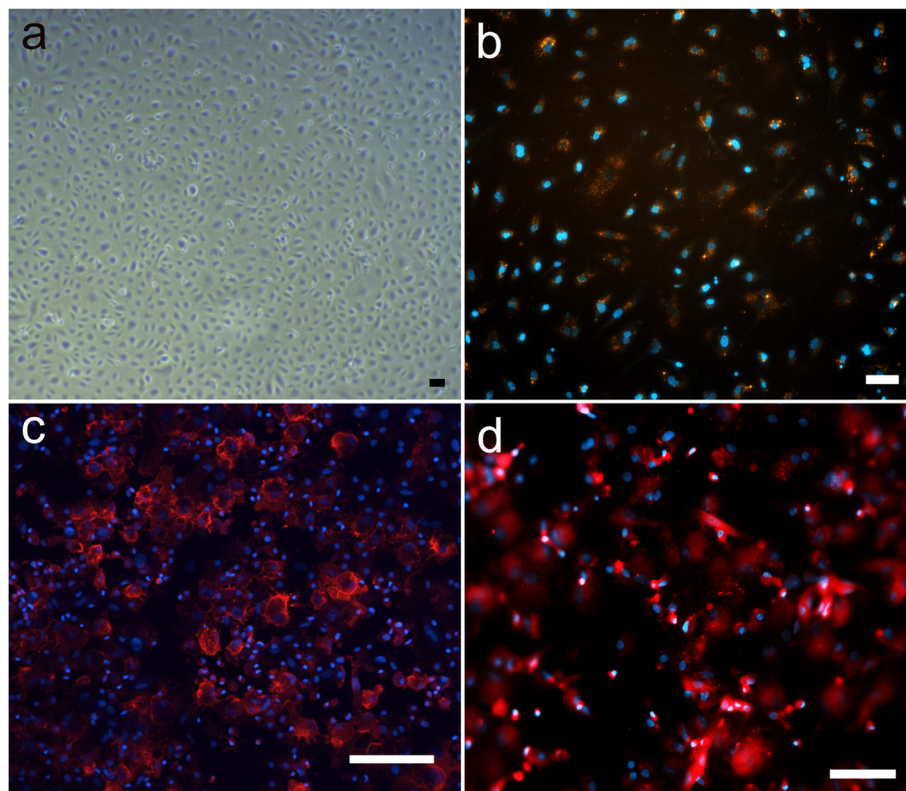
Fig. 5 Inverted brightfield and immunofluorescence microscopy of endothelial colony forming cells (ECFC). Inverted brightfield microscopy showed cobblestone-like appearance (**a**). Fluorescent microscopic images of ECFC show nuclei in blue (DAPI; **b,c,d**) in colocalization with DiI-acLDL (orange, **b**), CD31 (red, **c**) and von Willebrand factor (red, **d**). Scale bars represent 100 μm (**b,c,d**) or 200 μm (**a**) respectively
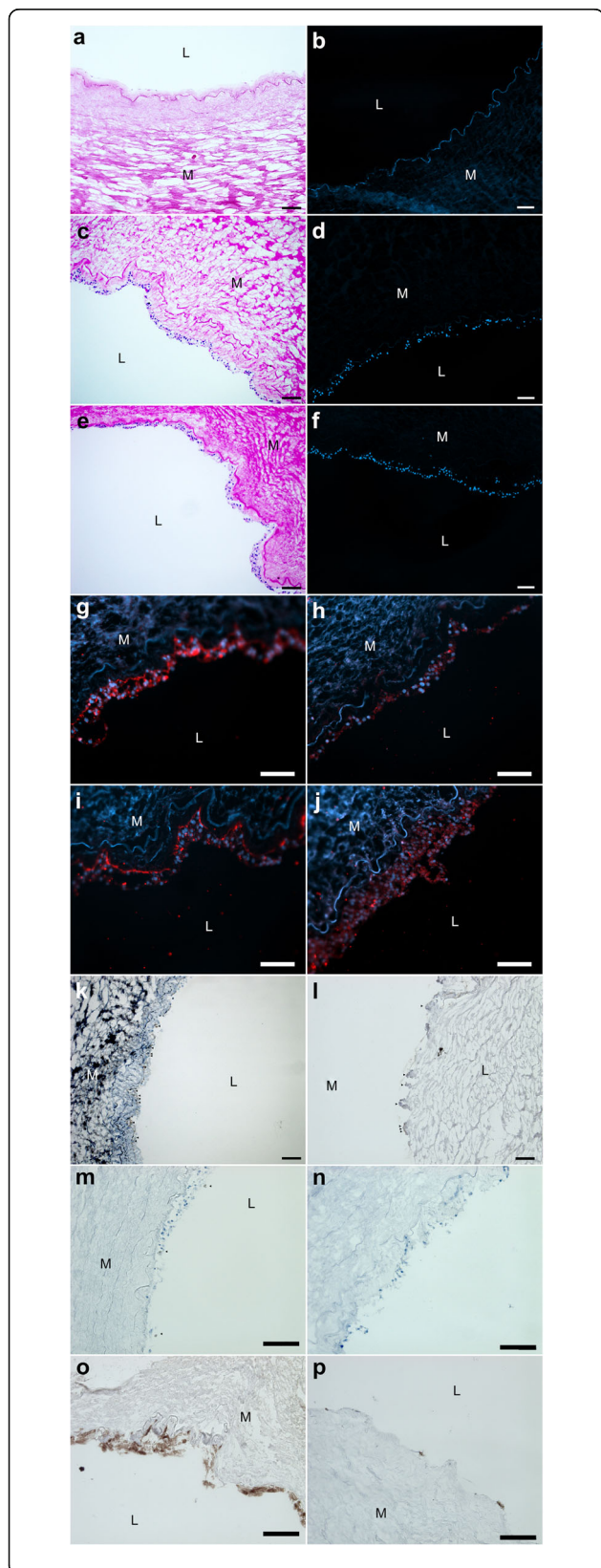
Fig. 6 Inverted brightfield and immunofluorescence microscopy of recellularized extracellular matrix (ECM) chips. ECM-chips were seeded with endothelialcolony forming cells (ECFC) in monoculture (**a**, **b**) or in coculture with rat (rMSC, **c-k**, **m**, **n**) or human mesenchymal stromal cells (hMSC, l, **o**, **p**) andincubated for 14 (**a-d**, **g**, **h**, **m**) or 23 days (**e**, **f**, **i**, **j**, **k**, **l**, **n-p**). H&E (**a**, **c**, **e**), DAPI (**b**, **d**, **f**), vWF (**g**, **i**) and CD31 (**h**, **j**, **o**) staining revealed confluent cellattachment on luminal ECM-chip side. A trend towards layered cell growth was observed in samples incubated for 23 days (**e**, **f**, **i**, **j**). CD90 (**k**, **l**, arrows),HNA (**m**, **n**, **p**) staining was observed. Scale bar represents 100 μm

Seeding of co-cultured hECFC with rMSC on ECM-chips

Easily available rat mesenchymal stromal cells (rMSC) were used for co-culture applications. Matrices seeded with hECFC in co-culture with rMSC showed confluent cell attachment to luminal ECM-chips on all recellularized samples. Cell growth remained exclusively along the luminal chip side and no infiltration of cells into the tunica media or adventitia was observed. This was true for both 14d ($n = 8$, Fig. 6c-d) and 23d ($n = 5$, Fig. 6e-f) culture periods. Longer incubation times favored layered cell growth, as this was observed in samples incubated for 23 days more frequently and more distinctly than after 14 days of culture. Cell nuclei appeared rounded in both H&E- and DAPI-staining for all co-culture approaches. To define the cell origin of seeded cells, immunofluorescence staining was performed for CD31 and vWF as well as CD90 and HNA. Impressive colocalized signal of both CD31 and vWF in regard to DAPI-Signal was observed in confluent cell layers (Fig. 6g-j). The positive immunofluorescent signal appeared in the respective cell areas. Notably, subendothelial vWF-signal, consistent with the typical endothelial cell vWF-storage location, was observed in both culture periods. Furthermore, vWF-Signal was intensified after 23 days of culture (Fig. 6g,i). Scattered CD90-positive staining showed presence of MSC after 23 days for co-culture with rat or human MSC (Fig. 6k [rat], Fig. 6m [human], arrows) while negative control showed no positive signal (Suppl.). However, HNA staining indicated that most of CD 31 and VWF-positive cells originated from rMSC. Only a few HNA positive cells could be found after 14 (Fig. 6m) and none after 23 days (Fig. 6n) of culture.

Seeding of co-cultured hECFC with hMSC on ECM-chips

Human mesenchymal stromal cells (hMSC) were also used for co-culture applications. Matrices seeded with hECFC in co-culture with hMSC showed partially confluent cell attachment to luminal ECM-chips after 23 days of culture (Fig. 6l). Immunohistological staining was performed for CD31 (Fig. 6o) and CD90 (Fig. 6l). Again, CD31 positive staining was observed. CD90-positive staining showed presence of hMSC after 23 days

(Fig. 6l). Few HNA positive cells were found after 23 days of culture (Fig. 6p).

Discussion

In this study we evaluate the capability of ECFC acquired through peripheral blood draw from hospitalized patients to reendothelialize decellularized BCA chips when applied in co-culture with rMSC and hMSC. The results may help to better estimate seeding capabilities of ECFC derived from the intended target group for reendothelialization.

Opposite to autologous vessels, TEVG are not a scarce material and could be implanted at an early disease stage. Ideally, artificial surface reaction through current non-biological devices could be avoided and, as a result, TEVG would be implanted in tissue with fewer inflammatory alterations. Constructive remodeling [46] and further improved patency rates could be obtained by this strategy. In order to acquire readily available and therefore transplantable scaffolds for recellularization, discarded BCAs were decellularized using a combination of decellularization techniques for gentle yet effective cell removal. To prevent inferior mechanical properties [47] and reduced recellularization capabilities through known drastic ECM-modification [48] by sodium dodecyl sulphate (SDS), the main reasons for both early and late graft failure, we modified the clinically successfully applied SDS-free protocol by Olausson et al. [49] Also, a SDS-free approach might evade removal and alteration of base membrane proteins and both less confluent and atypical cell growth [50]. Cell lysis was therefore initiated through a freeze-thaw cycle and incubation with deionized water [51]. Further cell lysis and cell debris removal was obtained by a combination of incubation with trypsin, Triton X-100 and DNase. While non-ionic detergent Triton X-100 is known to affect sGAG modification mildly [50] and was used in lower concentrations than comparable protocols [49, 50], sGAG content was significantly reduced after five detergent-enzymatic treatment cycles. Successful decellularization through sufficient DNA reduction to < 50 ng/mg dry weight and absence of cell nuclei in respective histology [51] was achieved after three detergent-enzymatic cycles, a prerequisite to avoid chronic inflammation and allow constructive remodeling when using scaffolds of xenogenic origin [52]. We limited the exposure of specimens accordingly.

Evaluating mechanical properties at defined time points we saw varying mechanical properties throughout our proposed decellularization protocol. An expected but statistically insignificant decline of strength retention and Youngs Modulus E col. following freeze-thaw treatment may be explained by minor ECM disruption of mainly collagen fibers [51]. A preservation of mechanical properties at statistically significant lower values following SDT but mostly comparable results to native controls following additional peracetic acid (PAA) sterilization process was observed. PAA sterilization has been linked with altered mechanical properties due to oxygen free radical reactivity and crosslinking leading to both tissue specific biaxial strength increase (submucosa) and decrease (bladder) [53, 54] but was used as PAA treated ECM showed unaltered or improved reseeding capabilities [55, 56] before. Considering preservation of key mechanical components and sGAG content as well as no detectable cell growth beyond the luminal graft side indicating retained ECM characteristics., the proposed decellularization and sterilization process seems to be favorable. In summary the decellularized and sterilized graft, suitable for recellularization, closely mimics native mechanical characteristics while altered mechanical characteristics may be observed during the decellularization process.

While using ECFC obtained from healthy individuals for recellularization approaches has become common practice and is performed successfully, it does not address the goal to develop autologous treatment options for the intended high-risk cardiovascular target group sufficiently. Krawiec et al. [35] were the first to identify and use adipose-derived stromal cells obtained from a cardiovascular risk group as a potential cell source for TEVG generation while expressing the need to evaluate additional cell groups used for tissue engineering. Altered function and reduced ECFC numbers have not only been observed in aging patients, but also in patients suffering from diabetes, hypertension and chronic renal failure, all being risk factors for PAD [57, 58] and indicating a key role of ECFC in cardiovascular disease [40–42]. We therefore evaluated both, the isolation and seeding efficiency of ECFC from high-risk donor populations in this study. Our results demonstrate that patient-derived ECFC can be isolated through peripheral blood draw and expanded successfully ex vivo.

To answer the vital question whether patient-derived ECFC may grow on decellularized xenogenic matrices, BCA-chips were recellularized. In contrast to published data stating successful recellularization using healthy ECFC [25, 54–56], decellularized BCA-chips seeded with patient-derived ECFC showed unsatisfactory seeding efficiency. As improved vasculogenic properties of peripheral blood ECFC co-implanted with MSC have been reported, we hypothesized that especially impaired patient-derived ECFC are dependent on perivascular support [29, 59]. ECFC and MSC are known to interact via both, cell-cell-contacts and paracrine mechanisms. We therefore assumed co-implantation could help both cell types to maintain their respective cell function and

enable remodeling as well as anastomosis healing upon implantation in vivo and exposure to patient-specific serum. Additionally, MSC have shown to be both, immune evasive and immunosuppressive and can therefore create a low inflammatory environment [60], suitable for constructive remodeling [46]. To explore our hypothesis we used both rat bone-marrow MSC (rMSC) due to easy obtainability and reported low immunogenicity [61] as well as human umbilical cord MSC (hMSC). Published research showed both positive and limiting effects in regard to cell proliferation and survival when comparing allogenic and xenogenic co-culture of ECFC and MSC [62–64]. However, so far only a limited amount of data has been collected and may lead to a distortion of the results in both a positive and negative emphasis.

Unexpectedly, by using a xenogenic co-seeding approach we were able to show that while CD31 and vWF expression in EC typical patterns occurred, these cells did not stain positive for HNA. Therefore, rMSC seemed to express both, CD31 and vWF, and outnumbered ECFC after 14 and 23 days of culture. Under static conditions, ECFC did not survive in great numbers but may have rather supported the differentiation of MSC towards endothelial fate. Co-culture of hMSC and ECFC under similar seeding and cell-culture conditions showed inferior partial reendothelialization compared to rMSC co-culture. Differing seeding-efficiency and cell-survival may be attributed to either heterogeneous ECFC or varying MSC-sources or both. Additionally, different culture-mediums for MSC could have influenced cell behavior. In summary, comparable to unsatisfactory results in regard to seeding capability of ECFC isolated from high-cardiovascular-risk patients reported previously [65], we saw low seeding capability in co-seeding experiments with MSC [29].

Our findings serve as a reminder that sick cells from patients might provide different characteristics from young and healthy cells. So far, we have only seeded ECM-chips in a two-dimensional cell-culture approach of TEVG-chips of only 0.5 cm^2. It remains possible that confluent coverage and function of ECFC and MSC will remain intact and show proper function upon exposure to in vivo conditions. Also, regular function of patient-derived MSC is still unclear and should be investigated through rigorous functional testing as others have shown intimal hyperplasia leading to graft-failure upon implantation in vivo [66]. While we have shown comparable mechanical attributes for decellularized scaffolds, in depth biomechanical analysis especially for smaller loads without pre-strain and multiple directions are still to be addressed, preferably using direct testing methods to omit overestimating mechanical characteristics [67].

In order to facilitate the translation of our collected data into clinical applications, additional research is required. In a first step the application of our findings should be evaluated to create a bypass graft from both human ECFC and human MSC of reasonable lengths under physiological flow and pressure conditions, possibly using bioreactors. This would also address the vital question if sick human MSC can be as beneficial as healthy rat MSC. This could be addressed in an animal-free cell and culture medium model using realistically achievable cell counts for seeding. To develop a patient-derived autologous TEVG, its reendothelialization in cylindrical form, maturation and implantation would be the logical next step.

Conclusion

In this proof-of-concept study we are the first to show the inability of patient-derived ECFC, isolated from patients who display a corresponding deposition due to their age and cardiovascular risk factors for the development of PAD, to form a confluent endothelial layer on decellularized bovine carotid arteries. Successful endothelialization was achieved upon co-culture of patient-derived ECFC with healthy rat MSC and partial endothelialization was observed for the co-culture of patient-derived ECFC with healthy human MSC. Under static conditions, MSC formed a confluent cell layer while expressing typical endothelial cell markers. Furthermore, we show a refined decellularization strategy for widely available BCAs to retain key mechanic and ECM characteristics through an SDS-free approach to be used as small-diameter bypass for patients with PAD.

Methods

All methods were carried out in accordance with relevant guidelines and regulations. Special permission was obtained for all experimental procedures with local committees and institutions where applicable.

Vessel harvesting

BCAs were obtained from a slaughterhouse and transported in cooled phosphate buffered saline (PBS) pH 7.4 (PBS, Biochrom, Berlin, Germany) to the laboratory facilities of the Department of Surgery, where surplus tissue was removed. Vessels were washed with PBS and stored frozen at – 80 °C until further use.

Preparation of Acellular matrices

The standard decellularization treatment (SDT) consisted of three steps as visualized in Fig. 1:

Step 1 Freeze-Thaw-Treatment: BCA were frozen at – 80 °C for > 24 h and then thawed to 5 °C.
Step 2 Osmotic Treatment: BCA were rinsed with deionized water for 48 h on an elliptical tube roller

mixer (RM 5, Glaswarenfabrik Karl Hecht, Sondheim, Germany).

Step 3 Multi-Cyclic Detergent-Enzymatic Treatment:
Multi-cyclic detergent-enzymatic treatment was performed daily for three consecutive days on a roller mixer at 37 °C. BCA were treated each day with 0.05% Trypsin (Sigma-Aldrich, St. Louis, MO, USA) for 2 h, 0.1% Triton-X 100 (Roth, Karlsruhe, Germany) for 4 h, both diluted in 0.05% EGTA (Sigma-Aldrich), and 8 mg/mL DNase-I (Roche Diagnostics, Risch, Switzerland) for 2 h. DNase-I was dissolved in DNase reaction buffer containing 10 mM Tris-HCl, 2.5 mM MgCl2 and 0.5 mM CaCl2 at pH 7.6 at room temperature (RT). Vessels were washed with PBS between treatment-steps. BCAs were stored in PBS solution containing 1% Penicillin/Streptomycin (Biochrom) at 5 °C. *Step 3* was prolonged to 5 days to evaluate sGAG content.

Biochemical analysis of Acellular matrices
Tissue samples of native and decellularized BCA were homogenized and lyophilized. For all biochemical analysis, processed specimens were compared to native controls using 10 mg dry weight samples.

sGAG-content of Acellular matrices
Sulfated glycosaminoglycans (sGAG) content was measured following osmotic treatment and after each Multi-Cyclic Detergent-Enzymatic Treatment for 5 days using the previously published protocol by Farndale et al. [68] Native and decellularized tissue samples as well as Chondroitin-4-Sulphate (0–200 µg/mL, Roth) to acquire a standard curve, were incubated in papain-containing-buffer, mixed with 1,9-Dimethyl-methylene blue (DMMB) at equal parts and measured at a wavelength of 525 nm using the NanoDrop 2000C spectrophotometer (Thermo Fisher Scientific, Waltham, MA, USA).

DNA-content of Acellular matrices
DNA-Content was obtained using DNeasy Blood & Tissue Kit (Qiagen, Venlo, Netherlands) according to the manufacturer's instructions. Samples were measured using the NanoDrop 2000C.

Mechanical analysis of Acellular matrices
Acellular Matrices were cut into 5 mm wide rings with 5 mm diameters. The thickness was measured while using a digital gage (accuracy: ± 0.1 mm; Mitutoyo, Andover, UK). Subsequently the ring specimens were mounted on two custom made wire hooks and finally subjected to low strain rate uniaxial tensile loading to failure testing by means of an Bose tensile machine device (BOSE ElectroForce LM1, Bose

Corporation, Eden Prairie, MN, USA). Specimens were manually prestrained up to approximately 1 N and subsequently loaded until failure at 0.166 mm/s, while applied force and displacement was acquired at a 100 Hz sample rate. Further data analysis was executed using a routine written in MATLAB (The MathWorks, Inc., Natick, MA, USA) converting force (F, N) and displacement (d, mm) to engineering stress (σ, MPa) and strain (ε, adimensional). The stress-strain curve of each sample was plotted, and the following parameters were calculated: elastic phase modulus (E ela, MPa) and collagen phase modulus (E col., MPa), representing Young's modulus under low and high strain determined as linear part of the stress-strain-curve, respectively. Ultimate tensile strength (UTS, MPa), indicating at which stage the sample failed and the corresponding stress-strain-curve exhibits the first drop in load, furthermore the maximal stress (Max stress, MPa) as the highest stress experienced. Max strain, Failure strain and Trans strain are defined accordingly (adimensional). Finally, the point at which the slope of E ela and E col. meet (see Suppl.) defines Trans strain and the corresponding point on the stress-strain-curve provides Transition stress (MPa). Native ($n = 12$) and specimens having undergone freeze-thaw-Ttreatment, SDT and sterilization ($n = 8$ each) as well as SDT without freeze-thaw-treetment ($n = 9$) were compared.

Histological analysis of Acellular matrices
Native vessels and decellularized samples were fixed with 4% paraformaldehyde (PFA, Roth), dehydrated, paraffinized and cut into 7 µm thick sections. Sections were stained with hematoxylin (ITW Reagents, Darmstadt, Germany) and eosin (Morphisto, Frankfurt a.M., Germany) or DAPI (Sigma-Aldrich) to verify the absence of cellular elements and DNA residue. Immunohistochemical stainings for Laminin, Fibronectin, Collagen-I and Collagen-IV as well as conventional picrosirius red staining for collagen were performed to evaluate extracellular matrix components. Table 2 states primary and secondary antibodies used for histological analysis. Following deparaffinization and rehydration, all immunohistochemical samples underwent 3% peroxidase block and 0.1 M citrate buffer pH 6 antigen retrieval. Respective primary antibodies for fibronectin and collagen I staining were incubated for 2 h at 37 °C. Designated samples for laminin and collagen IV staining were blocked with 3% goat serum and incubated with primary (1 h) and secondary antibody (30 min, goat-anti-rabbit, ab6721, abcam) at 37 °C. All remaining steps were performed using LSAB2 Kit (K0675, Agilent Technologies, Santa Clara, CA, USA).

Table 2 Overview of antibodies used

Target	Host	Dilution	Cat.-No.	Manufacturer
Primary Antibodies				
Collagen-I	Mouse	1:400	H00001278-M03	Abnova, Taipei, Taiwan
Collagen-IV	Rabbit	1:400	Ab6586	abcam, Cambridge, UK
Fibronectin	Rabbit	1:400	Ab23751	abcam, Cambridge, UK
Laminin	Rabbit	1:50	Ab11575	abcam, Cambridge, UK
vWF	Rabbit	1:400	Ab6994	abcam, Cambridge, UK
CD31	Rabbit	1:100	Bs-0195R	Bioss Antibodies Inc. Woburn, USA
CD90	Rabbit	1:10	Ab92574	abcam, Cambridge, UK
HNA	Mouse	1:200	Ab191181	abcam, Cambridge, UK
Secondary Antibodies				
Rabbit	Goat	1:400	Ab6721	abcam, Cambridge, UK
Mouse	Donkey	1:400	715–035-150	Dianova, Hamburg, Germany
Rabbit	Goat	1:400	Ab150080	abcam, Cambridge, UK

Isolation of Endothelial Colony Forming Cells (ECFC)

ECFC were isolated similarly to previously published protocols [69, 70]. Following approval of the ethics committee of the Charité – Universitätsmedizin Berlin (EA1/256/14) and in accordance with the declaration of Helsinki, peripheral blood was obtained from hospitalized patients after informed consent. Blood samples were heparinized and treated separately for each patient. Mononuclear cells were isolated using Biocoll (Biochrom) density gradient centrifugation. Mononuclear cell suspension was subsequently plated on fibronectin-gelatin-coating (Fibronectin 0.005 mg/ml, Merck; Gelatin 0.2 mg/ml, Sigma-Aldrich) and incubated at 37 °C and 5% CO_2 for 4 days with EBM-2 medium (Lonza, Basel, Switzerland) supplemented with EGM-2 SingleQuots (Lonza), 18% Fetal Bovine Serum (FBS, Merck) and 1% Penicillin-Streptomycin (P/S, EGM-2) to reach a final concentration of 20% FBS in EGM-2.). Afterwards, all non-adherent cells were washed off with PBS, new EGM-2 medium was added, changed daily for 1 week and then every other day. ECFC were expanded by replating at 80–90% confluence.

Characterization of isolated ECFC

Cell cultures were assessed daily for cell growth, colony formation and absence of contamination with an Axiovert 40 CFL microscope (Carl Zeiss AG, Oberkochen, Germany). Isolated ECFC were fixated on microscope slides using the Cytospin (Cytospin 4, Thermo Fisher Scientific) procedure: Cells were trypsinized, aliquoted, centrifuged onto slides and fixated with Merckofix (Merck). Slides were then washed, incubated with protein block (Agilent Technologies) for 45 min (CD31) or PBS containing 1% bovine serum albumin (BSA, Agilent Technologies) and 0.2% Triton X-100 for 10 min (vWF) at RT. Antibodies were diluted in PBS containing 1% BSA and 1% goat serum. Samples were incubated with primary antibodies for 1 h at 37 °C (CD31) or overnight at 4 °C (vWF) before being incubated with the secondary antibody for 45 min at 37 °C. Afterwards, the cells were washed, counterstained with DAPI and mounted with Aquatex (Merck). Isolated ECFC were incubated with EGM-2 Medium containing 10 μg DiI-ac-LDL (Merck) for 4 h at 37 °C and 5% CO_2. The cells were then washed, counterstained with DAPI, fixated with 4% PFA and microscopically assessed.

rMSC isolation

Rat mesenchymal stromal cells (rMSC) were isolated from rat femur bone marrow according to a modified protocol after Soleimani and Nadri [71]. Bones serving as cell sources for rMSC Isolation had been discarded hind limbs from other animal experiments. All initial animal work was performed in accordance with local law and approved by the State Office of Health and Local Affairs (Landesamt für Gesundheit und Soziales, LAGeSo, Berlin, Germany; Reg. No. T 0139/13, T 0301/17 and O 0365/11). Briefly, following femur explantation, bones were sterilized in 70% Ethanol and manually snapped in half under sterile conditions. The intramedullary canal was rinsed with RPMI-Medium (Thermo-Fischer Scientific) supplemented with 10% FCS and 1% P/S, (RPMI), the cell-containing medium was transferred to a cell culture flask (Corning Inc.) and incubated at 37 °C 5% CO_2. After 4 days, the cell culture flasks were rinsed, inspected for adherent cells and fresh RPMI medium was added. rMSC were replated at 70% confluence.

41

Recellularization of acellular BCA matrices with hECFC or hECFC in coculture with rMSC or hMSC

All steps were performed under sterile conditions. Decellularized matrices were sterilized by incubation for 6 h with 0.2% Peracetic Acid (PAA) and 4% Ethanol (EtOH) followed by washing steps in sterile PBS until the pH was neutralized. The matrices were then cut to $0.5\,cm^2$ pieces and equilibrated in EGM-2 in 12-well plates overnight.

ECFC derived from high cardiovascular risk donors were used for all recellularization experiments. Expanded hECFC were trypsinized, washed and resuspended in EGM-2 before seeding on the luminal side of matrices in 80 µl EGM-2 containing 3.6×10^5 hECFC. Seeding medium consisting of equal parts of EGM-2 medium and M-199 medium (rMSC) containing 10% FBS and 1% P/S (seeding medium) or ATCC PCS-500-030 Medium supplemented with ATCC PCS-500-040 (hMSC) was prepared. Expanded hECFC and rMSC or human MSC (hMSC, human umbilical cord-derived mesenchymal stem cells, ATCC) were trypsinized, washed and resuspended in seeding medium. Approximately 80 µl of cell suspension containing 5.5×10^5 ECFC and 4.2×10^4 rMSC or hMSC was added to the luminal side of each matrix followed by 1 h incubation at 37 °C 5% CO_2. Subsequently, 4 mL of seeding medium was added and seeded matrices were incubated for 72 h at 37 °C and 5% CO_2. After 72 h matrices were transferred carefully to new 12 well plates. Incubation continued for 12 ($n = 8$) days in monoculture and 14 ($n = 6$) or 23 (rat ($n = 5$) or human ($n = 6$) MSC) days in co-culture experiments.

Analysis of Recellularized matrices

Native vessels and recellularized samples were embedded in Tissue Freezing Medium (Leica), snap-frozen and stored at − 80 °C. Cryostat sections (7 µm, Thermo Fisher Scientific) were prepared, fixed in cold acetone (Roth), air-dried and washed with PBS. Sections were stained with H&E and DAPI. To prove endothelial origin, CD31- and vWF-staining was performed. Following incubation in boiling 0.01 M Target Retrieval Solution pH 6 (Agilent Technologies) for 20 min, specimens were treated with blocking buffer containing 3% goat serum and 0.3% Triton X-100 for 45 min at RT. Antibodies were diluted in buffer containing 1% BSA, 1% goat serum and 0.3% Triton X-100. Primary antibodies were then applied to tissue samples and incubated at 4 °C overnight. The secondary antibody (1:400, ab150080, abcam) was applied to tissue samples following washing for 45 min at 37 °C. Specimens were then washed, counterstained with DAPI and coverslipped using Aquatex (Sigma-Aldrich). To show cell distribution of human- and MSC-origin CD90 and human nuclear antigen (HNA) histochemical staining was performed. Epitope retrieval by using the pressure cooker method for 5 min while specimens were placed in boiling TRIS/EDTA-buffer and

peroxidase blocking was performed for CD90 staining. Blocking was performed using protein block for HNA. Primary antibody (1:20, ab92574; 1:200, ab191181) was then applied and incubated over night at room-temperature. The secondary antibody (1:400, ab6721; 1:400, 715–035-150) was applied to tissue samples following washing for 45 min at 37 °C (CD90) or 30 min at RT (HNA). All remaining steps were performed using LSAB2 Kit (K0675, Agilent Technologies, Santa Clara, CA, USA). Microscopic evaluation was performed using Observer Z1 microscope (Carl Zeiss AG) or EVOS FL Auto microscope (Thermo-Fisher Scientific, Fig. 5c).

Statistical analysis

All calculations were performed using GraphPad Prism version 6.04 for Mac, GraphPad Software, La Jolla, CA, USA. Data was tested for normality using Shapiro-Wilk test. Statistical comparison was performed by either Friedman test (sGAG-content), Wilcoxon test (DNA-content) or Kruskal-Wallis test (mechanical data). Data is presented as median and interquartile range (IQR). *p*-Values below 0.05 were considered statistically significant. All graphs in this study show medians with the respective IQR.

Supplementary Information

The online version contains supplementary material available at https://doi.org/10.1186/s13036-021-00266-5.

> **Additional file 1.** Shows complete data of the mechanical experiment including stress-strain curves and negative control images for histological staining.

Authors' contributions
NS developed the project idea, performed the experiments and wrote the manuscript. PT helped during all parts of the project. EK helped with the analysis of the experiments including histology. ARS discussed results with us and performed the statistical evaluation. SM helped with the analysis of the experiments and statistical analysis. HN helped develop the project idea and helped with the analysis of the experiments. HE helped establish the decellularization technique and with the analysis of the experiments. DW helped with the mechanical analysis. JP discussed the results and proofread the manuscript. IMS developed the project idea, discussed the results and proofread the manuscript. KH developed the project idea, supervised the revision, helped with the analysis of the experiments and proofread the manuscript. BS developed the project idea, supervised the whole project and proofread the manuscript. The author(s) read and approved the final manuscript.

Seiffert *et al. Journal of Biological Engineering*   (2021) 15:15

Page 13 of 14

Declarations

Author details
[1]Charité – Universitätsmedizin Berlin, corporate member of Freie Universität Berlin and Humboldt- Universität zu Berlin, Department of Surgery, Campus Charité Mitte | Campus Virchow-Klinikum, Augustenburger Platz 1, 13353 Berlin, Germany. [2]Department for Trauma and Orthopedic Surgery, Vivantes-Hospital Spandau, Berlin, Germany. [3]Berlin Institute of Health at Charité – Universitätsmedizin Berlin, Charitéplatz 1, 10117 Berlin, Germany. [4]Charité – Universitätsmedizin Berlin, corporate member of Freie Universität Berlin and Humboldt- Universität zu Berlin, Julius Wolff Institute, Augustenburger Platz 1, 13353 Berlin, Germany. [5]Berlin Institute of Health at Charité – Universitätsmedizin Berlin, BIH Academy, Clinician Scientist Program, Charitéplatz 1, 10117 Berlin, Germany. [6]Department of General, Visceral and Transplant Surgery, University Hospital Münster, Münster, Germany.

References

1. Benjamin EJ, Virani SS, Callaway CW, Chamberlain AM, Chang AR, Cheng S, et al. Heart disease and stroke Statistics-2018 update: a report from the American Heart Association. Circulation. 2018;137(12):e67–492. https://doi.org/10.1161/CIR.0000000000000558.
2. Agarwal S, Pitcavage JM, Sud K, Thakkar B. Burden of readmissions among patients with critical limb ischemia. J Am Coll Cardiol. 2017;69(15):1897–908. https://doi.org/10.1016/j.jacc.2017.02.040.
3. Arruda-Olson AM, Moussa Pacha H, Afzal N, Abram S, Lewis BR, Isseh I, et al. Burden of hospitalization in clinically diagnosed peripheral artery disease: a community-based study. Vasc Med. 2018;23(1):23–31. https://doi.org/10.1177/1358863X17736152.
4. Mahoney EM, Wang K, Keo HH, Duval S, Smolderen KG, Cohen DJ, et al. Vascular hospitalization rates and costs in patients with peripheral artery disease in the United States. Circ Cardiovasc Qual Outcomes. 2010;3(6):642–51. https://doi.org/10.1161/CIRCOUTCOMES.109.930735.
5. Kullo IJ, Rooke TW. Peripheral artery disease. N Engl J Med. 2016;374:861–71 Massachusetts Medical Society.
6. Klinkert P, Post PN, Breslau PJ, van Bockel JH. Saphenous vein versus PTFE for above-knee femoropopliteal bypass. A review of the literature. Eur J Vasc Endovasc Surg. 2004;27(4):357–62. https://doi.org/10.1016/j.ejvs.2003.12.027.
7. Faries PL, Logerfo FW, Arora S, Hook S, Pulling MC, Akbari CM, et al. A comparative study of alternative conduits for lower extremity revascularization: all-autogenous conduit versus prosthetic grafts. J Vasc Surg. 2000;32(6):1080–90. https://doi.org/10.1067/mva.2000.111279.
8. Ambler GK, Twine CP. Graft type for femoro-popliteal bypass surgery. Cochrane Database Syst Rev. 2018;2:CD001487.
9. Chlupác J, Filová E, Bacáková L. Blood vessel replacement: 50 years of development and tissue engineering paradigms in vascular surgery. Physiol Res. 2009;58(Suppl 2):S119–39.
10. Bosma J, Turkçan K, Assink J, Wisselink W, Vahl AC. Long-term quality of life and mobility after prosthetic above-the-knee bypass surgery. Ann Vasc Surg. 2012;26(2):225–32. https://doi.org/10.1016/j.avsg.2011.05.029.
11. Seifu DG, Purnama A, Mequanint K, Mantovani D. Small-diameter vascular tissue engineering. Nat Rev Cardiol. 2013;10(7):410–21. https://doi.org/10.1038/nrcardio.2013.77.
12. L'Heureux N, Dusserre N, Marini A, Garrido S, de la Fuente L, McAllister T. Technology insight: the evolution of tissue-engineered vascular grafts--from research to clinical practice. Nat Clin Pract Cardiovasc Med. 2007;4:389–95 Nat Publ Group.
13. Natasha G, Tan A, Gundogan B, Farhatnia Y, Nayyer L, Mahdibeiraghdar S, et al. Tissue engineering vascular grafts a fortiori: looking back and going forward. Expert Opin Biol Ther. 2015;15:231–44.
14. Pashneh-Tala S, MacNeil S, Claeyssens F. The tissue-engineered vascular graft-past, present, and future. Tissue Eng Part B Rev. 2016;22(1):68–100. https://doi.org/10.1089/ten.teb.2015.0100.
15. Huang AH, Niklason LE. Engineering of arteries in vitro. Cell Mol Life Sci. 2014;71(11):2103–18. https://doi.org/10.1007/s00018-013-1546-3.
16. Roy S, Silacci P, Stergiopulos N. Biomechanical proprieties of decellularized porcine common carotid arteries. American journal of physiology-heart and circulatory physiology. Am Physiol Soc. 2005;289:H1567–76.
17. Gui L, Muto A, Chan SA, Breuer CK, Niklason LE. Development of decellularized human umbilical arteries as small-diameter vascular grafts. Tissue Eng Part A. 2009;15(9):2665–76. https://doi.org/10.1089/ten.tea.2008.0526.
18. Hillebrandt KH, Everwien H, Haep N, Keshi E, Pratschke J, Sauer IM. Strategies based on organ decellularization and recellularization. Transpl Int. 2019;32(6):571–85. https://doi.org/10.1111/tri.13462.
19. Colunga T, Dalton S. Building blood vessels with vascular progenitor cells. Trends Mol Med. 2018;24(7):630–41. https://doi.org/10.1016/j.molmed.2018.05.002.
20. Dahan N, Sarig U, Bronshtein T, Baruch L, Karram T, Hoffman A, et al. Dynamic autologous Reendothelialization of small-caliber arterial extracellular matrix: a preclinical large animal study. Tissue Eng Part A. 2017;23(1-2):69–79. https://doi.org/10.1089/ten.tea.2016.0126.
21. Pineda DM, Dougherty MJ, Wismer MC, Carroll C, Tyagi S, Troutman DA, et al. Bovine carotid artery xenografts for hemodialysis access. J Vasc Surg. 2017;65(6):1729–34. https://doi.org/10.1016/j.jvs.2016.12.109.
22. Farber A, Major K, Wagner WH, Cohen JL, Cossman DV, Lauterbach SR, et al. Cryopreserved saphenous vein allografts in infrainguinal revascularization: analysis of 240 grafts. J Vasc Surg. 2003;38(1):15–21. https://doi.org/10.1016/S0741-5214(03)00330-6.
23. Zilla P, Bezuidenhout D, Human P. Prosthetic vascular grafts: wrong models, wrong questions and no healing. Biomaterials. 2007;28(34):5009–27. https://doi.org/10.1016/j.biomaterials.2007.07.017.
24. Casscells W. Migration of smooth muscle and endothelial cells. Critical events in restenosis. Circulation. 1992;86(3):723–9. https://doi.org/10.1161/01.CIR.86.3.723.
25. Borschel GH, Huang Y-C, Calve S, Arruda EM, Lynch JB, Dow DE, et al. Tissue engineering of recellularized small-diameter vascular grafts. Tissue Eng. 2005;11(5-6):778–86. https://doi.org/10.1089/ten.2005.11.778.
26. Quint C, Kondo Y, Manson RJ, Lawson JH, Dardik A, Niklason LE. Decellularized tissue-engineered blood vessel as an arterial conduit. Proc Natl Acad Sci U S A. 2011;108(22):9214–9. https://doi.org/10.1073/pnas.1019506108.
27. Tiwari A, Salacinski HJ, Hamilton G, Seifalian AM. Tissue engineering of vascular bypass grafts: role of endothelial cell extraction. Eur J Vasc Endovasc Surg. 2001;21(3):193–201. https://doi.org/10.1053/ejvs.2001.1316.
28. Cho S-W, Lim SH, Kim I-K, Hong YS, Kim S-S, Yoo KJ, et al. Small-diameter blood vessels engineered with bone marrow-derived cells. Ann Surg. 2005;241(3):506–15. https://doi.org/10.1097/01.sla.0000154268.12239.ed.
29. Melero-Martin JM, De Obaldia ME, Kang S-Y, Khan ZA, Yuan L, Oettgen P, et al. Engineering robust and functional vascular networks in vivo with human adult and cord blood-derived progenitor cells. Circ Res. 2008;103(2):194–202. https://doi.org/10.1161/CIRCRESAHA.108.178590.
30. Melchiorri AJ, Bracaglia LG, Kimerer LK, Hibino N, Fisher JP. In vitro Endothelialization of biodegradable vascular grafts via endothelial progenitor cell seeding and maturation in a tubular perfusion system bioreactor. Tissue Eng Part C Methods. 2016;22(7):663–70. https://doi.org/10.1089/ten.tec.2015.0562.
31. Hofmann NA, Reinisch A, Strunk D. Isolation and large scale expansion of adult human endothelial colony forming progenitor cells. J Vis Exp. 2009; Available from:. https://doi.org/10.3791/1524.
32. Ensley AE, Nerem RM, Anderson DEJ, Hanson SR, Hinds MT. Fluid shear stress alters the hemostatic properties of endothelial outgrowth cells. Tissue Eng Part A. 2012;18(1-2):127–36. https://doi.org/10.1089/ten.tea.2010.0290.
33. Glynn JJ, Hinds MT. Endothelial outgrowth cells: function and performance in vascular grafts. Tissue Eng Part B Rev. 2014;20:294–303 online.liebertpub.com.
34. Peters EB. Endothelial progenitor cells for the vascularization of engineered tissues. Tissue Eng Part B Rev. 2018;24(1):1–24. https://doi.org/10.1089/ten.teb.2017.0127.

35. Krawiec JT, Weinbaum JS, Liao H-T, Ramaswamy AK, Pezzone DJ, Josowitz AD, et al. In vivo functional evaluation of tissue-engineered vascular grafts fabricated using human adipose-derived stem cells from high cardiovascular risk populations. Tissue Eng Part A; 2016;22:765–775. Mary Ann Liebert, Inc, New Rochelle.

36. Maiti SK, Shivakumar MU, Mohan D, Kumar N, Singh KP. Mesenchymal stem cells of different origin-seeded bioceramic construct in regeneration of bone defect in rabbit. Tissue Eng Regen Med. 2018;15(4):477–92. https://doi.org/10.1007/s13770-018-0129-7.

37. Le Blanc K, Ringdén O. Immunomodulation by mesenchymal stem cells and clinical experience. J Intern Med; 2007;262:509–525 Wiley Online Library.

38. Wang K, Lin R-Z, Melero-Martin JM. Bioengineering human vascular networks: trends and directions in endothelial and perivascular cell sources. Cell Mol Life Sci. 2019;76(3):421–39. https://doi.org/10.1007/s00018-018-2939-0.

39. Au P, Daheron LM, Duda DG, Cohen KS, Tyrrell JA, Lanning RM, et al. Differential in vivo potential of endothelial progenitor cells from human umbilical cord blood and adult peripheral blood to form functional long-lasting vessels. Blood. 2008; 111(3):1302–5. https://doi.org/10.1182/blood-2007-06-094318.

40. Fadini GP, Losordo D, Dimmeler S. Critical reevaluation of endothelial progenitor cell phenotypes for therapeutic and diagnostic use. Circ Res. 2012;110(4):624–37. https://doi.org/10.1161/CIRCRESAHA.111.243386.

41. Umemura T, Soga J, Hidaka T, Takemoto H, Nakamura S, Jitsuiki D, et al. Aging and hypertension are independent risk factors for reduced number of circulating endothelial progenitor cells. Am J Hypertens. 2008;21(11): 1203–9. https://doi.org/10.1038/ajh.2008.278.

42. Choi J-H, Kim KL, Huh W, Kim B, Byun J, Suh W, et al. Decreased number and impaired angiogenic function of endothelial progenitor cells in patients with chronic renal failure. Arterioscler Thromb Vasc biol. Am Heart Assoc. 2004;24:1246–52.

43. Ranjan AK, Kumar U, Hardikar AA, Poddar P, Nair PD, Hardikar AA. Human blood vessel-derived endothelial progenitors for endothelialization of small diameter vascular prosthesis. PLoS One. 2009;4(11):e7718. https://doi.org/10.1371/journal.pone.0007718.

44. Stroncek JD, Ren LC, Klitzman B, Reichert WM. Patient-derived endothelial progenitor cells improve vascular graft patency in a rodent model. Acta Biomater. 2012;8(1):201–8. https://doi.org/10.1016/j.actbio.2011.09.002.

45. Fernandez CE, Achneck HE, Reichert WM, Truskey GA. Biological and engineering design considerations for vascular tissue engineered blood vessels (TEBVs). Curr Opin Chem Eng. 2014;3:83–90. https://doi.org/10.1016/j.coche.2013.12.001.

46. Londono R, Badylak SF. Biomaterials from Decellularized tissues. In: Neves NM, Reis RL, editors. Biomaterials from nature for advanced devices and therapies. Hoboken: Wiley; 2016. p. 190–210. https://doi.org/10.1002/9781119126218.ch12.

47. Mancuso L, Gualerzi A, Boschetti F, Loy F, Cao G. Decellularized ovine arteries as small-diameter vascular grafts. Biomed Mater. 2014;9(4):045011. https://doi.org/10.1088/1748-6041/9/4/045011.

48. Gratzer PF, Harrison RD, Woods T. Matrix alteration and not residual sodium dodecyl sulfate cytotoxicity affects the cellular repopulation of a decellularized matrix. Tissue Eng. 2006;12(10):2975–83. https://doi.org/10.1089/ten.2006.12.2975.

49. Olausson M, Patil PB, Kuna VK, Chougule P, Hernandez N, Methe K, et al. Transplantation of an allogeneic vein bioengineered with autologous stem cells: a proof-of-concept study. Lancet. 2012;380(9838):230–7. https://doi.org/10.1016/S0140-6736(12)60633-3.

50. Faulk DM, Carruthers CA, Warner HJ, Kramer CR, Reing JE, Zhang L, et al. The effect of detergents on the basement membrane complex of a biologic scaffold material. Acta Biomater. 2014;10(1):183–93. https://doi.org/10.1016/j.actbio.2013.09.006.

51. Crapo PM, Gilbert TW, Badylak SF. An overview of tissue and whole organ decellularization processes. Biomaterials. 2011;32(12):3233–43. https://doi.org/10.1016/j.biomaterials.2011.01.057.

52. Keane TJ, Swinehart IT, Badylak SF. Methods of tissue decellularization used for preparation of biologic scaffolds and in vivo relevance. Methods. 2015; 84:25–34. https://doi.org/10.1016/j.ymeth.2015.03.005.

53. Delgado LM, Pandit A, Zeugolis DI. Influence of sterilisation methods on collagen-based devices stability and properties. Expert Rev Med Devices. 2014;11(3):305–14. https://doi.org/10.1586/17434440.2014.900436.

54. Freytes DO, Badylak SF, Webster TJ, Geddes LA, Rundell AE. Biaxial strength of multilaminated extracellular matrix scaffolds. Biomaterials. 2004;25(12): 2353–61. https://doi.org/10.1016/j.biomaterials.2003.09.015.

55. Hodde JP, Record RD, Tullius RS, Badylak SF. Retention of endothelial cell adherence to porcine-derived extracellular matrix after disinfection and sterilization. Tissue Eng. 2002;8(2):225–34. https://doi.org/10.1089/107632702753724996.

56. Matuska AM, McFetridge PS. The effect of terminal sterilization on structural and biophysical properties of a decellularized collagen-based scaffold; implications for stem cell adhesion. J Biomed Mater Res B Appl Biomater. 2015;103(2):397–406. https://doi.org/10.1002/jbm.b.33213.

57. Ouriel K. Peripheral arterial disease. Lancet. 2001;358(9289):1257–64. https://doi.org/10.1016/S0140-6736(01)06351-6.

58. Wattanakit K, Folsom AR, Selvin E, Coresh J, Hirsch AT, Weatherley BD. Kidney function and risk of peripheral arterial disease: results from the atherosclerosis risk in communities (ARIC) study. J Am Soc Nephrol. 2007; 18(2):629–36. https://doi.org/10.1681/ASN.2005111204.

59. Pill K, Hofmann S, Redl H, Holnthoner W. Vascularization mediated by mesenchymal stem cells from bone marrow and adipose tissue: a comparison. Cell Regen (Lond). 2015;4:8.

60. Cunnane EM, Weinbaum JS, O'Brien FJ, Vorp DA. Future perspectives on the role of stem cells and extracellular vesicles in vascular tissue regeneration. Front Cardiovasc Med. 2018;5:86. https://doi.org/10.3389/fcvm.2018.00086.

61. Lee M, Jeong SY, Ha J, Kim M, Jin HJ, Kwon S-J, et al. Low immunogenicity of allogeneic human umbilical cord blood-derived mesenchymal stem cells in vitro and in vivo. Biochem Biophys Res Commun. 2014;446(4):983–9. https://doi.org/10.1016/j.bbrc.2014.03.051.

62. Reichert D, Friedrichs J, Ritter S, Käubler T, Werner C, Bornhäuser M, et al. Phenotypic, Morphological and Adhesive Differences of Human Hematopoietic Progenitor Cells Cultured on Murine versus Human Mesenchymal Stromal Cells. Sci Rep. 2015;5:15680.

63. Steiner D, Köhn K, Beier JP, Stürzl M, Horch RE, Arkudas A. Cocultivation of Mesenchymal stem cells and endothelial progenitor cells reveals Antiapoptotic and Proangiogenic effects. Cells Tissues Organs. 2017;204(5-6): 218–27. https://doi.org/10.1159/000478654.

64. Fang J-F, Huang X-N, Han X-Y, Ouyang X, Fan L, Zhao X, et al. Combined transplantation of Mesenchymal stem cells and endothelial progenitor cells restores cavernous nerve injury-related erectile dysfunction. J Sex Med. 2018;15(3):284–95. https://doi.org/10.1016/j.jsxm.2018.01.005.

65. Stroncek JD, Grant BS, Brown MA, Povsic TJ, Truskey GA, Reichert WM. Comparison of endothelial cell phenotypic markers of late-outgrowth endothelial progenitor cells isolated from patients with coronary artery disease and healthy volunteers. Tissue Eng Part A. 2009;15(11):3473–86. https://doi.org/10.1089/ten.tea.2008.0673.

66. Rotmans JI, Heyligers JMM, Verhagen HJM, Velema E, Nagtegaal MM, de Kleijn DPV, et al. In vivo cell seeding with anti-CD34 antibodies successfully accelerates endothelialization but stimulates intimal hyperplasia in porcine arteriovenous expanded polytetrafluoroethylene grafts. Circulation. 2005; 112(1):12–8. https://doi.org/10.1161/CIRCULATIONAHA.104.504407.

67. Geelhoed WJ, Lalai RA, Sinnige JH, Jongeleen PJ, Storm C, Rotmans JI. Indirect burst pressure measurements for the mechanical assessment of biological vessels. Tissue Eng Part C Methods. 2019;25(8):472–8. https://doi.org/10.1089/ten.tec.2019.0133.

68. Farndale RW, Buttle DJ, Barrett AJ. Improved quantitation and discrimination of sulphated glycosaminoglycans by use of dimethylmethylene blue. Biochim Biophys Acta. 1986;883(2):173–7. https://doi.org/10.1016/0304-4165(86)90306-5.

69. Vasa M, Fichtlscherer S, Adler K, Aicher A, Martin H, Zeiher AM, et al. Increase in circulating endothelial progenitor cells by statin therapy in patients with stable coronary artery disease. Circulation. 2001;103(24):2885–90. https://doi.org/10.1161/hc2401.092816.

70. Melero-Martin JM, Khan ZA, Picard A, Wu X, Paruchuri S, Bischoff J. In vivo vasculogenic potential of human blood-derived endothelial progenitor cells. Blood. 2007;109(11):4761–8. https://doi.org/10.1182/blood-2006-12-062471.

71. Soleimani M, Nadri S. A protocol for isolation and culture of mesenchymal stem cells from mouse bone marrow. Nat Protoc. 2009;4(1):102–6. https://doi.org/10.1038/nprot.2008.221.

Publisher's Note

H. Napierala, K.-H. Hillebrandt, N. Haep, P. Tang, M. Tintemann, J. Gassner, M. Noesser, H. Everwien, N. Seiffert, M. Kluge, E. Teegen, D. Polenz, S. Lippert, D. Geisel, A. Reutzel Selke, N. Raschzok, A. Andreou, J. Pratschke, I.M. Sauer, B. Struecker, **Engineering an endocrine Neo-Pancreas by repopulation of a decellularized rat pancreas with islets of Langerhans**, Sci. Rep. 7 (2017) 41777
DOI: http://dx.doi.org/10.1038/srep41777
PubMed PMID: 28150744
Impact Factor: 4,379 im Jahr 2020

SCIENTIFIC REPORTS

Engineering an endocrine Neo-Pancreas by repopulation of a decellularized rat pancreas with islets of Langerhans

H. Napierala[1], K.-H. Hillebrandt[1], N. Haep[1], P. Tang[1], M. Tintemann[1], J. Gassner[1], M. Noesser[1], H. Everwien[1], N. Seiffert[1], M. Kluge[1], E. Teegen[1], D. Polenz[1], S. Lippert[1], D. Geisel[2], A. Reutzel Selke[1], N. Raschzok[1], A. Andreou[1], J. Pratschke[1], I. M. Sauer[1] & B. Struecker[1,3]

Decellularization of pancreata and repopulation of these non-immunogenic matrices with islets and endothelial cells could provide transplantable, endocrine Neo- Pancreata. In this study, rat pancreata were perfusion decellularized and repopulated with intact islets, comparing three perfusion routes (Artery, Portal Vein, Pancreatic Duct). Decellularization effectively removed all cellular components but conserved the pancreas specific extracellular matrix. Digital subtraction angiography of the matrices showed a conserved integrity of the decellularized vascular system but a contrast emersion into the parenchyma via the decellularized pancreatic duct. Islets infused via the pancreatic duct leaked from the ductular system into the peri-ductular decellularized space despite their magnitude. TUNEL staining and Glucose stimulated insulin secretion revealed that islets were viable and functional after the process. We present the first available protocol for perfusion decellularization of rat pancreata via three different perfusion routes. Furthermore, we provide first proof-of-concept for the repopulation of the decellularized rat pancreata with functional islets of Langerhans. The presented technique can serve as a bioengineering platform to generate implantable and functional endocrine Neo-Pancreata.

Type 1 diabetes mellitus (T1DM) is one of the most cost-intensive chronic diseases worldwide[1,2]. Insulin was discovered more than 90 years ago and has since been the main therapeutic agent in the management of T1DM; however, in some cases, exogenous insulin replacement is not able to provide the necessary metabolic regulation to prevent primary (hypoglycemic episodes)[3] and secondary long-term complications (e.g., vasculopathy, cardiovascular diseases, diabetic nephropathy, neuropathy and retinopathy)[4]. In these severe cases, B-cell replacement through pancreas or islet transplantation may be indicated.

Pancreas transplantation is a well-established procedure and (with regard to long term metabolic function) superior to islet transplantation[5]. However, in addition to rejection, major and occasionally life-threatening complications, such as post- transplant-pancreatitis, infections and thrombosis, continue to result in approximately 10% graft loss. Islet transplantation appears to be an alternative because it is less invasive and is therefore considered safer[6]. Although the indications to islet (auto-) transplantations are currently being expanded[7], metabolic function after islet transplantation continues to suffer from various issues, such as the need for immunosuppression and graft-site specific problems like hypoxia[8], partial portal vein thrombosis[9,10] and the instant blood-mediated inflammatory reaction (IBMIR)[11].

With the development of novel tissue engineering techniques (e.g., decellularization and recellularization; Fig. 1), the above-mentioned issues could be overcome[12]. The intent of decellularization is to remove all cellular and antigenic material from an organ while preserving the innate and possibly non-immunogeneic, extracellular matrix (ECM). This matrix could be used for the bioengineering of transplantable organs via repopulation with (autologous) cells[13–16]. The ECM represents a biochemically, geometrically and spatially ideal platform[17],

[1]Department of Surgery, Campus Charité Mitte and Campus Virchow Klinikum, Charité - Universitätsmedizin Berlin, Germany. [2]Department of Radiolgoy, Charité – Universitätsmedizin Berlin, Germany. [3]Berlin Institute of Health (BIH), Berlin, Germany. Correspondence and requests for materials should be addressed to I.M.S. (email: Igor.Sauer@charite.de)
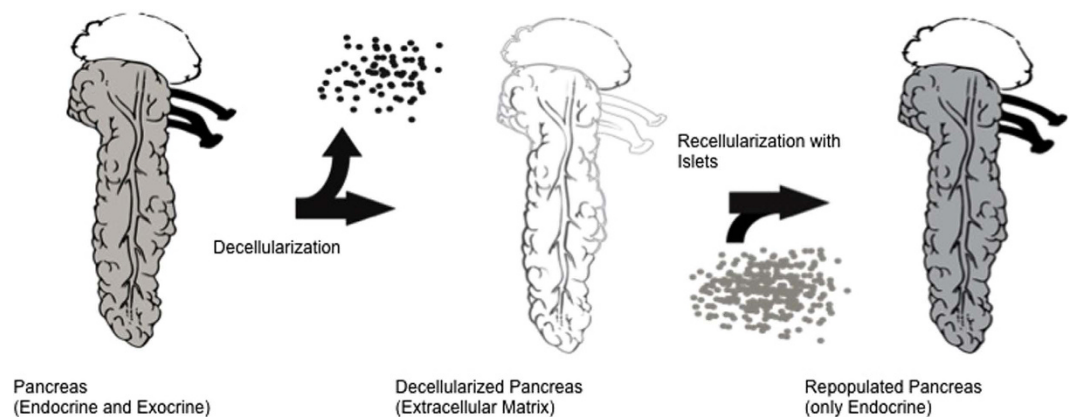
Figure 1. Concept to generate an Endocrine Neo-Pancreas. A (xenogene) pancreas is decellularized by perfusion with alkaline detergents. The resulting non-immunogenic matrix conserves the organ specific extracellular matrix including the vascular and ductular protein network. The matrix is then repopulated by infusion of islets and endothelial cells to generate a functional and implantable organ.

preserves basic matrix components, such as proteins and growth factors[18], and retains an intact vasculature[17]. This environment could be the key to improved long-term islet survival and function after transplantation[6].

Furthermore, by applying this technique it appears possible to engineer a solely endocrine Neo-Pancreas, which would prevent post-transplant pancreatitis because exocrine cells would not be used for the repopulation of the organ. The need for post-transplant immunosuppression could in the future be avoided, given that a protocol for the differentiation of fibroblasts into beta-like cells is already available[19].

However, surprisingly, a limited number of studies have been published reporting on pancreas decellularization and recellularization[1,20–23] compared with other organs. To the best of our knowledge, no study is currently available reporting on whole rat pancreas decellularization, although a decellularized rat pancreas would render an interesting platform for tissue engineering experiments. Furthermore, no data is available on the repopulation of decellularized pancreas matrices with intact islets. Thus, it remains unclear, if the decellularized, parenchymal space can be repopulated with whole, intact islets, which are significantly bigger than other cells[24].

Our aim was to find a rapid and reproducible protocol to decellularize whole rat pancreata and repopulate these matrices with intact Islets of Langerhans. Pancreas perfusion is possible through various perfusion routes (portal vein, aorta, extrahepatic bile duct and consecutively the pancreatic duct); thus, we evaluated these routes regarding decellularization effectiveness, ECM conservation, general handling and the possibility to infuse whole islets into the matrix. Furthermore, we evaluated if islets are still viable and functional after the process by *ex vivo* perfusion and glucose stimulated insulin secretion of repopulated Neo pancreata.

Results

Macroscopic observations during decellularization.
During perfusion decellularization, a gradual loss of brownish color could be observed in all three groups until the organs appeared lucent (Fig. 2A–D).

After 1 hour (initial perfusion with Triton X-100) the organs remained opaque but elucidated compared with the beginning of the experiment (Fig. 2B). After 3 hours (end-point of the perfusion with SDS), the organs were completely translucent (Fig. 2C). This did not change until the end of the protocol (Fig. 2D). Macroscopically, the generated scaffolds were completely cell free but remained an intact network of vessel-like-structures.

Histological evaluation of decellularized matrices.
Macroscopic observations were confirmed by H/E staining (Fig. 3): no cellular material was stained in the decellularized matrix, whereas the lobular structure of the pancreas could be preserved. Additionally, the connective tissue septa, as well as the ductal and vascular network were preserved in all specimens. Sirius red and Alcian Blue stainings were performed to visualize collagen fibers and acidic sulfated mucopolysaccharides as abundant components of the ECM, respectively (Fig. 3). The decellularized ECM appeared identical to that of the controls in all cases. Microscopically, no relevant differences were observed between the three experimental groups (Fig. 3).

Immunohistochemical stainings were performed to visualize collagen IV, fibronectin and laminin as abundant components of the ECM for a qualitative evaluation of the ECM after decellularization compared with the controls (Fig. 3). In all cases, the matrix proteins were detected inside the matrix and their distribution appeared comparable to native tissue. Again, no relevant differences were observed between the three experimental groups (Fig. 3).

Biochemical analysis of decellularized matrices.
In all three experimental groups, the total DNA content declined significantly compared with the controls (Arterial Perfusion: $44.24 \pm 11.58\,\mu g$ ($p < 0.05$); Portal Venous Perfusion: $67.49 \pm 27.68\,\mu g$ ($p < 0.5$); Pancreatic duct perfusion: $59.73 \pm 15.89\,\mu g$ ($p < 0.5$); C: $687.0 \pm 168.3\,\mu g$ ($n = 6$); Fig. 4A). No statistically significant differences between the three groups were found. The conservation of the main ECM components was confirmed via biochemical analysis showing remaining sGAG and hydroxyproline content in the matrix. A trend towards higher values could be observed for the sGAG
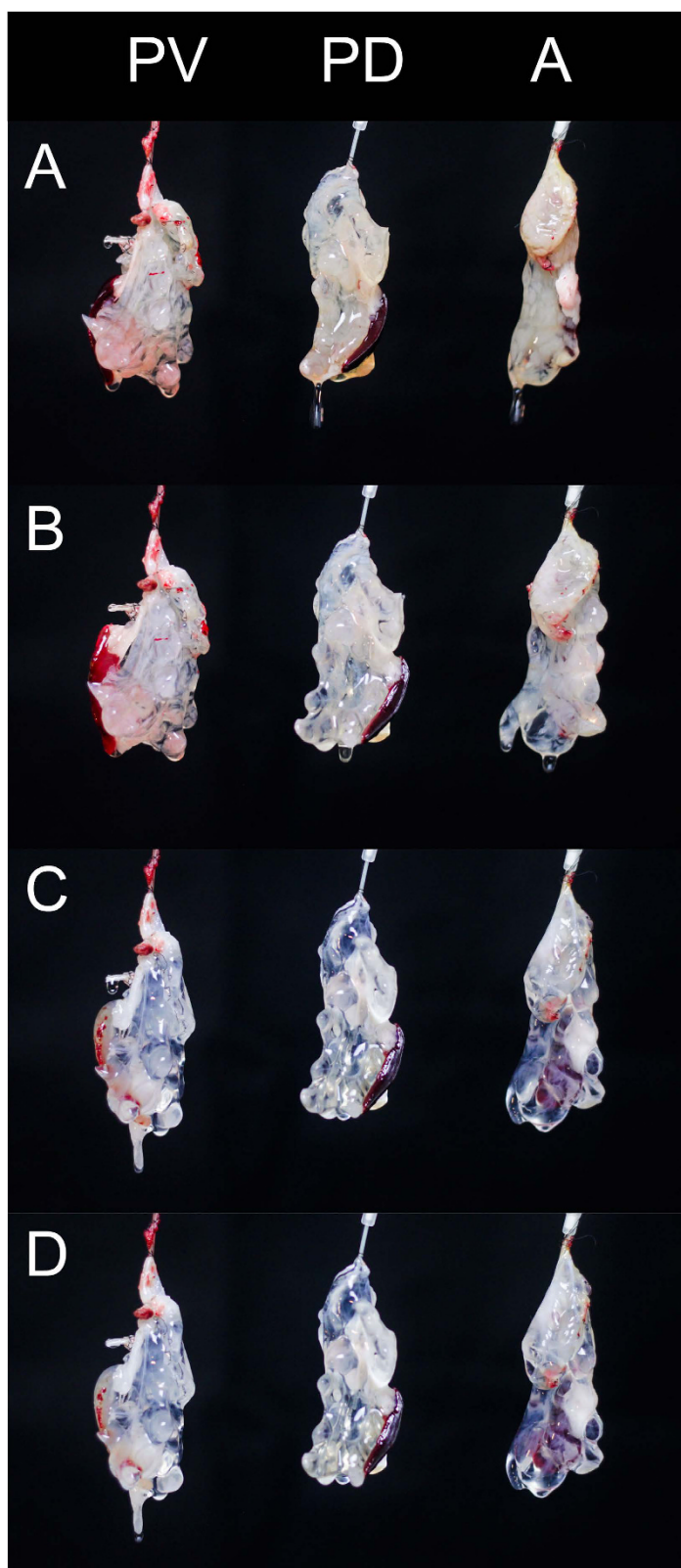
Figure 2. Macroscopic observations during decellularization. Time course of perfusion of three rat pancreata cannulated via the portal vein (PV), the pancreatic duct (PD) or the arterial system (A). At the initiation of the perfusion pancreata appear yellow to brown. Attached to the pancreata is the spleen in dark brown. One hour after perfusion with Triton X-100 pancreata start to lose their color and elucidate. After 2 hours of perfusion with SDS the pancreata appear completely transparent. The spleen is still brown because splenic blood vessels were ligated and not perfused. At the end of the decellularization process the organ structure is still conserved but the cellular components are removed.
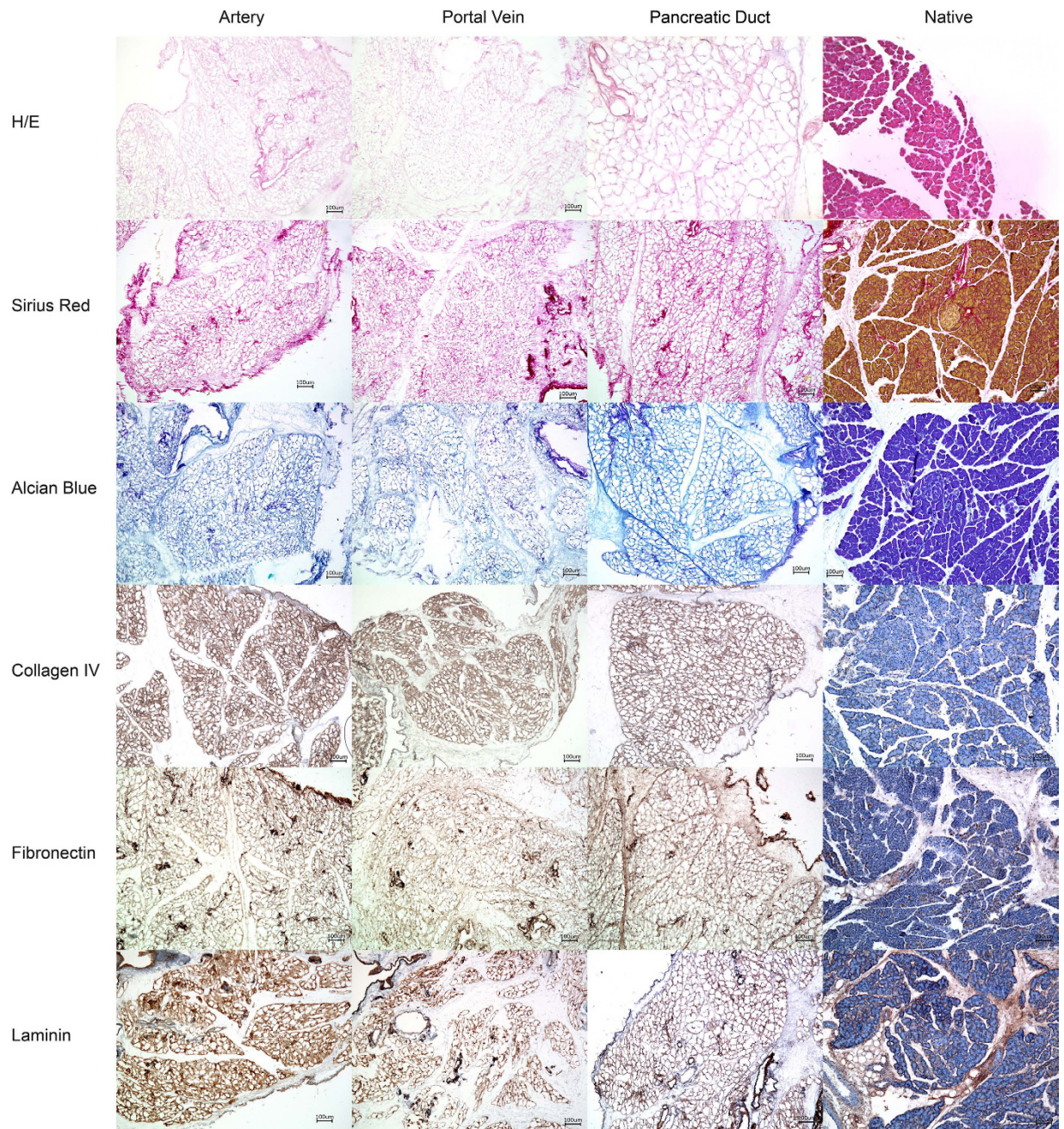
Figure 3. Histology of the decellularized pancreata. Pancreata that were decellularized via the Artery, the Portal Vein or the Pancreatic Duct were stained with different methods to analyze the organ structure after decellularization and compared with native controls: No remaining cells were found inside the decellularized organs but the characteristic lobular microarchitecture of the organ was preserved. Key matrix proteins (Collagen IV, Fibronectin and Laminin) were visualized by immunohistochemical stainings. No significant differences were observed between the three experimental groups. Key matrix proteins remained in the matrices.

content/dry weight in the experimental groups compared with the native controls (A: $62.14 \pm 10.52 \, \mu g/mg$ ($p < 0.5$); PV: $56.26 \pm 15.06 \, \mu g/mg$; BD: $60.32 \pm 25.58 \, \mu g/mg$; C: $8.076 \pm 4.081 \, \mu g/mg$; Fig. 4B). However, the only significant difference was found between the arterial perfusion group and the native controls. The collagen content/dry weight slightly increased in the three groups with different perfusion routes compared with the native controls (A: $164.3 \pm 70.67 \, \mu g/mg$; PV: $108.9 \pm 66.69 \, \mu g/mg$; BD: $287.4 \pm 159 \, \mu g/mg$; C: $13.01 \pm 2.573 \, \mu g/mg$; Fig. 4C). However, no significant differences could be found between the groups.

Contamination analysis of decellularized matrices. When a cell culture is contaminated with germs the culture medium becomes cloudy. Therefore, light absorbance levels of the culture medium was measured
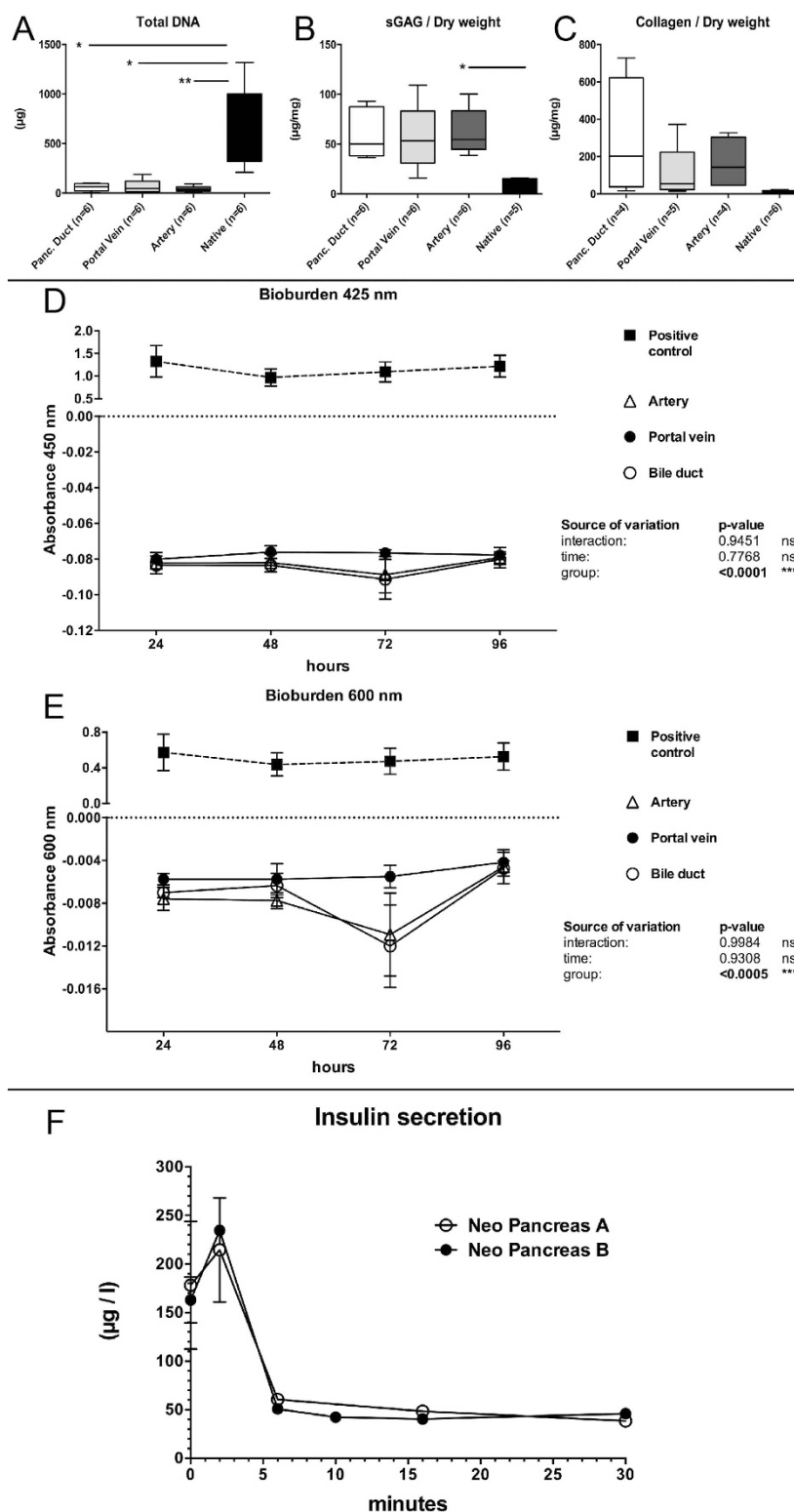
Figure 4. Biochemical evaluation. The amount of DNA significantly declined in all experimental groups compared to native controls (**A**). No statistically significant differences were observed between the experimental groups. The content of sulfated Glycosaminoglycans (sGAG) per dry weight (**B**) increased compared to native controls due to a loss of cellular protein mass. No statistically significant differences were observed between the experimental groups. The collagen content per dry weight (**C**) increased compared to native controls due to a loss of cellular protein mass. No statistically significant differences were observed between the experimental groups. Bioburden testing at 425 nm (**D**) and 600 nm (**E**) revealed that all experiments were sterile and not contaminated. Insulin analysis revealed that Insulin levels in the perfusate initially increased after high glucose perfusion and then were constant until the end of the perfusion (**F**).
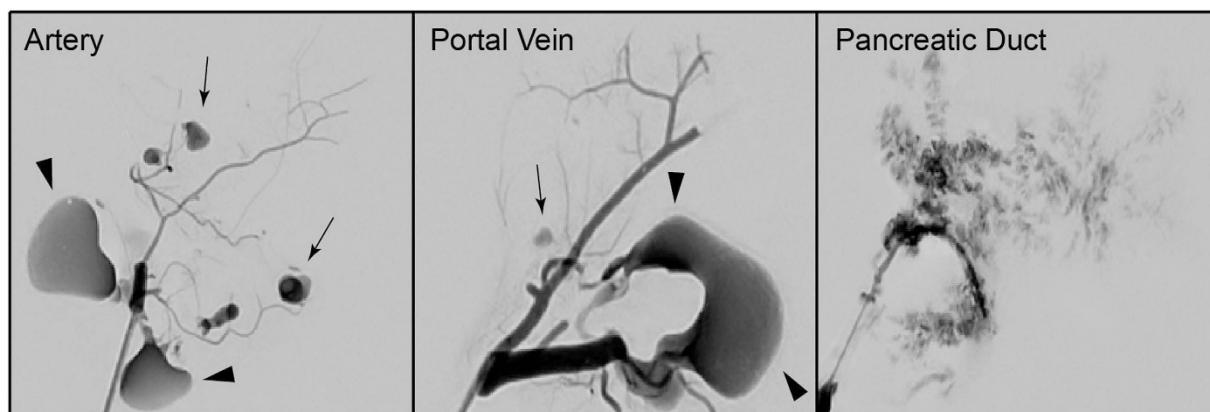
Figure 5. Digital subtraction angiography (DSA) of decellularized pancreata. DSA revealed a major difference between pancreata, which were decellularized via the Artey or the Portal Vein and the Pancreatic Duct: Contrast agent that was infused via the vascular system followed the conserved vascular protein network and leaked into the decellularized parenchymal space at the ends of the intraparenchymatous vessels (black arrows). When infused via the pancreatic duct, the contrast agent followed the ductular system, too, but leaked into the decellularized parenchymal space along all along the ductular system. Some contrast agent leaked through extra-pancreatic vessels outside the organs (black arrowheads).
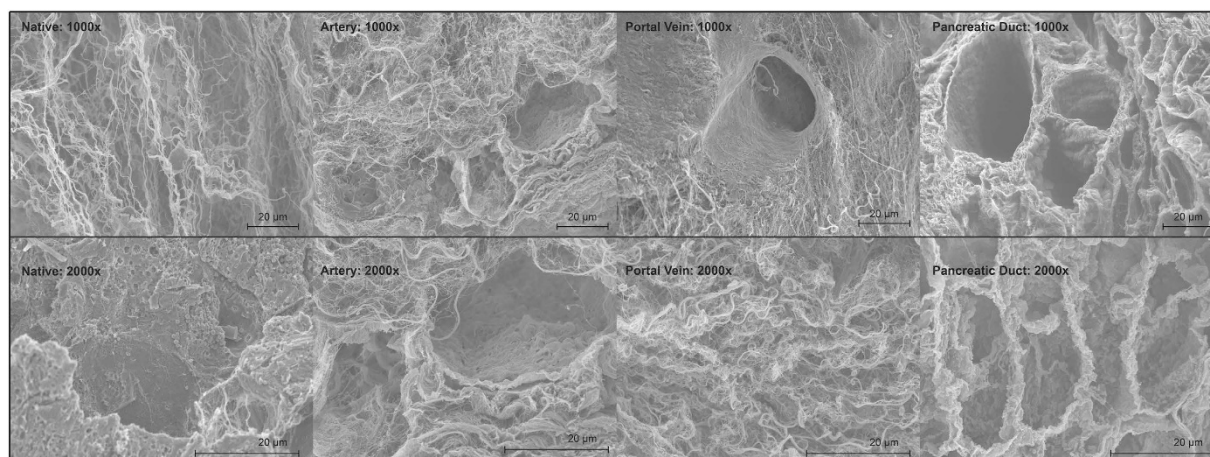
Figure 6. Scanning electron microscopy (SEM) of decellularized pancreata. SEM at a magnification of 1000 and 2000 was performed to analyze the matrix composition after decellularization via the different perfusion routes and compare them with native controls. SEM showed intact protein fibers of the decellularized pancreata and empty cellular spaces compared to native controls. No significant differences were observed between the three experimental groups.

at 425 and 600 nm to analyze its turbidity and to quantify sterility of the decellularized matrices[25]. Bioburden analysis showed no change in the absorbance of any of the three experimental groups compared with the positive controls at both wavelengths throughout the experiment (Fig. 4D+E), indicating that the decellularized matrices remained sterile 96 hours after the process.

Digital subtraction analysis of decellularized matrices. The integrity of the vascular system within the decellularized pancreas was confirmed by angiography: Infusion of contrast agent via the arterial system and the portal vein showed an intact framework of the vessels with sparse emersion of contrast agent at the distal ends of the intra-pancreatic capillaries (Fig. 5). Angiography of the pancreatic duct showed a diffuse emersion of contrast agent along the ductular system into the parenchymal space (Fig. 5).

Scanning electron microscopy (SEM) of decellularized matrices. A comparison of native and decellularized pancreata demonstrated the preservation of the three-dimensional microstructure after decellularization (Fig. 6). SEM images of decellularized pancreata showed the conservation of matrix components. In contrast to the native controls, empty spaces surrounded by networks consisting of fibers with different calibers can be found inside the ECM. Intact protein networks of the blood vessels could be confirmed by the appearance of the
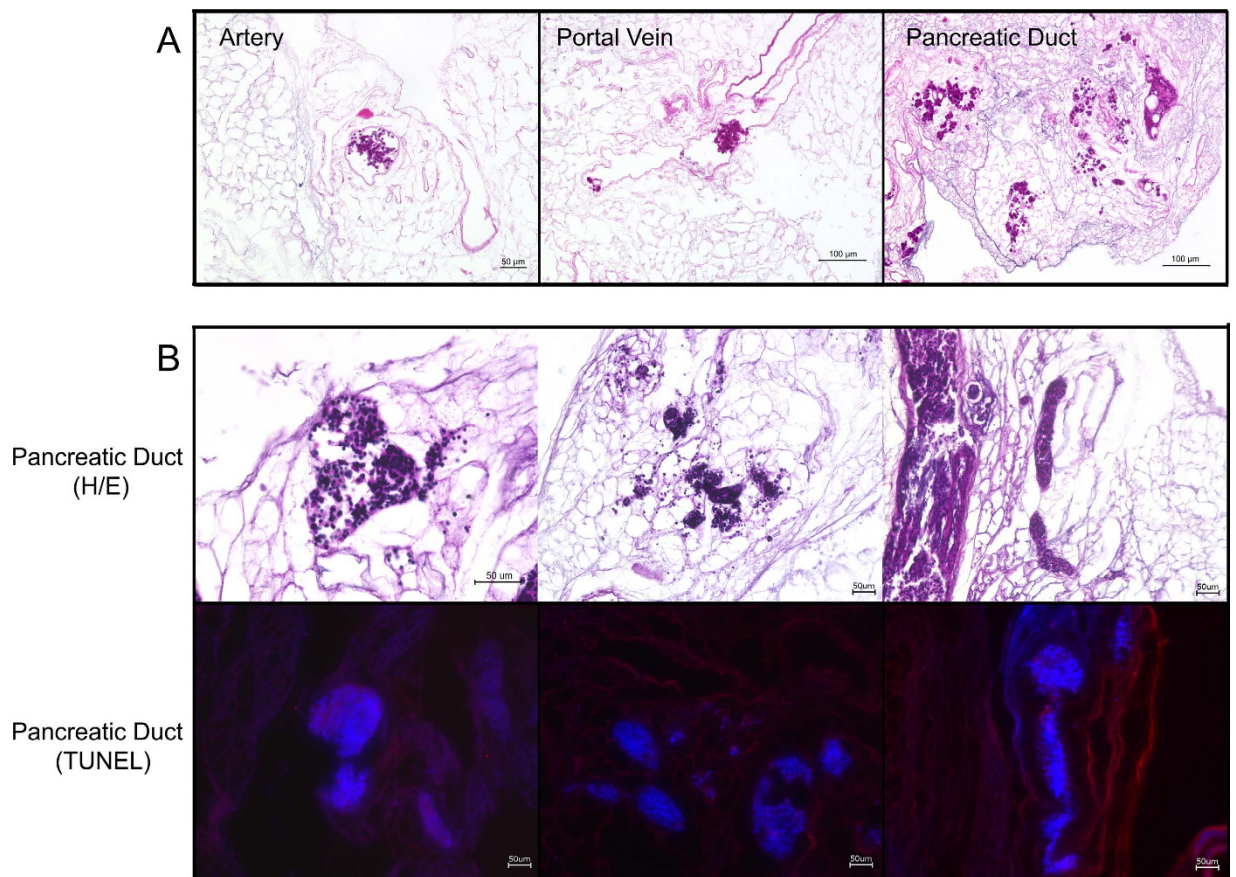
Figure 7. H/E and TUNEL staining of the repopulated pancreata. At first the optimal route for the repopulation process was evaluated (**A**): When infused via the vascular system either islets were stuck inside the protein network of the vessels or were flushed through the organ. When infused via the pancreatic duct, islets leaked into peri-ductular parenchymal space. More islets were found in the pancreas repopulated via the pancreatic duct. Therefore further repopulation experiments were performed via the pancreatic duct (**B**): H/E staining confirmed the previous observations and showed many intact islets inside the decellularized space. TUNEL staining (red) revealed that islets are TUNEL negative and DAPI positive (blue) and therefore viable after the process.

internal elastic lamina without any residual endothelial cells. In the examined specimens, no relevant differences between the experimental groups were observed.

Evaluation of the repopulation process.   During repopulation, islets were observed inside the vascular or ductular network of the decellularized pancreas, depending on the infusion route. Islets followed the flow of the perfusate inside the network from proximal to distal into the periphery of the organ. Some islets then leaked from the visible vascular or ductular network and entered the decellularized parenchymal matrix, while others remained inside the decellularized vessels. Interestingly, islets infused via the pancreatic duct seemed to enter the parenchymal matrix faster and easier. This observation was confirmed by H/E staining of the repopulated matrices (Fig. 7): In total, more islets were found inside the organ, when infused via the pancreatic duct, compared to the aorta or the portal vein. Furthermore, more of these islets leaked into the parenchymal space. Since only a limited amount of islets and no other cells were infused, the majority of the decellularized space remained empty (Fig. 7).

Based on these observations two additional rat pancreata were repopulated via the pancreatic duct and used for *ex vivo* perfusion and glucose stimulated insulin secretion (GSIS) testing. In these experiments 17500 islets each were infused, using a multi-step recellularization protocol. Seeding efficiency of Experiment A and B was 81.96% and 84.5%, respectively.

Viability and functionality of the Neo Pancreas grafts.   At the beginning of the high glucose stimulation, insulin levels were $178 \pm 66\,\mu g/l$ and $163 \pm 24\,\mu g/l$, respectively. After 2 minutes of high glucose perfusion insulin in the perfusate increased to the highest values at $215 \pm 54\,\mu g/l$ and $235\,\mu g/l$, respectively. Then, insulin constantly decreased and was $39\,\mu g/l$ and $46\,\mu g/l$ after 30 minutes of perfusion (Fig. 4F). Even after 90 minutes of perfusion, insulin was still detectable in the perfusate ($22\,\mu g/l$ and $40\,\mu g/l$, respectively; data not shown) indicating an insulin production of the islets during the whole experiment.

H/E and TUNEL staining confirmed that most of the islets remained intact after the manual infusion. Islets inside the decellularized pancreas matrix were negative for TUNEL staining, even after six hours of *ex vivo* perfusion for the GSIS testing, showing that islets remained viable after the process (Fig. 7).

Discussion

The decellularization and recellularization of parenchymal organs has in recent years emerged in the field of tissue engineering. This interesting new technique could provide several improvements: by removing all cellular material from an allogeneic or even xenogeneic organ, a less immunogenic three-dimensional scaffold can be generated that can be repopulated with xenogeneic, allogeneic or autologous cells. If the endothelial integrity inside the vascular network is re-established by e.g. re-endothelialization[26] the engineered organ could finally be implanted *in vivo*. Recent proof-of-concept studies showed promising *in-vivo* results for various recellularized organs such as the heart, lung, liver and kidney[27–30] but available data on pancreas decellularization remain limited[1,20–23].

We provide the first protocol for rat pancreas decellularization and recellularization with whole islets. To analyze the impact of the perfusion route, three different experimental groups, that were identical with regard to applied perfusates, flow rates and duration, were evaluated. Interestingly, in contrast to our own results in the liver[31] and to the results of Goh et al.[21], who stated that decellularization via the pancreatic duct was insufficient, in the presented study, the perfusion route only appeared to have a minor impact on decellularization efficiency. In none of the examined specimens any remaining cells were found and the microstructures of the decellularized organs, including immunohistochemical stainings of the important matrix components, were comparable.

The only major difference between the three experimental groups was revealed by angiography: While contrast agent given via the vascular system remained mainly inside the framework of the vascular system and only leaked in to parenchyma at the distal ends of the capillaries, contrast agent infused via the pancreatic duct followed the ductular system but spilled into the parenchymal space all along the ductular system. Thus, we hypothesized that the pancreatic duct could be the best perfusion route for repopulation of decellularized pancreas matrices: Islets represent units of different cells and are significantly larger than single cells[24]. If the basal lamina of the vascular network is still intact after decellularization, infused islets should not be able to pass through the vascular protein network into the decellularized parenchymal space. We infused islets through the arterial system or the portal venous system or the pancreatic duct and confirmed our angiographic observations: When given via the vascular system, a high amount of the islets either remained inside the vascular system and got stuck or islets were just flushed through the organ. In contrast, islets given via the pancreatic duct left the ductular system and were found inside the parenchyma. Interestingly, a recent publication on human pancreas decellularization showed a survival of islets cultured on slices of the decellularized pancreas in a perifusion chamber. However, whole decellularized pancreata were not repopulated with islets, possibly due to their size[22].

In our study, functionality of the repopulated grafts was evaluated by *ex vivo* perfusion and glucose stimulated insulin secretion testing: Compared to physiological levels, we found relatively high glucose levels in the perfusate, which can be explained by a high number of islets used for the repopulation. Then, we found higher levels at the beginning of the perfusion with high glucose medium than we expected. This finding may result from different reasons: During the three hours of perfusion with low glucose medium we used a closed circuit to save perfusion medium. Then, after initiation of perfusion with high glucose the circuit was opened and fresh (high glucose) medium was inserted. Thus, secreted insulin might have accumulated in the circuit before initiation of high glucose perfusion. Furthermore, at least some islets will have been damaged during the process of repopulation and therefore some insulin might have been released from perished islets. However, we are able to show a clear increase of insulin after initiation of perfusion with high glucose medium and found constant insulin levels during the further perfusion even with the open circuit. These findings clearly show that islets are functional after the repopulation process, as confirmed by TUNEL staining after the perfusion experiments.

If the vascular (and ductular) protein network of the organ is conserved, the cellular integrity of these structures can also be re-assembled with (for example) endothelial cells, as shown by Orlando et al.[17]. Complete re-endothelialization will be essential because thrombosis will otherwise become a major issue after implantation[32]. In our study, the conservation of the vascular system was examined via macroscopic observation and confirmed in histological stainings, scanning electron microscopy and angiography. Thus, after parenchymal repopulation with islets, our next step will be the re-endothelialization of the vascular protein network.

However, we provide the first proof-of-concept that the parenchymal space of a decellularized pancreas can be repopulated with islets, despite their great size. We hypothesize that islets can leak into the parenchymal matrix through ruptures in the basal membrane of I) the conserved vascular protein network or even better II) through the protein network of the ductular system. In our experiments, repopulation via the pancreatic ductular system showed the most promising results. TUNEL staining and glucose stimulated insulin secretion revealed that islets remain viable and functional after the process.

Conclusion

To the best of our knowledge, we herein present the first available protocol for whole rat pancreas decellularization and recellularization with islets of Langerhans and compare three perfusion routes (arterial, venous and ductular). We provide proof-of-concept that the repopulation of decellularized rat pancreata is possible via the pancreatic duct and that islets remain viable and functional after the process. The presented technique can serve as a bioengineering platform for further recellularization and implantation studies.

Methods

Animals. All animal work was performed in accordance with local law and approved by the State Office of Health and Local Affairs (LAGeSo, Berlin, Germany; Reg. No. T0139/13, O0262/13 and O264/13).

Forty-four male and female F344 DPP IV-, Wistar and Lewis eGFP rats (FEM, Charité, Berlin, Germany) weighing between 150 and 400 g were used for the decellularization experiments.

Fifteen female outbred Wistar rats (Harlan Sprague Dawley Inc., Indianapolis, IN, USA) weighing between 300 and 400 g were used for the islet isolation procedure.

Sterile conditions were maintained throughout all surgical procedures.

Rat Pancreas Harvesting. Rats were anaesthetized via the inhalation of isoflurane (abbvie, North Chicago, IL, USA) (3.5% for induction/2% for maintenance) and administered a subcutaneous injection of ketamine (Pfizer, New York City, NY, USA) (10 mg/kg), medetomidine hydrochloride (cp pharma, Burgdorf, Germany) (0.1 mg/kg) and metamizol (ratiopharm, Burgdorf, Germany) (100 mg/kg).

For perfusion via the portal vein (PV) and the abdominal aorta (A), the protocol for donor pancreatectomy published by Klempnauer and Settje[33] was modified. We cannulated the designated vessel after injecting 500 IE of heparin (Rotexmedia, Trittau, Germany) in the inferior vena cava. The portal vein was cannulated retrogradely with a shortened 17 G catheter (Becton, Dickinson and Company, Franklin Lakes, NJ, USA). The aorta was cannulated retrogradely with a 17 G catheter after preparation of all branches. For the perfusion via the pancreatic duct (PD), the major duodenal papilla was exposed and ligated once with Silk 5–0. A small incision was made at common bile duct and a shortened 24 G catheter (Becton, Dickinson and Company) was inserted anterogradely.

All explanted organs were placed in a 100 ml beaker filled with cold Ringer-Lactate buffer and directly used for decellularization (PV, A and PD), or direct preparation for further analyses (Controls).

Perfusion Decellularization. To avoid contamination, the complete procedure was performed under sterile conditions in a laminar airflow cabinet (Heraeus Instruments, Hanau, Germany). The cannulated pancreata were connected to a perfusion system and 1% Triton X100 (Carl Roth, Karlsruhe, Germany) was perfused at 10 ml/min. for 60 minutes through the portal vein. Next, 0.5% sodium dodecyl sulfate (SDS) (Carl Roth) was used as a perfusate for 120 minutes. Again 1% Triton X-100 was used to perfuse the organs for 15 minutes at 10 ml/min. Then, phosphate-buffered saline solution pH 7.4 (PBS) (Biochrom, Berlin, Germany) was rinsed through the organs at 2 ml/min. for 4 hours.

Islet isolation. Islet isolation was performed as described by Schubert et al.[34]. After euthanasia, a digestion solution containing Collagenase (Sigma-Aldrich, St. Louis, MO, USA) and DNase I (F. Hoffmann-La Roche, Basel, Switzerland) was injected anterogradely into the common bile duct. The pancreata were digested for 15 min., islets were isolated with a discontinuous Ficoll (Sigma-Aldrich) gradient and cultured in RPMI 1640 (Gibco, ThermoScientific, Venlo, Netherlands) supplemented with 10% (vol/vol) FBS (Biochrom). Purity and the amount of islets were determined using dithizone staining (Sigma-Aldrich).

Recellularization. At first recellularization was performed to test the best perfusion route: Isolated islets were reseeded on the decellularized matrix via a single-step perfusion technique. Approximately 2,000 islets in 3 ml islet medium each were manually infused via the portal vein or the aorta or the pancreatic duct. The repopulation process was performed under a M651 surgical microscope (Leica Microsystems, Wetzlar, Germany) and filmed with a MC170HD microscope camera (Leica Microsystems).

Further pancreata were recellularized with a modified technique via the pancreatic duct to test viability and functionality of the islets after the process: Decellularized pancreata were perfused with PBS 1 ml/min. overnight at room temperature. One hour before recellularization the organs were transferred into a petri dish filled with islet medium and incubated at 37 °C (95% O_2/5% CO_2). Recellularization was conducted using a 3-step manual infusion technique. At first, all cannulated outflows of the decellularized pancreas matrices were closed and 5 ml islet medium was infused via the extrahepatic bile duct. In total 6 ml islet medium with approximately 17,500 islets was infused via the same route consisting of 2 min. infusion periods followed by 5 min. of static seeding.

***Ex-vivo* Perfusion and Glucose stimulated Insulin Secretion (GSIS).** After repopulation, the recellularized organs were connected to the perfusion reactor, kept at 37 °C (Fig. 8) but were not perfused for one hour to permit adherence of the islets inside the matrix. Then, the organs were perfused for 180 min. with low glucose islet medium (4 mmol/l) followed by a 90 min. perfusion with high glucose islet medium (20 mmol/l). Perfusion was performed via the cannulated arterial system. Perfusate freely flew out of the pancreas into the perfusion chamber. Samples from the effluent inside the perfusion chamber were taken using a syringe at different time points and stored at −20 °C before further analyses (Fig. 4F). Seeding efficiency was calculated by dithizone staining of the remaining islets inside the petri dish and inside the reactor at the end of the adherence time.

Histological evaluation. Paraformaldehyde-fixed (Herbeta Arzneimittel, Berlin, Germany) and paraffin-embedded (Sigma-Aldrich) tissue sections were cut 5-μm-thick and stained with Hematoxylin and Eosin (AppliChem, Darmstadt, Germany), Alcian Blue (Morphisto, Frankfurt am Main, Germany) and Sirius Red (Sigma-Aldrich).

The immunohistochemistry staining for Collagen IV and Laminin used a 3% hydrogen peroxide solution, antigen retrieval with a 0.01 M citrate buffer (Agilent Technologies, Glostrup, Denmark) and 3% goat serum for blocking (Agilent Technologies). The sections were then incubated 1:400 with a rabbit anti-mouse polyclonal collagen IV antibody (Abcam, Cambridge, United Kingdom, Cat #ab6586) or 1:50 with a rabbit anti-mouse polyclonal laminin antibody (Abcam, Cat #ab11575) for 1 hour at 37 °C. The secondary goat anti-rabbit HRP antibody (Abcam, Cat #ab6721) was diluted 1:400 and incubated for 30 minutes followed by visualization with 3,3′-Diaminobenzidine (Agilent Technologies). Fibronectin staining included antigen retrieval with a 0.01 M citrate buffer, peroxidase block (Agilent Technologies) and protein block (Agilent Technologies). Sections were then incubated 1:100 with a rabbit polyclonal fibronectin antibody (Abcam, Cat #ab23751) at room temperature
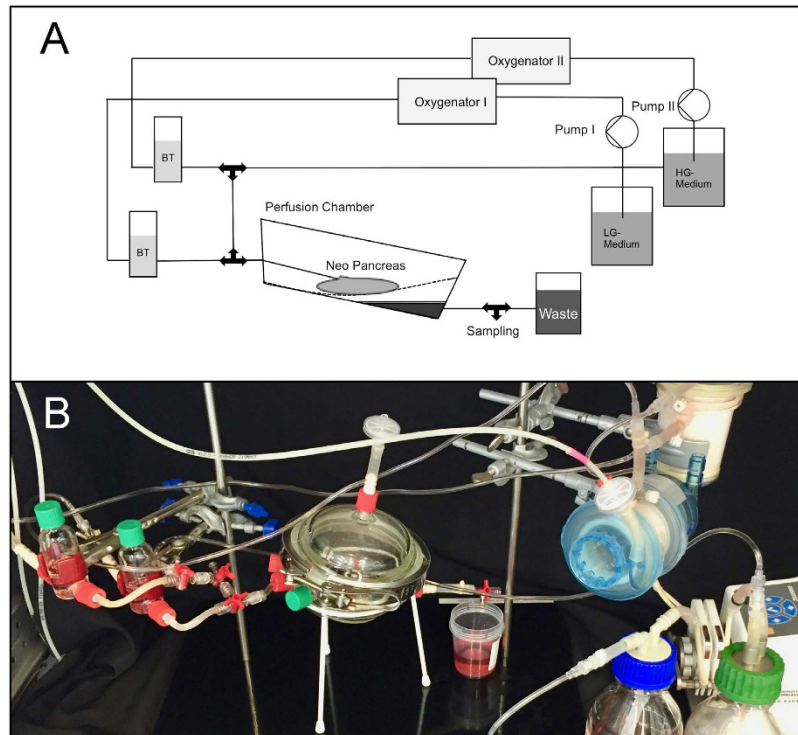
Figure 8. Scheme and photograph of the bioreactor for *ex vivo* perfusion. The reactor consisted of a perfusion chamber and two separate circuits for low and high glucose medium, each consisting of a pump, an oxygenator and a bubble trap. Two circuits were used to constantly circulate and oxygenate the perfusion medium and to ensure a fast switch from low to high glucose perfusion.

overnight. LSAB System-HRP (Agilent Technologies) was used according manufacturer's instructions and 3, 3′-Diaminobenzidine as substrate for visualization. Finally, all sections were counterstained with Mayer's hematoxylin and mounted with Aquatex (Merck, Darmstadt, Germany).

To detect apoptosis inside the repopulated pancreas grafts we performed terminal deoxynucleotidyl transferase dUTP nick end labeling (TUNEL) staining using an *In-Situ* Cell Death Detection Kit, Fluorescein (F. Hoffmann-La Roche). To stain the tissue we used the labeling protocol for difficult tissue provided by the manufacturer. Afterwards the tissue was counterstained with DAPI (Sigma-Aldrich).

Images were recorded with a BZ-9000 BIOREVO microscope (Keyence, Osaka, Japan).

Biochemical analysis. For biochemical analysis, diethylpyrocarbonate (DEPC) (AppliChem) was added to the samples ($n = 6$ for each group), and they were homogenized with an Ultra-Turrax T25 (Janke & Kunkel IKA Labortechnik, Staufen, Germany). For DNA quantification, the DNeasy Blood & Tissue Kit (Qiagen, Venlo, Netherlands) was used to purify the DNA according to the protocol for small sample sizes provided by the manufacturer. The DNA content was measured using a NanoDrop 2000 C UV-Vis Spectrophotometer (ThermoScientific, Venlo, Netherlands) with a pre-configuration for DNA at 260 nm. For hydroxyproline detection, the Total Collagen Assay (QuickZyme, Leiden, Netherlands) was used following the instructions of the manufacturer. The hydroxyproline content was measured at an absorbance maximum of 570 nm with a FluoStar Optima (BMG Labtech, Ortenberg, Germany) and run against a standard curve (6–300 μg/ml). The sGAG content was determined using a method described by Farndale *et al.*[35]. 1 ml of a 1,9-Dimethylmethylene blue (Sigma-Aldrich) color reagent was mixed with the same amount of sample solution that had been incubated in a buffer containing papain and run directly at 525 nm on the NanoDrop 2000 C. A standard curve (0–200 μg/ml) was obtained using Chondroitin-4-Sulphate (Carl Roth) with the same method.

A rat insulin ELISA (Mercodia AB, Uppsala, Sweden) was used to measure insulin levels in the perfusate. The protocol was performed according to the protocol provided by the manufacturer.

Bioburden analysis. To check for bacterial contamination, 5 ml of the perfusion perfusate was mixed with 7 ml SOC medium in a partially opened 15 ml Falcon tube. The mixture was incubated at 37 °C and absorbance at 425 and 600 nm was run against blank SOC medium with PBS after 24, 48, 72 and 96 hours using the NanoDrop 2000 C.

Digital Subtraction Angiography. To visualize ductal and vascular anatomy, digital subtraction angiography was performed in cooperation with the department of Radiology. A 1:1 mixture of Lipiodol (Guerbet, Villepinte, France) and Histoacryl (B. Braun, Melsungen, Germany) was used as a contrast agent. Images were acquired with an Allura Xper FD20/20 (Philips Medical Systems, Hamburg, Germany) angiography unit. After

55

flushing with 10% glucose solution, the contrast agent was injected manually into the cannulated portal vein, artery and pancreatic duct under fluoroscopic control.

Scanning electron microscopy (SEM).   Scanning electron microscopy was performed by the electron microscopy core facility at the Charité Universitätsmedizin Berlin. The samples were fixated with 2.5% glutaraldehyde in 0.1 M sodium cacodylate buffer, rinsed, post-fixated with 1% osmium tetroxide and rinsed again. Then, the specimens were dehydrated with an ascending row of ethanol and critical-point-dried in a Polaron E3000 (Quorum Technologies, Laughton, United Kingdom). The samples were mounted on an aluminum pin and sputter-coated with a gold/palladium alloy to generate conductivity with a MED 020 (BAL-TEC, Balzers, Liechtenstein).

Pictures were taken with a DSM 982 Gemini (Zeiss, Oberkochen, Germany).

Statistical analysis.   Statistical analysis and visualization were performed using Prism 6.0 g for Mac OS X (GraphPad Software Inc., La Jolla, CA, USA). Numeric data were expressed as the means $\pm$ standard error of means (SEM). Because a normal distribution could not be assumed due to the small sample size, group comparisons were performed using the Kruskal-Wallis test followed by Dunn's multiple comparison analysis. Probability values $p < 0.05$ were regarded as statistically significant.

References

1. Mirmalek-Sani, S. H. *et al.* Porcine pancreas extracellular matrix as a platform for endocrine pancreas bioengineering. *Biomaterials* **34,** 5488–5495 (2013).
2. Imperatore, G. *et al.* Projections of Type 1 and Type 2 Diabetes Burden in the U.S. Population Aged < 20 Years Through 2050: dynamic modeling of incidence, mortality and population growth. *Diabetes Care* **35,** 2515–2520 (2012).
3. Frier, B. M. Hypoglycaemia in diabetes mellitus: epidemiology and clinical implications. *Nat Rev Endocrinol* **10,** 711–722 (2014).
4. Atkinson, M. A., Eisenbarth, G. S. & Michels, A. W. Type 1 diabetes. *Lancet* **383,** 69–82 (2014).
5. Barton, F. B. *et al.* Improvement in outcomes of clinical islet transplantation: 1999–2010. *Diabetes Care* **35,** 1436–1445 (2012).
6. Ludwig, B., Ludwig, S., Steffen, A., Saeger, H. D. & Bornstein, S. R. Islet versus pancreas transplantation in type 1 diabetes: competitive or complementary? *Curr Diab Rep* **10,** 506–511 (2010).
7. Balzano, G.*et al.* Autologous islet transplantation in patients requiring pancreatectomy: a broader spectrum of indications beyond chronic pancreatitis. *Am J Transplant*, doi: 10.1111/ajt.13656 (2015 Dec 22) [Epub ahead of print].
8. Olsson, R., Olerud, J., Pettersson, U. & Carlsson, P. O. Increased numbers of low-oxygenated pancreatic islets after intraportal islet transplantation. *Diabetes* **60,** 2350–2353 (2011).
9. Kawahara, T., Kin, T. & Shapiro, A. M. A comparison of islet autotransplantation with allotransplantation and factors elevating acute portal pressure in clinical islet transplantation. *J. Hepato-Biliary-Pancreat. Sci.* **19,** 281–288 (2012).
10. Kawahara, T. *et al.* Portal vein thrombosis is a potentially preventable complication in clinical islet transplantation. *Am J Transplant* **11,** 2700–2707 (2011).
11. Naziruddin, B. *et al.* Evidence for instant blood-mediated inflammatory reaction in clinical autologous islet transplantation. *Am J Transplant* **14,** 428–437 (2014).
12. Struecker, B., Raschzok, N. & Sauer, I. M. Liver support strategies: cutting- edge technologies. *Nat. Rev. Gastroenterol. Hepatol.* **11,** 166–176 (2014).
13. Song, J. J. & Ott, H. C. Organ engineering based on decellularized matrix scaffolds. *Trends Mol. Med.* **17,** 424–432 (2011).
14. Orlando, G. *et al.* Regenerative medicine as applied to solid organ transplantation: current status and future challenges. *Transpl. Int.* **24,** 223–232 (2011).
15. Badylak, S. F., Weiss, D. J., Caplan, A. & Macchiarini, P. Engineered whole organs and complex tissues. *Lancet* **379,** 943–952 (2012).
16. Sullivan, D. C. *et al.* Decellularization methods of porcine kidneys for whole organ engineering using a high-throughput system. *Biomaterials* **33,** 7756–7764 (2012).
17. Orlando, G. *et al.* Production and implantation of renal extracellular matrix scaffolds from porcine kidneys as a platform for renal bioengineering investigations. *Ann Surg* **256,** 363–370 (2012).
18. Wang, Y. *et al.* Lineage restriction of human hepatic stem cells to mature fates is made efficient by tissue-specific biomatrix scaffolds. *Hepatology* **53,** 293–305 (2011).
19. Zhu, S. *et al.* Human pancreatic beta-like cells converted from fibroblasts. *Nat. Commun.* **7,** 10080 (2016).
20. De Carlo, E. *et al.* Pancreatic acellular matrix supports islet survival and function in a synthetic tubular device: *in vitro* and *in vivo* studies. *INT J MOL MED* **25,** 195–202 (2010).
21. Goh, S. K. *et al.* Perfusion-decellularized pancreas as a natural 3D scaffold for pancreatic tissue and whole organ engineering. *Biomaterials* **34,** 6760–6772 (2013).
22. Peloso, A. *et al.* The Human Pancreas as a Source of Protolerogenic Extracellular Matrix Scaffold for a New-generation Bioartificial Endocrine Pancreas. *Ann Surg*, doi: 10.1097/sla.0000000000001364 (2015 Nov 26) [Epub ahead of print].
23. Wu, D. *et al.* 3D Culture of MIN-6 Cells on Decellularized Pancreatic Scaffold: *In Vitro* and *In Vivo* Study. *Biomed Res Int 2015* 432645 (2015).
24. von Mach, M. A. *et al.* Size of pancreatic islets of Langerhans: a key parameter for viability after cryopreservation. *Acta Diabetol* **40,** 123–129 (2003).
25. Guyette, J. P., Gilpin, S. E., Charest, J. M., Tapias, L. F., Ren, X. & Ott, H. C. Perfusion decellularization of whole organs. *Nat. Prot.* **9,** 1451–1468 (2014).
26. Crapo, P. M., Gilbert, T. W. & Badylak, S. F. An overview of tissue and whole organ decellularization processes. *Biomaterials* **32,** 3233–3243 (2011).
27. Ott, H. C. *et al.* Perfusion-decellularized matrix: using nature's platform to engineer a bioartificial heart. *Nat. Med.* **14,** 213–221 (2008).
28. Ott, H. C. *et al.* Regeneration and orthotopic transplantation of a bioartificial lung. *Nat. Med.* **16,** 927–933 (2010).
29. Song, J. J. *et al.* Regeneration and experimental orthotopic transplantation of a bioengineered kidney. *Nat. Med.* **19,** 646–651 (2013).
30. Uygun, B. E. *et al.* Organ reengineering through development of a transplantable recellularized liver graft using decellularized liver matrix. *Nat. Med.* **16,** 814–820 (2010).
31. Struecker, B. *et al.* Improved rat liver decellularization by arterial perfusion under oscillating pressure conditions. *J Tissue Eng Regen Med*, doi: 10.1002/term.1948 (2014 Sep 4) [Epub ahead of print].
32. Jiang, B., Akgun, B., Lam, R. C., Ameer, G. A. & Wertheim, J. A. A polymer- extracellular matrix composite with improved thromboresistance and recellularization properties. *Acta biomater.* **18,** 50–58 (2015).
33. Klempnauer, J. & Settje, A. Vascularized pancreas transplantation in the rat–details of the microsurgical techniques, results, and complications. *Transpl. Int.* **2,** 84–91 (1989).

34. Schubert, U. *et al.* Transplantation of pancreatic islets to adrenal gland is promoted by agonists of growth-hormone-releasing hormone. *Proc. Natl. Acad. Sci. USA* **110,** 2288–2293 (2013).
35. Farndale, R. W., Buttle, D. J. & Barrett, A. J. Improved quantitation and discrimination of sulphated glycosaminoglycans by use of dimethylmethylene blue. *Biochim. Biophys. Acta* **883,** 173–177 (1986).

Acknowledgements

Author Contributions

H.N. developed the project idea, performed the experiments and contributed to main parts of the manuscript. K.H. helped during all parts of the project. N.H. helped establishing the *ex vivo* perfusion and helped with the analysis of the experiments. P.T. helped during all parts of the project. M.T. helped with the analysis of the *ex vivo* perfusion and the histological evaluation of the Neo Pancreata. J.G. helped establishing the *ex vivo* perfusion and helped with the analysis of the experiments. M.N. helped establishing the *ex vivo* perfusion and helped with the analysis of the experiments. H.E. helped establishing the *ex vivo* perfusion and helped with the analysis of the experiments. N.S. helped with the analysis of the experiments including histology. M.K. helped with the analysis of the experiments including histology. E.T. discussed results with us and performed the statistical evaluation. D.P. developed the cannulation technique for rat pancreata and performed the explantations. S.L. helped with the analysis of the experiments including histology. D.G. performed the angiographies of the decellularized pancreata. A.R.-S. discussed results with us and performed the statistical evaluation. A.A. discussed results with us and performed the statistical evaluation. N.R. developed the project idea, discussed the results and proofread the manuscript. J.P. developed the project idea, discussed the results and proofread the manuscript. I.M.S. developed the project idea, discussed the results and proofread the manuscript. B.S. developed the project idea, supervised the whole project and wrote the manuscript.

Additional Information

Competing financial interests: The authors declare no competing financial interests.

How to cite this article: Napierala, H. *et al.* Engineering an endocrine Neo-Pancreas by repopulation of a decellularized rat pancreas with islets of Langerhans. *Sci. Rep.* **7**, 41777; doi: 10.1038/srep41777 (2017).

Publisher's note: Springer Nature remains neutral with regard to jurisdictional claims in published maps and institutional affiliations.

H. Everwien, E. Keshi, K.H. Hillebrandt, B. Ludwig, M. Weinhart, P. Tang, A.S. Beierle, H. Napierala, J.M. Gassner, N. Seiffert, S. Moosburner, D. Geisel, A. Reutzel-Selke, B. Strücker, J. Pratschke, N. Haep, I.M. Sauer, **Engineering an endothelialized, endocrine Neo-Pancreas: Evaluation of islet functionality in an ex vivo model**, Acta Biomater. 117 (2020) 213–225.
DOI: http://dx.doi.org/10.1016/j.actbio.2020.09.022
PubMed PMID: 32949822
Impact Factor: 8,947 im Jahr 2020

12. LEBENSLAUF

Mein Lebenslauf wird aus datenschutzrechtlichen Gründen in der elektronischen Version meiner Arbeit nicht veröffentlicht.

13. Vollständige Publikationsliste

N. Seiffert, P. Tang, E. Keshi, A. Reutzel-Selke, S. Moosburner, H. Everwien, D. Wulsten, H. Napierala, J. Pratschke, I.M. Sauer, K.H. Hillebrandt, B. Struecker, **In vitro recellularization of decellularized bovine carotid arteries using human endothelial colony forming cells**, J. Biol. Eng. 15 (2021) 15.
DOI: http://dx.doi.org/10.1186/s13036-021-00266-5
PubMed PMID: 33882982
Impact Factor: 4,355 im Jahr 2020

H. Everwien, E. Keshi, K.H. Hillebrandt, B. Ludwig, M. Weinhart, P. Tang, A.S. Beierle, H. Napierala, J.M. Gassner, N. Seiffert, S. Moosburner, D. Geisel, A. Reutzel-Selke, B. Strücker, J. Pratschke, N. Haep, I.M. Sauer, **Engineering an endothelialized, endocrine Neo-Pancreas: Evaluation of islet functionality in an ex vivo model**, Acta Biomater. 117 (2020) 213–225.
DOI: http://dx.doi.org/10.1016/j.actbio.2020.09.022
PubMed PMID: 32949822
Impact Factor: 8,947 im Jahr 2020

A. Butter, K. Aliyev, K.-H. Hillebrandt, N. Raschzok, M. Kluge, N. Seiffert, P. Tang, H. Napierala, A.I. Muhamma, A. Reutzel-Selke, A. Andreou, J. Pratschke, I.M. Sauer, B. Struecker, **Evolution of graft morphology and function after recellularization of decellularized rat livers**, J. Tissue Eng. Regen. Med. 12 (2018) e807–e816.
DOI: http://dx.doi.org/10.1002/term.2383
PubMed PMID: 27957815
Impact Factor: 3,963 im Jahr 2020

H. Napierala, K.-H. Hillebrandt, N. Haep, P. Tang, M. Tintemann, J. Gassner, M. Noesser, H. Everwien, N. Seiffert, M. Kluge, E. Teegen, D. Polenz, S. Lippert, D. Geisel, A. Reutzel Selke, N. Raschzok, A. Andreou, J. Pratschke, I.M. Sauer, B. Struecker, **Engineering an endocrine Neo-Pancreas by repopulation of a decellularized rat pancreas with islets of Langerhans**, Sci. Rep. 7 (2017) 41777
DOI: http://dx.doi.org/10.1038/srep41777
PubMed PMID: 28150744
Impact Factor: 4,379 im Jahr 2020

14. Danksagung

Vieles wäre ohne ihre Hilfe nicht möglich gewesen. Nicht zuletzt möchte ich mich bei Martin Knoop für seine Motivation und tatkräftige Unterstützung bedanken.

Ein großes Dankeschön geht auch an meine Freundinnen und Freunde, die stets an mich geglaubt und an guten und schlechteren Tagen in jeglicher Art und Weise mich unterstützt haben.